2014-12-01

Fabrication, Characterization, Optimization and Application Development of Novel Thin-layer Chromatography Plates

Supriya Singh Kanyal
Brigham Young University - Provo

Fabrication, Characterization, Optimization and Application Development of Novel Thin-Layer Chromatography Plates

Supriya Singh Kanyal

A dissertation submitted to the faculty of
Brigham Young University
in partial fulfillment of the requirements for the degree of

Doctor of Philosophy

Matthew R. Linford, Chair
David V. Dearden
Daniel E. Austin
Robert C. Davis
Richard A. Vanfleet

Department of Chemistry and Biochemistry

Brigham Young University

December 2014

ABSTRACT

Fabrication, Characterization, Optimization and Application Development of Novel Thin-Layer Chromatography Plates

Supriya Singh Kanyal
Department of Chemistry and Biochemistry, BYU
Doctor of Philosophy

This dissertation describes advances in the microfabrication of thin layer chromatography (TLC) plates. These plates are prepared by the patterning of carbon nanotube (CNT) forests on substrates, followed by their infiltration with an inorganic material. This document is divided into ten sections or chapters. Chapter 1 reviews the basics of conventional TLC technology. This technology has not changed substantially in decades. This chapter also mentions some of the downsides of the conventional approach, which include unwanted interactions of the binder in the plates with the analytes, relatively slow development times, and only moderately high efficiencies. Chapter 2 focuses primarily on the tuning of the iron catalyst used to grow the CNTs, which directly influences the diameters of the CNTs grown that are produced. Chapter 3 focuses on the atomic layer deposition (ALD) of SiO_2 from a silicon precursor and ozone onto carbon-nanotubes to obtain an aluminum free stationary phase. This approach allowed us to overcome the tailing issues associated with the earlier plates prepared in our laboratory. Chapter 4 is a study of the hydroxylation state of the silica in our TLC plates. A linear correlation was obtained between the $SiOH^+/Si^+$ time-of-flight secondary ion mass spectrometry (ToF-SIMS) peak ratio and the isolated silanol peak position at ca. 3740 cm^{-1} in the diffuse reflectance infrared spectroscopy (DRIFT) spectra. We also compared the hydroxylation efficiencies on our plates of ammonium hydroxide and HF. Chapter 5 reports a series of improvements in TLC plate preparation. The first is the low-pressure chemical vapor deposition (LPCVD) of silicon nitride onto CNTs, which can be used to make very robust TLC plates that have the necessary SiO_2 surfaces. These TLC plates are the best we have prepared to date. We also describe here the ALD deposition of ZnO into these devices, which can make them fluorescent. Chapters 6 – 10 consist of contributions to Surface Science Spectra (SSS) of ToF-SIMS spectra of the materials used in our microfabrication process. SSS is a peer-reviewed database that has been useful to many in the surface community. The ToF-SIMS spectra archived include those of (i) Si/SiO_2, (ii) $Si/SiO_2/Al_2O_3$, (iii) $Si/SiO_2/Al_2O_3/Fe$, (iv) $Si/SiO_2/Fe$ (annealed at 750 °C in H_2), and (v) $Si/SiO_2/Al_2O_3/Fe_{(annealed)}/CNTs$. Both positive and negative ion spectra have been submitted. In summary, the present work is a description of advances in the development, thorough characterization, optimization, and application development of microfabricated thin layer chromatography plates that are superior to their commercial counterparts.

Keywords: Microfabrication, thin layer chromatography, carbon nanotubes, atomic layer deposition, silica, zinc oxide, low-pressure chemical vapor deposition, SIMS

ACKNOWLEDGEMENTS

I acknowledge the invaluable mentorship, suggestions, encouragement and support from Dr. Matthew R. Linford. His direction and guidance have helped me improve my skills and knowledge tremendously.

I am also thankful to my committee members, Dr. Daniel E. Austin, Dr. David V. Dearden, Dr. Rob C. Davis and Dr. Richard A. Vanfleet for their insightful suggestions and comments throughout my graduate studies.

I am thankful to all my colleagues and lab members in Dr. Linford's group who have helped me: David S. Jensen, Bhupinder Singh, David Hung, Anubhav Diwan, Landon A. Wiest, Guilin Jiang and Cody Cushman.

I thank BYU cleanroom and Utah Nanofab for the opportunity to let me work inside their fabrication facility.

I am grateful to the Department of Chemistry and Biochemistry for giving me the opportunity to earn my doctoral degree in analytical chemistry.

Last but not least, I am very grateful to my family, friends and chotu for all the love and support--especially my life's inspiration, my parents, Deepa Kanyal and Kripal S. Kanyal.

TABLE OF CONTENTS

LIST OF FIGURES

LIST OF TABLES

1. Chapter: Introduction

1.1. Technique

TLC, or thin layer chromatography, is one of the oldest chromatography techniques. In TLC, a sample is dissolved in a suitable solvent and applied as a spot or a band approximately 1-1.5 cm above the lower edge of a TLC plate. The actual position of the band depends on the type of chromatography (normal or preparative). The spotted plate is then dried to remove the solvent, which helps ensure a good separation. Often, in the case of a two-trough developing chamber, the plate will be placed in a trough in this chamber after it has been saturated with the vapors of a developing solvent. The developing solvent will then be added to the trough in which the plate is located to a level just below the sample spot. As the eluent migrates through the sorbent, the sample components also migrate. Ideally the migration of the analytes takes place at different rates, which will result in their separation. When the solvent front has reached a desired point, usually near top of the sorbent layer, the plate is removed and dried. Visualization of the spots or bands on the developed layer is typically performed either under UV light, or via chemical treatment/derivatization. The TLC plates on the market suffer from various drawbacks and limitations, which include inhomogeneities in the adsorbent bed, and the fact that the binders present in commercial plates may interact with analytes and compromise their separations (see Figure 1.2).

1.2. History

The origins of TLC date back to 1938 when Schraiber, working with Izmailov, separated alkaloids present in belladonna (*Atropa belladonna* L.) at the Khar'kov Chemistry and Pharmacy

Research Institute.[1, 2] They used a thin layer of adsorbent coated on a microscopic slide. This method required very small amount of both stationary and mobile phases.

Apart from separating alkaloids, Schraiber is considered to be the first person to employ fluorescence as a method for detecting separated spots on a TLC plate. In 1941, shortly after his work, Consden, Gordon and Martin invented paper chromatography.[3] Unfortunately, Schraiber's work was not well understood by other scientists, and it was not until 1951 that the technique was rediscovered by Kirchner et al., who used coated glass slides to separate terpenes and aldehydes.[4-6] Two decades later Kirchner was still publishing in this field.[7-9] In 1956, Stahl coined the term *thin-layer chromatography.*[10, 11] He also invented an automatic spreader for TLC plates,[12] working from 1960 to 1980 to develop the technique.[13-23] As part of these efforts, he convinced Merck to make TLC plates commercially so that the technique could become a widely accepted analytical tool.

1.3. Stationary phases used

1.3.1. Silica Gel

Most commercially available TLC plates on the market use silica gel as the stationary phase. The silica gel employed can be of high purity. It can be unmodified, or modified with a bonded phase. Properties of the silica that may include its particle diameter, pore volume, pore size, surface area, and chemical nature are similar to those important for liquid chromatography. However, in TLC a small amount of a binder is usually added to the particles to enhance the adhesion of the stationary phase to itself and to the substrate. The commonly used binders fall into two categories: inorganic and organic binders. Organic or polymeric binders such as the polymethacrylates make TLC plates more rugged and allow for the use of high amounts of polar

solvents. TLC plates containing inorganic binders are less rugged. However, TLC plates containing inorganic binders are recommended when the plate derivatization requires charring for visualization. Gypsum, an inorganic binder, is used extensively for producing TLC plates. All of these binders, inorganic or organic, will affect analyte retention, at least to a small degree, because the analytes will interact at least to a small degree with the binder.

1.3.2. Reversed and modified phases

Reversed phases often contain alkyl chains with varying numbers of carbon atoms, *n*, and may be designated as C_n. As expected, these phases generally exhibit very poor wettability due to their strongly hydrophobic natures. That is, the use of high concentrations of water in the development solvent may not be possible. In particular, when *n* is large, the alkyl content of the phases is high, even the presence of a small amount of water in the mobile phase may keep it from wetting the stationary phase. Precoated plates with a polar bonded phase such as amino-, nitrile-, and diol-bonded phase have also made a remarkable progress in various applications.[24]

1.3.3. Alumina

While alumina or aluminum oxide is the second most widely used stationary phase after silica gel, it is not a close second place.[25, 26] TLC plates prepared with alumina are not nearly as popular as those made from silica. The properties of alumina are somewhat similar to those of silica. In general, alumina TLC plates have efficiencies comparable to or less than those of silica coated TLC plates. This stationary phase will often be prepared by heating aluminum hydroxide $Al(OH)_3$ at high temperature (~500 °C).

1.3.4. Magnesia

Magnesia or magnesium silicate has the chemical formula MgO_3Si. It is rarely used today. It was, however, employed in earlier TLC separations involving plant material such as carotenoids. Magnesium silicate is generally prepared by heating magnesium hydroxide at about 350 °C. Further heating at higher temperatures causes a decrease in retention. The chromatographic characteristics of magnesium silicate are again similar to those of silica gel, where the only major difference is that magnesia is basic, which silica gel is intrinsically acidic.[27]

1.3.5. Kieselguhr

Kieselguhr, or diatomaceous earth, is a naturally occurring white or off white powder that is formed by the accumulation of amorphous silica from dead, single celled algae. It is found largely in marine sediments.[28] Kieselguhr has relatively larger pores, and hence has a very low surface area (1 – 5 m^2/g). In general, its particle size varies from 10 – 250 µm. It is, however, used as a support layer for stationary phases and not as a primary adsorbent film.[29-31]

1.3.6. Cellulose

Cellulose is an organic material that consists of D-glucopyranose units coupled together by glycosidic linkages. It is the most abundantly found polymer in nature. Cellulose is present in most vegetation. The two forms of cellulose used in TLC are native cellulose (fibrous) and micro-crystalline cellulose.[32-36] Micro-crystalline cellulose is prepared by the partial hydrolysis of cellulose. Native cellulose has between 400 and 500 units per chain while micro-crystalline cellulose has between 40 and 200. Cellulose is not very commonly used in TLC, but it has been applied in the separation of various amino acid mixtures.

1.3.7. Polyamides

Various polyamides have also been employed as stationary phases in TLC, including polyamide 6,6 (Nylon 6,6), polyhexamethylenediamine, polyamide 6 (Nylon 6), polyaminoundecanoic acid, aminopolycapro-lactame, and polyamide 11 (Nylon 11).[37] These are synthesized by condensing a dicarboxylic acid with a diamine, with the resulting structure, in general, represented by the following formula:

$-[NH-(CH_2)_6-NH-CO-(CH_2)_x-C)]_n$

(if x = 4 then the product is Nylon 6,6, if x = 8 then the product is Nylon 6,10 etc.).

The polyamides have two types of functionalities. The aliphatic chains are hydrophobic. Their amide linkages are polar and can hydrogen bond to analytes.

1.4. Capillary Flow

Capillary forces play a major role in TLC.[38] In general, higher numbers of cavities/voids in a material cause it to have higher surface energy, and this energy is lowered when a mobile phase comes in contact with it.

The energy change of a mobile phase or stationary phase as the mobile phase comes in contact with the porous medium can be given by,

$$\Delta E = \gamma V_m / D$$

where

γ is the surface tension of mobile phase

V_m is molar volume of mobile phase

D is the diameter of pore

For a traditional TLC plate, the overall velocity of the mobile phase decreases with increasing distance of development. In other words

$X_f = \sqrt{kt}$

Where,

$k = 2K_0 d_p\,(\gamma/\eta)\cos\theta$

K_0 is defined as the permeability constant of adsorbent layer

X_f is the mobile phase front position

k is the flow constant

γ is the surface tension

η is the mobile phase velocity

θ is the contact angle

1.5. Resolution

Resolution[38] or R_s is defined in chromatography as the degree of separation of two compounds and can be defined as:

$$Rs = \frac{t_2 - t_1}{\frac{1}{2}(w_{t1} - w_{t2})}$$

Where, t_1 and t_2 are the retention times of the peaks and W_1 and W_2 are the peak width. Baseline resolution is achieved at $R_s = 1.25$.

1.6. Applications

Thin layer chromatography has been applied to a variety of pharmaceutical applications. Some of these include the identification of drugs of abuse and toxic substances in biological fluids,[39, 40] and analysis of complex and dirty samples that are very difficult to analyze by other techniques. TLC can also be used for stability and content uniformity testing,[41, 42] and for authentication of label claims of pharmaceutical products.[43] It has been used to test for overdose of disease preventing drugs in farm animals.[44, 45] Class fractionation and speciation of lipids are done to a significant extent by thin layer chromatography.[46-48] Standardization of plant materials used as traditional medicines is widely performed using thin-layer chromatography.[49] Thin-layer chromatography is often used for screening large numbers of samples because of enhanced sample throughput via parallel separations, and ease of post chromatographic derivatization that improves method selectivity and specificity. It continues to be widely used by organic chemists. In short, thin layer chromatography is an important, practical, and widely used analytical technique. There are, however, limitations to the state of the art plates. Conventional TLC plates use a binder that may interfere with separations and analyte visualization. The long development times in TLC have been a significant and recurring concern for many years. It's limiting resolving power and issues related to non-uniform adsorbent beds are also issues.

1.7. Newer substrates

The purpose of this section is to identify newer substrates that have been developed for thin layer chromatography.

1.7.1. Monoliths as a stationary phase

A monolith is basically a solid porous material with meso and micropores. Monoliths have potential in chromatography because they can be designed to have high permeability and therefore allow high mobile phase velocities.[34] Macroporous monoliths were introduced as possible stationary phases for TLC 16 years ago.[6] Schulz, in his work in this area,[50, 51] referred to this approach as UTLC (ultrathin layer chromatography). These UTLC plates were made via the hydrolytic polycondensation of a liquid film of an alkoxysilane on a glass plate. The separation of pesticides, pharmaceutically active ingredients, phenols, and plasticizers was performed on these plates. Comparison of these UTLC devices with TLC and High Performance TLC (HPTLC) plates clearly showed improvement in detection limits, migration times, and lower solvent consumption.[7] However, problems with these monolithic based TLC plate included higher R_f values, higher plate heights, and lower resolution. In 2009, Boichenko et al. proposed a method for preparing monolithic TLC plates by optimizing a sol gel synthesis on the plate.[52] Their method involved the acid hydrolysis of tetraethoxyorthosilicate (TEOS) and a catalyst (HF) in ethanol (the solvent). Additives in their synthesis included dimethylformaldehyde and cetylpyridinium chloride. Their approach consisted of spreading their reaction mixture on a glass substrate, followed by drying of the monolith. Through the sol-gel process, the control of the structure of materials at the molecular level is possible. High speeds, short run distances, the possibility of plate regeneration, and the reduction of toxic organic solvents were a few of the advantages of their UTLC plates.[11] Disadvantages of monolithic layers for TLC may include the challenge of obtaining desired film thicknesses with appropriate pore structure, and prevention of monolith cracking.

1.7.2. Polymeric phases

Monolithic stationary phases for TLC have also been made from thin films of poly(butylmethacrylate-co-ethylene dimethacrylate) via in situ photopolymerization.[53] These porous, monolithic polymer layers were prepared by placing the polymerization mixture inside of a mold of desired thickness and by then exposing it to UV light. The resulting layers were ca. 50 – 200 μm thick. A separation of proteins and peptides was achieved with a migration time of about 5 – 6 min for a 6 cm migration distance, which was a very reasonable separation time. This separation was coupled with Matrix-assisted laser desorption ionization (MALDI) for detection. The advantage of this technique was the precise control of the reaction conditions, which gave the monolithic layers well-defined porosity, and thus improved the chromatographic performance. Moreover the lack of a binder in the adsorbent layer also improved the separation efficiencies and retention characteristics of the material.

1.7.3. Glancing angle deposition (GLAD)

Glancing angle deposition, or GLAD,[54-60] (see Figure 1.1) has been exploited by Bezuidenhout et al.[61-64] to prepare UTLC plates. In GLAD, one's substrate is tilted, so that the flux of atoms approaching a surface is at a glancing angle (α). The GLAD technique results in deposition of a porous nanostructured thin film of SiO_2. Plates made by this method were termed nanostructured-UTLC (NS-UTLC) since the sorbent layer obtained was just 10 μm thick. It is a physical vapor deposition technique that utilizes computer controlled biaxial substrate motion to grow nano-columns. Different shapes that include helices, vertical post, square spirals and zig-zags can be grown. This method allows for growth of nanostructured layers with controllable film architectures, macroporosity and thickness.

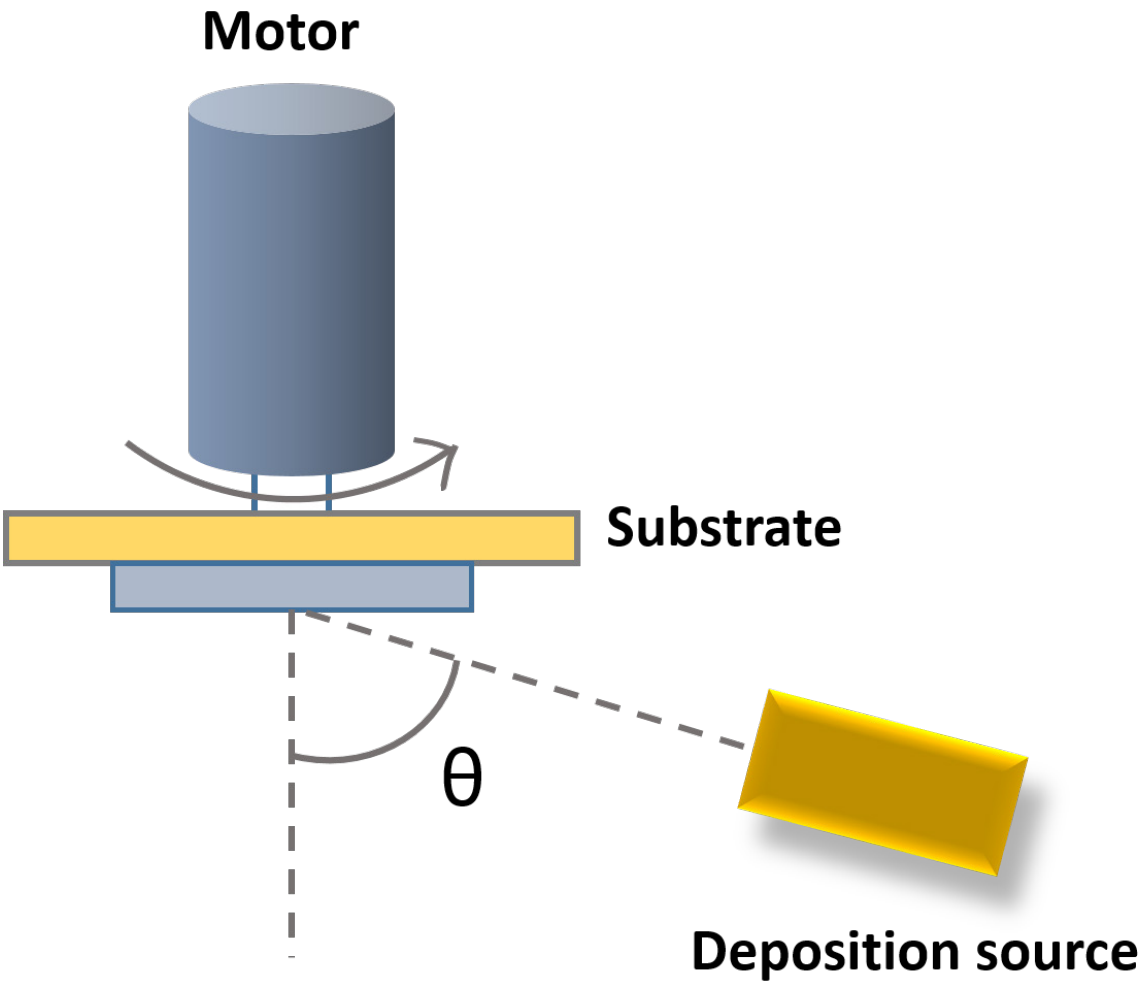

Figure 1.1. The schematic of GLAD technique.

It was observed that the quality of a TLC separation on GLAD plates is dependent largely on the deposition angle. For example, a good separation of an Analtech test dye mixture was obtained on plates prepared at a higher deposition angle. Film thickness also has an effect on separation quality, e.g., dyes were well separated in a short distance of 5 mm on 5 µm and 7 µm films in an elution time of less than 5 min. Nevertheless, the technique suffers from various problems that include: 1) non uniformity of the film out of the plane because of the shadowing effects of adjacent columns that block the incoming flux of atoms during column growth, 2) Lower resolution compared to HPTLC separations, and 3) Lower specific surface area, leading to weak solute retention and fronting. Further optimization of the plate was shown in 2010 when Brett et *al.*[64] used GLAD to fabricate a 4.6 – 5.3 µm normal phase silica UTLC stationary phases with several types of in-plane macropore anisotropies. Channel-like structures were shown to affect separation behaviors on anisotropic media. A customized chromatogram extraction technique and dye separations were used to quantify the GLAD stationary phase performance. Theoretical plate numbers and plate heights of a separated yellow dye showed the potential of the anisotropic stationary phases and provided an impetus for their future exploration.

1.7.4. Electrospun polymers

The Olesik group at Ohio State has worked on films of electrospun fibers as stationary phases for thin layer chromatography.[65-70] In the electrospinning technique, a high voltage is applied to a liquid droplet. The resulting charging of the droplet results in repulsions inside the liquid that lead to its deformation. Beyond some critical point, the droplet erupts as a continuous stream of fibers that are collected at a grounded collector. The mats of fibers produced in this way

have been used for TLC. This technique has the advantage of only requiring moderately complex equipment.

1.8. Improving chromatography characteristics via microfabrication

Microfabrication is widely utilized in the semiconductor industries for making MOSFETS, CMOS devices, etc.[71-91] Microfabrication has also been used to produce TLC plates. (see Figure 1.3) An approach taken in the Linford group at Brigham Young University utilizes a framework of patterned carbon nanotubes.[92-97] Microfabrication allows for the precise placement of channels and an adsorbent bed on a substrate. This decreases the anisotropy in the plate, while simultaneously improving separation efficiencies and reducing analysis times.

1.8.1. General terminologies used

(1) $$R_F = \frac{Z_s}{Z_{sol}}$$

In this basic equation, Z_s is the analyte migration distance from the point of its application on the plate, and Z_{sol} is the solvent front migration distance also as measured from the point of analyte application (see Figure 1.4).[98] Efficiencies or numbers of theoretical plates were calculated from the following fundamental equation in chromatography:

(2) $$N = 16\left(\frac{Z_s}{W}\right)^2$$

where W is the width of the analyte band. Observed plate heights and variances were calculated using an equation described by Poole *et al*.[98]

(3) $$H_{obs} = \frac{\sigma^2_{chrom}}{R_F(Z_f - Z_o)}$$

Where, Z_o represents the distance between the solvent entry position and the position of the applied sample spot, and Z_f represents the distance the solvent has traveled from its entry position. That is, $Z_{sol} = Z_f - Z_o$ and Equation 3 reduces to:

(4) $$H_{obs} = \frac{\sigma^2_{chrom}}{R_F Z_{sol}}$$

However, for R_F as defined above, Equation 4 becomes:

(5) $$H_{obs} = \frac{\sigma^2_{chrom}}{Z_s}$$

In other words, H_{obs} is the quotient of the corrected variance, σ^2_{chrom}, as defined below, of the band and its migration distance.

From Poole,[98] the variance in the band, σ^2_{chrom}, was taken as:

(4) $$\sigma^2_{chrom} = \sigma^2_{obs} - \sigma^2_{SA} - \sigma^2_{den}$$

where σ^2_{obs} is the variance of the separated (developed) analyte band, σ^2_{SA} is the variance of the band at its point of application, and σ^2_{den} is the variance of the densitometer (scanning, surface ultraviolet-visible spectrometer) used. Here, $\sigma^2_{den} = 0$ (no densitometer was used).

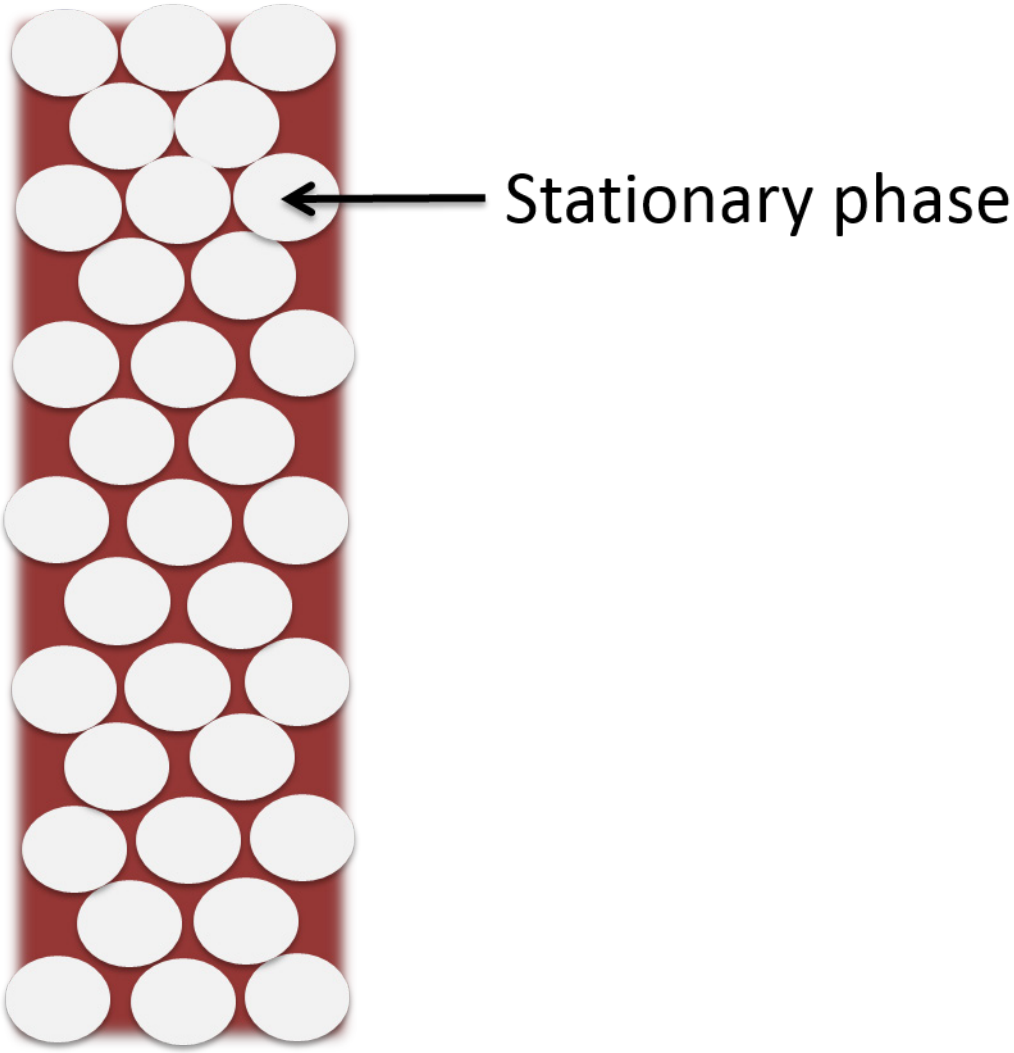

Figure 1.2. An idealized, top view of a particle based TLC plate. In many plates, the particles are not spherical and the particle size distribution is broad.

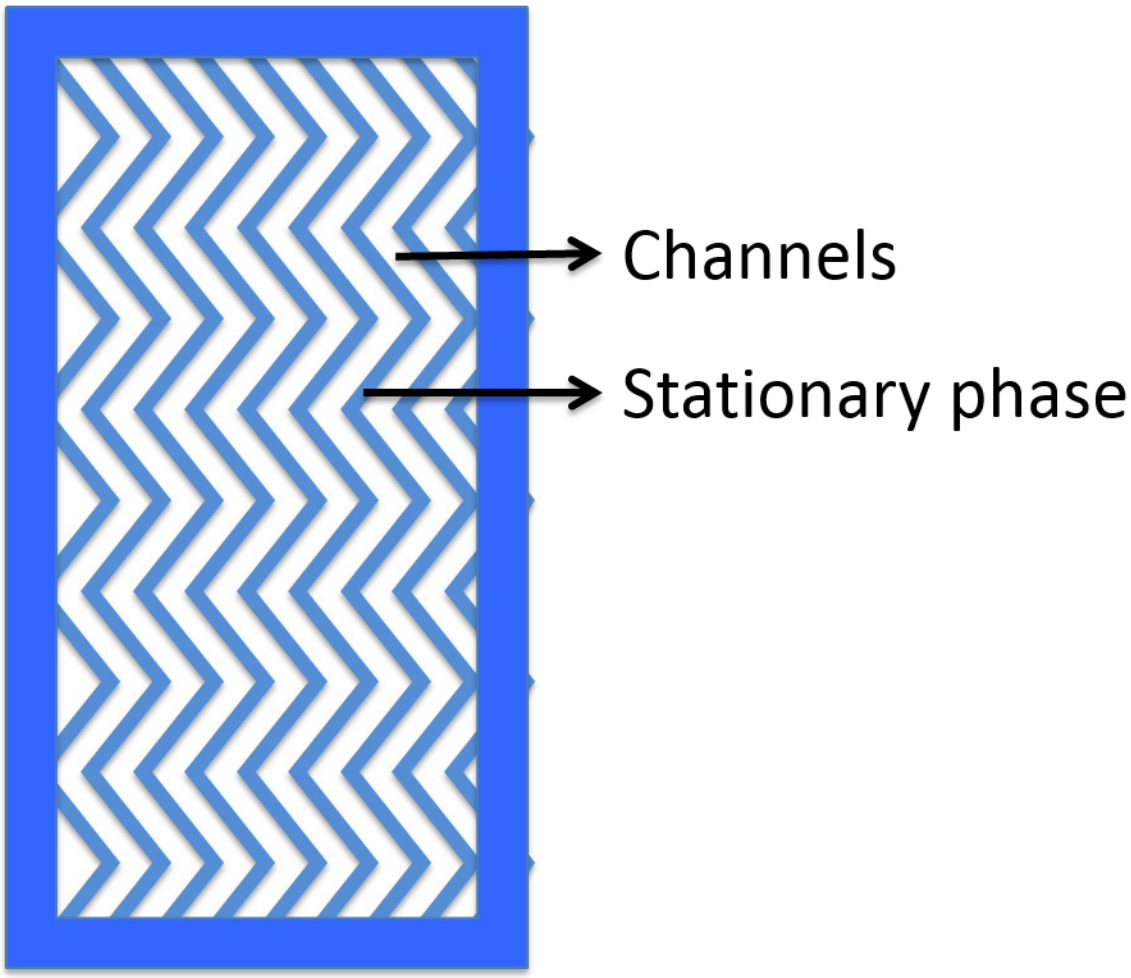

Figure 1.3. The geometry of the microfabricated TLC plates developed by the Linford group at BYU showing open regions (channels) and hedges (the stationary phase).[92, 93, 95, 96]

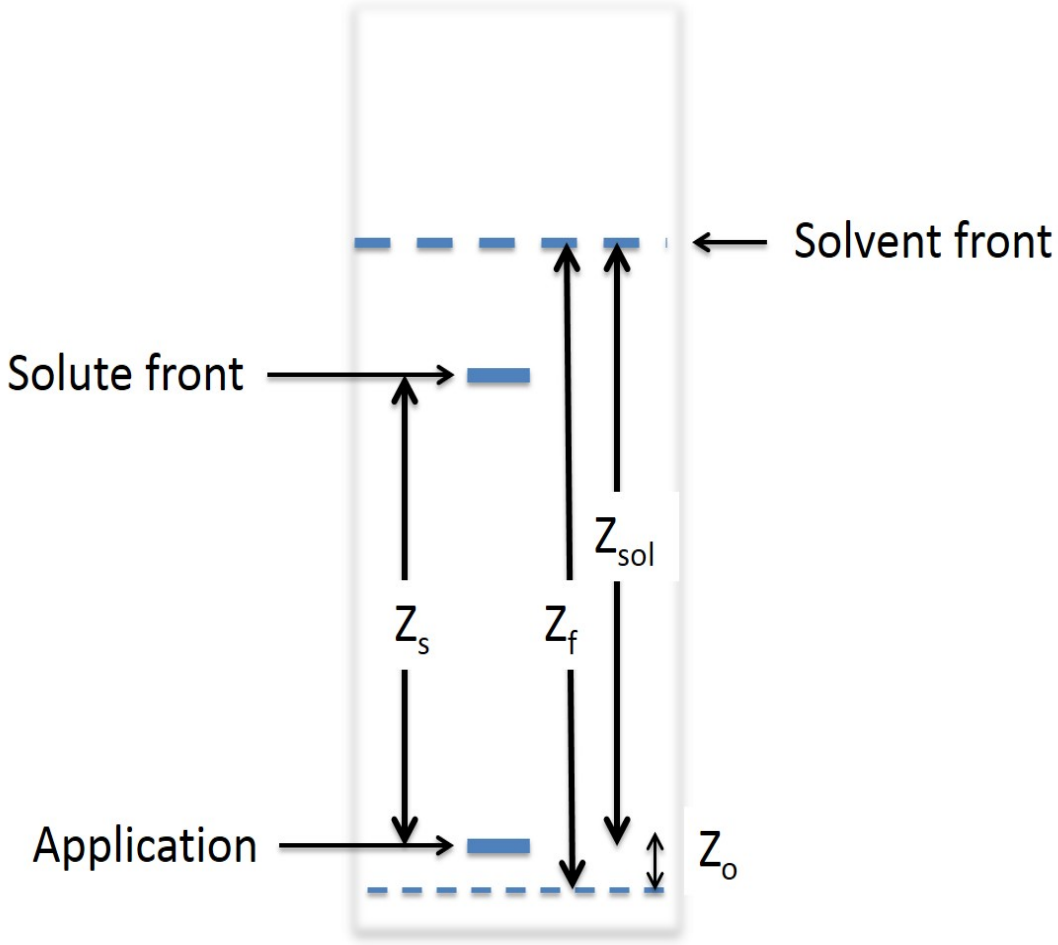

Figure 1.4. Various terms used in TLC.

1.9. Materials investigated in the microfabrication of TLC plates

1.9.1. Low-pressure chemical vapor deposition (LPCVD) of Silica

LPCVD of amorphous silicon (not silica) was the first inorganic material used to coat patterned Carbon nanotubes (CNT) scaffolds.[96] When this silicon was oxidized at elevated temperature to silica, a volume expansion of the silicon occurred. The distortions in the resulting chromatographic features (see Figure 1.5 limited the performance of these devices.

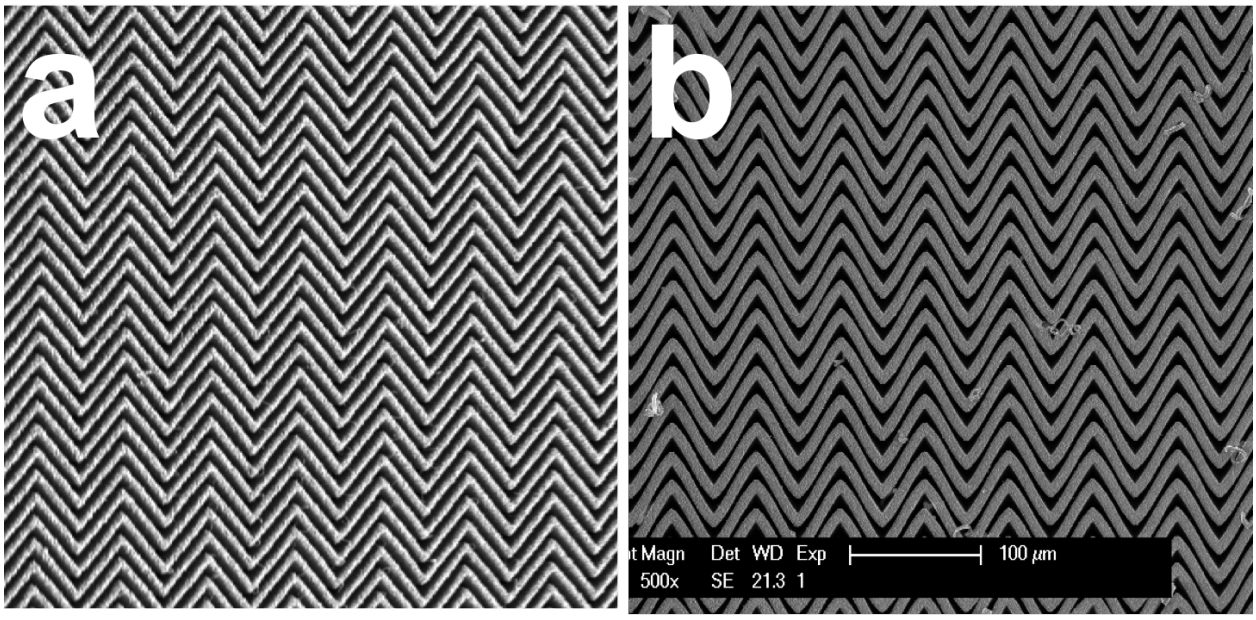

Figure 1.5. Features of LPCVD-silicon coated microfabricated plates via SEM (a) before, and, (b) after oxidation at 1000 °C.

1.9.2. Pseudo ALD or poor man ALD using amorphous carbon

In an attempt to reduce or eliminate feature distortion, a fast (pseudo) atomic layer deposition (ALD) of silica was explored.[99] This process utilized trimethyl aluminum (TMA) and tris(tert-butoxy) silanol as precursors, which were deposited in an ABAB type fashion. Prior to this deposition, the CNTs were treated with amorphous carbon or ozone to improve the adhesion of the silica film. Due to the presence of aluminum in the films, tailing was significant in the chromatography in a normal phase separation. Nevertheless, the plates could be treated with 3-aminopropyltriethoxysilane (APTES) to obtain an amino-bonded phase that yielded high efficiency separations.[92, 93]

1.9.3. True SiO_2 film and silicon nitride films

A true SiO_2 film, which was free of aluminum, was deposited via true atomic layer deposition. For the first time, a high efficiency, normal phase separation of a standard test mixture of dyes from CAMAG could be performed on an all-silica plate. Efficiencies of 40,000 – 140,000 plates/m were obtained. This work, along with even more recent work using LPCVD silicon nitride, is described in detail in this thesis.[97]

1.10. References

1. M. Schraiber and N. Izmailov, **3** (1.7) (1938).
2. M. Schreiber, *75 Years of Chromatography-an Historical Dialogue*. (Elsevier Scientific Publishing Company, New York, 1979).
3. R. Consden, A. H. Gordon and A. J. P. Martin, Bichem J. **38**, 224 (1944).
4. J. G. Kirchner, M. J. Miller and G. J. Keller, Anal Chem **23**, 420-425 (1951).
5. J. G. Kirchner, J. M. Miller and G. J. Keller, Anal Chem **23** (3), 420-425 (1951).
6. R. G. Rice, G. J. Keller and J. G. Kirchner, Anal Chem **23** (1), 194-195 (1951).
7. J. G. Kirchner, Chemtech **4** (2), 79-82 (1974).
8. J. G. Kirchner, J Chromatogr Sci **11** (4), 180-183 (1973).
9. J. G. Kirchner, J Chromatogr **82** (1), 101-115 (1973).
10. E. Stahl, Fresen Z Anal Chem **181**, 303-312 (1961).
11. E. Stahl, Z Anal Chem Freseniu **234** (1), 1-& (1968).
12. E. Stahl and J. Muller, J Chromatogr **189** (3), 293-297 (1980).
13. E. Stahl and W. Schild, Arznei-Forschung **19** (3), 314-& (1969).
14. E. Stahl and H. Jork, Z Anal Chem Freseniu **234** (1), 12-& (1968).
15. E. Stahl, Arch Pharm **306** (9), 693-696 (1973).
16. E. Stahl, Qual Plant Mater Veg **16** (1-4), 35-& (1968).
17. E. Stahl and E. Dumont, J Chromatogr Sci **7** (9), 517-& (1969).
18. E. Stahl, Angewandte Chemie-International Edition **3** (12), 784-& (1964).
19. E. Stahl and H. Bolliger, *Dünnschicht-chromatographie: Ein Laboratoriumshandbuch*. (Springer, Berlin, 1962).
20. E. Stahl, Cc/Phys Chem Earth (52), 10-10 (1979).

21. E. Stahl, Arznei-Forschung **19** (11), 1892-& (1969).

22. E. Stahl, Z Anal Chem Freseniu **236** (Apr), 294-& (1968).

23. E. Stahl, J Chromatogr **165** (1), 59-73 (1979).

24. N. Grinberg, *Stationary Phase in Thin-Layer Chromatograpy in Modern Thin-Layer Chromatography*. (Marcel Dekker, New York, 1990).

25. B. Klama and T. Kowalska, Jpc-J Planar Chromat **9** (1), 25-30 (1996).

26. M. Filip, V. Coman, R. Grecu, K. Albert and Z. Moldovan, Jpc-J Planar Chromat **17** (6), 424-430 (2004).

27. M. WaksmundzkaHajnos, Chromatographia **43** (11-12), 640-646 (1996).

28. O. Hadjadj-Aoul, R. Belabbes, S. Charchari, I. Belkadi, Y. Combret and J. C. Combret, Chromatographia **50** (11-12), 728-732 (1999).

29. H. C. Chiang and S. L. Lin, J Chromatogr **44** (1), 203-& (1969).

30. H. C. Chiang and R. G. Tseng, J Pharm Sci **58** (12), 1552-& (1969).

31. H. C. Chiang and T. M. Chiang, J Chromatogr **47** (1), 128-& (1970).

32. N. G. Camara and M. Lederer, J Pharmaceut Biomed **10** (5), 371-373 (1992).

33. T. K. X. Huynh, A. O. Kuhn and M. Lederer, J Chromatogr **626** (2), 301-304 (1992).

34. M. Lederer, J Chromatogr **604** (1), 55-62 (1992).

35. H. T. K. Xuan and M. Lederer, J Chromatogr **645** (1), 185-188 (1993).

36. H. T. K. Xuan and M. Lederer, J Chromatogr **635** (2), 346-348 (1993).

37. H. Szumilo and J. Flieger, Jpc-J Planar Chromat **9** (6), 462-466 (1996).

38. C. F. Poole, *The Essence of Chromatography*. (Elsevier science B. V., Amsterdam, 2003).

39. B. Fried and J. Sherma, (CRC Press, FL, 1996).

40. I. Ojanpera, K. Goebel and E. Vuori, Journal of Liquid Chromatography & Related Technologies **22** (161) (1999).

41. B. Renger, J Aoac Int **84** (4), 1217-1217 (2001).

42. M. E. Fallat, S. J. Rengers, B. L. Bachulis and B. A. Pruitt, J Trauma **34** (4), 560-564 (1993).

43. L. Gagliardi, D. De Orsi, M. R. Del Giudice, F. Gatta, R. Porra, P. Chimenti and D. Tonelli, Anal Chim Acta **457** (2), 187-198 (2002).

44. J. M. Poul and J. P. Abjean, Recl Med Vet **169** (1), 47-52 (1993).

45. J. M. Poul, V. Verlinde, J. P. Abjean and M. Laurentie, J Appl Toxicol **13** (2), 117-122 (1993).

46. S. Zellmer, J. Lasch and U. Rothe, J Lipid Res **38** (11), 2374-2379 (1997).

47. K. Ferenczi-Fodor, Z. Vegh, A. Nagy-Turak, B. Renger and M. Zeller, J Aoac Int **84** (4), 1265-1276 (2001).

48. G. Szepesi and S. Nyiredy, J Pharmaceut Biomed **10** (10-12), 1007-1015 (1992).

49. N. Galand, J. Pothier and C. Viel, J Chromatogr Sci **40** (10), 585-597 (2002).

50. H. E. Hauck and M. Schulz, Journal of Chromatographic Science **40** (10), 550-552 (2002).

51. H. E. Hauck, O. Bund, W. Fischer and M. Schulz, Jpc-J Planar Chromat **14** (4), 234-236 (2001).

52. *A. P. Boichenko*, The Open Surface Science Journal **1**, 40-45 (2009).

53. R. Bakry, G. K. Bonn, D. Mair and F. Svec, Anal Chem **79** (2), 486-493 (2007).

54. B. Dick, M. J. Brett and T. Smy, J Vac Sci Technol B **21** (1), 23-28 (2003).

55. F. Liu, M. T. Umlor, L. Shen, J. Weston, W. Eads, J. A. Barnard and G. J. Mankey, J Appl Phys **85** (8), 5486-5488 (1999).

56. K. Robbie, A. J. P. Hnatiw, M. J. Brett, R. I. MacDonald and J. N. McMullin, Electron Lett **33** (14), 1213-1214 (1997).

57. K. Robbie, J. C. Sit and M. J. Brett, J Vac Sci Technol B **16** (3), 1115-1122 (1998).

58. J. C. Sit, D. Vick, K. Robbie and M. J. Brett, J Mater Res **14** (4), 1197-1199 (1999).

59. D. X. Ye, Y. P. Zhao, G. R. Yang, Y. G. Zhao, G. C. Wang and T. M. Lu, Nanotechnology **13** (5), 615-618 (2002).

60. Y. P. Zhao, D. X. Ye, G. C. Wang and T. M. Lu, Nano Lett **2** (4), 351-354 (2002).

61. L. W. Bezuidenhout and M. J. Brett, J. Chromatogr., A **1183** (1-2), 179-185 (2008).

62. L. W. Bezuidenhout, N. Nazemifard, A. B. Jemere, D. J. Harrison and M. J. Brett, Lab Chip **11** (9), 1671-1678 (2011).

63. A. B. Jemere, L. W. Bezuidenhout, M. J. Brett and D. J. Harrison, Rapid Commun Mass Sp **24** (15), 2305-2311 (2010).

64. S. R. Jim, M. T. Taschuk, G. E. Morlock, L. W. Bezuidenhout, W. Schwack and M. J. Brett, Anal Chem **82** (12), 5349-5356 (2010).

65. T. Lu and S. V. Olesik, J Chromatogr B **912**, 98-104 (2013).

66. P. Kampalanonwat, P. Supaphol and G. E. Morlock, J Chromatogr A **1299**, 110-117 (2013).

67. J. E. Clark and S. V. Olesik, J Chromatogr A **1217** (27), 4655-4662 (2010).

68. T. Rojanarata, S. Plianwong, K. Su-uta, P. Opanasopit and T. Ngawhirunpat, Talanta **115**, 208-213 (2013).

69. X. Fang and S. V. Olesik, Anal Chim Acta **830**, 1-10 (2014).

70. M. C. Beilke, J. W. Zewe, J. E. Clark and S. V. Olesik, Anal Chim Acta **761**, 201-208 (2013).

71. H. E. Tu and Y. Xu, Applied Physics Letters **101** (5) (2012).

72. R. A. Minamisawa, M. Schmidt, L. Knoll, D. Buca, Q. T. Zhao, J. M. Hartmann, K. K. Bourdelle and S. Mantl, Ieee Electr Device L **33** (8), 1105-1107 (2012).

73. H. Takamizawa, Y. Shimizu, K. Inoue, T. Toyama, F. Yano, A. Nishida, T. Mogami, N. Okada, M. Kato, H. Uchida, K. Kitamoto, T. Miyagi, J. Kato and Y. Nagai, Applied Physics Letters **100** (25) (2012).

74. N. V. Nguyen, M. Xu, O. A. Kirillov, P. D. Ye, C. Wang, K. Cheung and J. S. Suehle, Applied Physics Letters **96** (5) (2010).

75. P. Michetti and G. Iannaccone, Ieee T Electron Dev **57** (7), 1616-1625 (2010).

76. L. Pei, A. Balls, C. Tippets, J. Abbott, M. R. Linford, J. A. Hu, A. Madan, D. D. Allred, R. R. Vanfleet and R. C. Davis, J Vac Sci Technol A **29** (2) (2011).

77. J. Y. Kwon, D. H. Lee, M. Chitambar, S. Maldonado, A. Tuteja and A. Boukai, Nano Letters **12** (10), 5143-5147 (2012).

78. S. S. Shah, J. Y. Lee, S. Verkhoturov, N. Tuleuova, E. A. Schweikert, E. Ramanculov and A. Revzin, Langmuir **24** (13), 6837-6844 (2008).

79. R. Rehammar, F. A. Ghavanini, R. Magnusson, J. M. Kinaret, P. Enoksson, H. Arwin and E. E. B. Campbell, Nano Letters **13** (2), 397-401 (2013).

80. M. Lee, Y. Jeon, T. Moon and S. Kim, ACS Nano **5** (4), 2629-2636 (2011).

81. C. Kopp, S. Bernabe, B. Ben Bakir, J. M. Fedeli, R. Orobtchouk, F. Schrank, H. Porte, L. Zimmermann and T. Tekin, Ieee J Sel Top Quant **17** (3), 498-509 (2011).

82. N. G. Wang, E. J. O'Sullivan, P. Herget, B. Rajendran, L. E. Krupp, L. T. Romankiw, B. C. Webb, R. Fontana, E. A. Duch, E. A. Joseph, S. L. Brown, X. L. Hu, G. M. Decad, N. Sturcken, K. L. Shepard and W. J. Gallagher, Journal of Applied Physics **111** (7) (2012).

83. M. J. R. Heck, H. W. Chen, A. W. Fang, B. R. Koch, D. Liang, H. Park, M. N. Sysak and J. E. Bowers, Ieee J Sel Top Quant **17** (2), 333-346 (2011).

84. H. Boubekeur, T. Mikolajick, J. Hopfner, C. Dehm, W. Pamler, J. Steiner, G. Kilian, B. O. Kolbesen, A. Bauer, L. Frey and H. Ryssel, Sol St Phen **76-77**, 9-14 (2001).

85. H. Ishikawa, Ifip Trans A **12**, 674-682 (1992).

86. P. M. Osterberg and S. D. Senturia, J Microelectromech S **6** (2), 107-118 (1997).

87. A. Luque, J. M. Quero, C. Hibert, P. Fluckiger and A. M. Ganan-Calvo, Sensor Actuat a-Phys **118** (1), 144-151 (2005).

88. K. Tsugawa, K. Kitatani, H. Noda, A. Hokazono, K. Hirose, M. Tajima and H. Kawarada, Diam Relat Mater **8** (2-5), 927-933 (1999).

89. J. Matovic, N. Adamovic, F. Radovanovic, Z. Jaksic and U. Schmid, Sensor Actuat B-Chem **170**, 137-142 (2012).

90. K. J. Lee, K. A. Tosser and R. G. Nuzzo, Adv Funct Mater **15** (4), 557-566 (2005).

91. J. Qing, K. N. Leung, T. J. King, X. M. Jiang and B. R. Appleton, Nucl Instrum Meth B **241** (1-4), 335-340 (2005).

92. D. S. Jensen, S. S. Kanyal, V. Gupta, M. A. Vail, A. E. Dadson, M. Engelhard, R. Vanfleet, R. C. Davis and M. R. Linford, Journal of Chromatography A **1257**, 195-203 (2012).

93. D. S. Jensen, S. S. Kanyal, N. Madaan, A. J. Miles, R. C. Davis, R. Vanfleet, M. A. Vail, A. E. Dadson and M. R. Linford, J Vac Sci Technol B **31** (3), 031203 (2013).

94. D. S. Jensen, S. S. Kanyal, N. Madaan, J. M. Hancock, A. E. Dadson, M. A. Vail, R. Vanfleet, V. Shutthanandan, Z. H. Zhu, M. H. Engelhard and M. R. Linford, Surf. Interface Anal. **45** (8), 1273-1282 (2013).

95. S. S. Kanyal, D. S. Jensen, A. J. Miles, A. E. Dadson, M. A. Vail, R. E. Olsen, S. Fabien, J. Nichols, R. Vanfleet, R. Davis and M. R. Linford, J. Vac. Sci Technol. B **31** (3), 031203 (2013).

96. J. Song, D. S. Jensen, D. N. Hutchison, B. Turner, T. Wood, A. Dadson, M. A. Vail, M. R. Linford, R. R. Vanfleet and R. C. Davis, Adv Funct Mater **21** (6), 1132-1139 (2011).

97. S. S. Kanyal, D. S. Jensen, A. E. Dadson, R. R. Vanfleet, R. C. Davis and M. R. Linford, J. Plan. Chrom. **27** (3), 151-156 (2014).

98. S. K. Poole and C. F. Poole, J Chromatogr A **1218** (19), 2648-2660 (2011).

99. D. Hausmann, J. Becker, S. L. Wang and R. G. Gordon, Science **298** (5592), 402-406 (2002).

2. Chapter: Effects of catalyst Thickness on the Fabrication and Peformance of Carbon Nanotube Thin Layer Chromatography Plates

2.1. Abstract

The effects of iron catalyst thickness on the fabrication and performance of microfabricated, binder-free, carbon nanotube (CNT) – templated, thin layer chromatography (TLC) plates are demonstrated. The iron catalyst was deposited at thicknesses ranging from 4 – 18 nm in increments of 2 nm. Its thickness plays a key role in governing the integrity and separation capabilities of microfabricated TLC plates, as determined using a test dye mixture. Atomic force microscopy (AFM) and scanning electron microscopy (SEM) show that smaller and more numerous catalyst nanoparticles are formed from thinner Fe layers, which in turn govern the diameters and densities of the CNTs. The average diameter of the Fe nanoparticles, D_p, is approximately six times the initial Fe film thickness, t_{Fe}: $D_p \approx 6\ t_{Fe}$. After deposition of relatively thick silicon layers on CNTs made with different Fe thicknesses, followed by oxidation, all of the resulting CNT-templated SiO_2 wires had nearly the same diameter. Consequently, their surface areas were very similar, although their areal densities on the TLC plates were not because thinner catalyst layers produce denser CNT forests. For t_{Fe} = 6 nm, nanotube growth appears to be base growth, not tip growth. Best TLC separations of a test dye mixture were obtained with plates prepared with 6 or 4 nm of catalyst. Calculations suggest a loss of surface area for TLC plates made with thicker Fe layers as a result of fewer, thicker CNTs, where the density of silica nanotubes (device surface area) goes approximately as $1/t_{Fe}^2$. While the focus of this paper is towards a greater understanding of the processing conditions that lead to the best TLC plates, a

baseline separation of three analgesics (caffeine, phenacetine, and propylphenazone) is shown on a normal phase TLC plate grown with 6 nm of iron.

2.2. Introduction

A recent trend in modern liquid chromatography is the exploration of new materials and processing methods for the production of thin layer chromatography (TLC) plates. Monolithic silica (10 μm), ultra-thin-layer chromatography (UTLC) plates[1] were introduced in 2001 by Schulz et al. and sold by Merck. Compared with TLC and HPTLC plates, Ultra-Thin-Layer Chromatography (UTLC) plates showed clear improvements in detection limits, migration times, and solvent consumption. Problems with these new plates included higher R_f values, higher plate heights, and thus lower resolution. (The R_f value is the distance the analyte has moved divided by the distance the mobile phase has traveled from the point where the analyte mixture is spotted. The 'plate height' in chromatography is a measure of the efficiency of a separation; the lower the plate height the higher the efficiency.) Boichenko et al. have also recently used a sol-gel process to prepare monolithic thin films of silica for TLC, demonstrating high speeds and short-distance separations.[2] Frolova et al. investigated the factors affecting the various sorption and stability characteristics of silica monoliths for TLC.[3] Svek et al. have developed monolithic porous polymer layers of poly(butylmethacrylate-*co*-ethylene dimethacrylate) to separate peptides and proteins.[4] Urbanova et al. prepared thin monolithic hydrophobic gradients for thin layer chromatography for separating peptides in 2-D.[5] Benzuidenhout et al. prepared UTLC plates using glancing angle deposition (GLAD).[1, 6] Different feature shapes such as helices, vertical posts, and zig-zags could be grown. Another type of UTLC plate was recently prepared by Olesik et al. in 2009 through

electrospinning of nanofibers.[7] Their materials showed enhanced efficiencies in chromatographic separations, good analysis times and low solvent consumption. They also reported UTLC devices made from carbon nanofibers.[8]

Since their discovery in 1991, carbon nanotubes (CNTs) have shown potential in various fields, including electronics, the medicinal and biological sciences, and in analytical chemistry.[9-17] Along these lines, we have recently microfabricated TLC plates from patterned, carbon nanotube (CNT) forest templates, where in our first effort,[18] vertically aligned CNT forests[19, 20] were conformally infiltrated with silicon and then oxidized to make SiO_2 (see Figure 1.5). This oxidation also removed the CNT forest template, yielding a white material. Some reasonable, rapid separations were demonstrated with these materials: efficiencies of ca. 75,000 theoretical plates per meter (N/m). Nevertheless, the oxidation of Si to SiO_2 caused a volume expansion that sometimes led to substantial distortion of the features. To improve upon this first process, CNT forests were primed with carbon and Al_2O_3 so that they could be directly coated via a pseudo atomic layer deposition (ψ-ALD) of SiO_2,[21] i.e., a material that would not require subsequent oxidation.[22] The resulting materials were coated with an amino silane, [23] which led to some high efficiency separations (H_{obs} of ca. 1.6 – 7.7 μm, ca. 100,000 – 270,000 N/m). As a third effort,[24] the microfabrication procedure was simplified through the replacement of the carbon and Al_2O_3 priming layers with an ozone treatment. The resulting plates showed the highest efficiencies we have seen to date (H_{obs} of -0.6 – 15.2 μm, ca. 58,000 – 1,865,000 N/M). We have also performed a multi-technique characterization of the key materials used to make these different plates.[25]

These previous studies have raised the need for a careful exploration of the deposition/fabrication parameters that govern TLC plate microfabrication. Accordingly, we focus

herein on the iron catalyst film that is essential for CNT growth, varying its thickness, t_{Fe}, from 4 to 18 nm in 2 nm increments. Field-emission scanning electron microscopy (FEG-SEM), and atomic force microscopy (AFM) are used to characterize the catalyst nanoparticles formed during annealing of the Fe films in H_2. We demonstrate that the width and areal densities of the CNTs depend strongly on the initial catalyst thickness, and that thicker nanotubes yield poor quality TLC plates. Surface area measurements and calculations indicate that the lower quality of these plates is due to a lower areal density of CNT-templated SiO_2 nanowires. For the study reported herein we use our simplest deposition scheme, which is the direct, conformal coating of CNTs with Si, followed by its oxidation.[18] Surface hydroxylation is then performed with ammonium hydroxide at pH 10.0,[26] and the chromatographic performance of these plates is evaluated.

Of course, the properties of CNTs are known to depend on processing parameters such as gas composition, annealing and catalyst thickness,[27-31] e.g., Davis and coworkers studied the effects of iron catalyst thickness on sidewall straightness in vertically aligned carbon nanotube forests in microelectromechanical systems (MEMS).[32] However, none of these studies has been applied to the microfabrication of TLC plates from CNT frameworks.

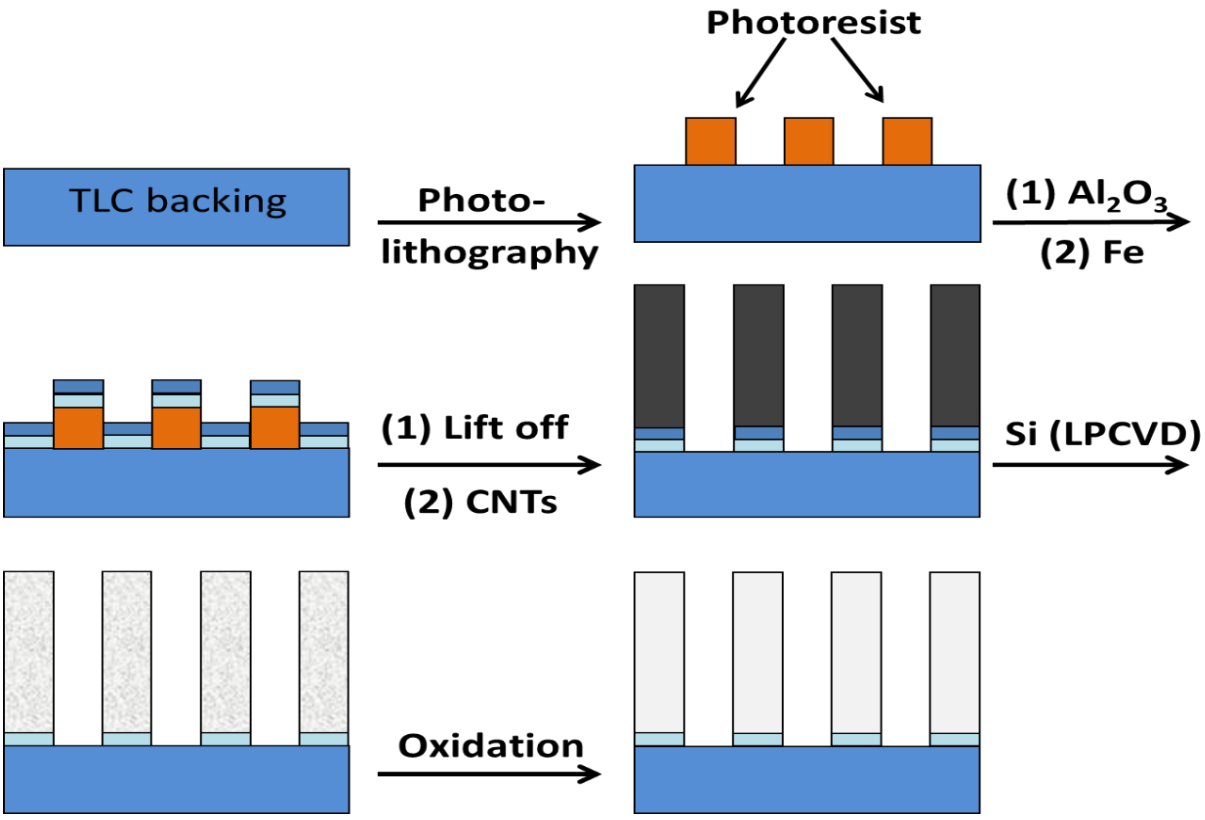

Figure 2.1. Microfabrication scheme for TLC plates. Surfaces are photolithographically patterned. Al_2O_3 and Fe are deposited sequentially. The devices then undergo lift-off of the photoresist, leaving a pattern of Fe on Al_2O_3, which is followed by CNT growth, infiltration of Si by low-pressure chemical vapor deposition (LPCVD) of SiH_4, and oxidation to remove the CNT framework and convert Si to SiO_2.

2.3. Experimental

2.3.1. Fabrication process

In general, TLC plates were prepared as described previously (See figure 2.1).[18] Briefly, we photolithographically patterned silicon wafers with photoresist and then deposited thin films of alumina (35 nm) and iron (6 nm). This was followed by lift off of the photoresist. CNTs were then grown at 750 °C in the presence of C_2H_4 gas and H_2. CNTs were infiltrated with amorphous silicon, and the CNTs were removed at high temperatures (1000 °C) in an oxidizing environment leaving silica nanotubes.

2.3.2. Hydroxylation

Because of the high temperature growth and oxidation conditions, silica surfaces can be assumed to have very low surface silanol concentrations.[33-36] Therefore, all samples were hydrated in NH_4OH at pH 10.0 at room temperature for 18 h.[26]

2.3.3. Surface/Materials Characterization

Scanning electron microscopy (SEM) was performed with a Helios NanoLab™ 600 instrument, (FEI, Hillsboro, OR), atomic force microscopy (AFM) with a Digital Instruments (Tonawanda, NY) Dimension 3100 instrument in tapping mode, and transmission electron microscopy (TEM) with a Tecnai F30 (FEI Company, Hilsboro, OR).

ImageJ software ('Image Processing and Analysis in Java' version 1.45 obtained from nih.gov) was used to estimate the diameters of the Fe nanoparticles, as follows:

$$Dp = 2\sqrt{A/\pi} \qquad (1)$$

Where A is the average area of the nanoparticles as determined by the software and D_p is the average particle diameter.

2.3.4. Materials

Commercial HPTLC and TLC plates were obtained from EMD Millipore, Darmstadt Germany (Silica Gel 60, F) and Analtech (silica gel GF, Newark, DE), respectively. Triethylamine 99.8%, was obtained from Sigma Aldrich (Saint Louis, MI). A mixture of analgesics was prepared by mixing caffeine (90 ng/μL), phenacetine (62.5 ng/μL), and propylphenazone (55 ng/μL) in ethanol.

2.3.5. Separation of a CAMAG Test Dye Mixture

A test dye solution containing five dyes: indophenol, ariabel red, Sudan blue II, Sudan IV, and dimethylaminoazobenzene was obtained from CAMAG (Muttenz, Switzerland) and diluted in hexanes to 3% of its original concentration. Plates were spotted with a microcapillary (CAMAG, Switzerland) 5 mm above the bottom edge of the plate, dried at 120 °C for one min, and developed in a twin trough chamber (CAMAG, Muttenz, Switzerland) that had been presaturated with the vapors of toluene for 10 min. After conditioning of the plate for 2 min in the developing chamber in the presence of the developing solvent, toluene (3 mL) was added at the bottom of the plate, and development took place over a distance of 25 mm from the point of analyte application.

2.3.6. Separations of Analgesics

The mixture of three analgesics (see above) was spotted onto microfabricated TLC plates with a sample volume of either 1.8 or 3.6 μL with a Linomat 5 (CAMAG, Muttenz, Switzerland). Bands were 3 mm wide, and positioned 5 mm above the bottom of the plate. After spotting, plates

were dried on a hotplate at 120 °C for two min. Development of these plates was as before (see previous paragraph) in a twin trough chamber, i.e., the chamber was presaturated with mobile phase vapors for 10 min, the plate was equilibrated with the mobile phase for 2 min, and the mobile phase (3 mL) was then added to the bottom of the plate. The development distance was 35 mm. Some method development was attempted; the separations were performed with different mobile phases (vide infra). Plate visualization was with a TLC Visualizer (CAMAG, Muttenz, Switzerland) and a TLC Scanner 4 (CAMAG, Muttenz, Switzerland) at 254 nm.

2.3.7. Surface Area Measurements and DRIFT

Silica was scraped off of 12 microfabricated TLC plates (previously used for chromatography but washed extensively with methanol and then water to remove the analytes) and then dried/dehydrated in an oven at 120 °C for 24 h. The surface area of the silica nanowires was then measured by BET (Tristar II, Micromeritics, GA, USA). The surface area measurement was also done for HPTLC (Merck) and Analtech TLC particles. Diffuse reflectance infrared Fourier transform spectroscopy (DRIFT) spectra (512 scans at 4 cm^{-1} resolution) were collected from undiluted adsorbant material of microfabricated TLC, HPTLC (Merck, NJ, USA) and TLC (Analtech, Newark, DE, USA) plates using a Nicolet 6700 FT-IR spectrometer (Thermo Scientific, Waltham, MA, USA).

2.4. Results and discussions

To understand the effects of Fe thickness on iron nanoparticle formation, CNT growth, and TLC performance, iron layers of different thicknesses (4 – 18 nm) were deposited onto ca. 30 nm Al_2O_3 films and then annealed in H_2. The film thicknesses were monitored via Atomic Force Microscopy (AFM). The alumina is necessary for preventing the formation of an iron silicide, which is inactive in nanotube growth and therefore represents a poisoning of the Fe catalyst.[37] After annealing, SEM of the iron surfaces shows the presence of nanoparticles (see Figure 2.2) that become steadily larger and coarser as the initial thickness of the Fe film increases. The Si/SiO_2 substrate, the Al_2O_3 barrier layer, the Fe layer before and after annealing, and also a CNT forest grown from Fe nanoparticles have been characterized by X-ray photoelectron spectroscopy (XPS), valence band spectroscopy, time-of-flight secondary ion mass spectrometry (ToF-SIMS), Rutherford Backscattering (RBS), and Helium Ion Microscopy (HIM) for a single (6 nm) layer of iron.[25] This characterization confirmed that the materials had been deposited correctly – the material compositions were as expected.

These data can be fit reasonably well, especially above t_{Fe} = 6 nm, to a straight line that passes through the origin, giving: $D_p = 6.1\ t_{Fe}$ ($D_p \approx 6\ t_{Fe}$). The particle diameters at t_{Fe} = 4 and 6 nm do not seem to follow this same trend, which is reflected in the fact that the data are better fit to a line with a non-zero intercept (see Figure 2.3). Of course, this suggests that more than one mechanism is most likely operative in nanoparticle formation and a straight line (with or without an intercept) is not fully adequate to describe the data over their full range. Indeed, the formation of nanoparticles from thin iron layers is known to be complex, where the resulting particles often exhibit a wide range of sizes and may even be bimodal.[38] Histograms of the nanoparticle diameters

for the different t_{Fe} values in this study (see Figure 2.10) reveal broad distributions that in some instances show bimodality. AFM images (see Figure 2.4) were also taken of each Fe nanoparticle surface. They confirm the increase in Fe nanoparticle size with increasing t_{Fe}.

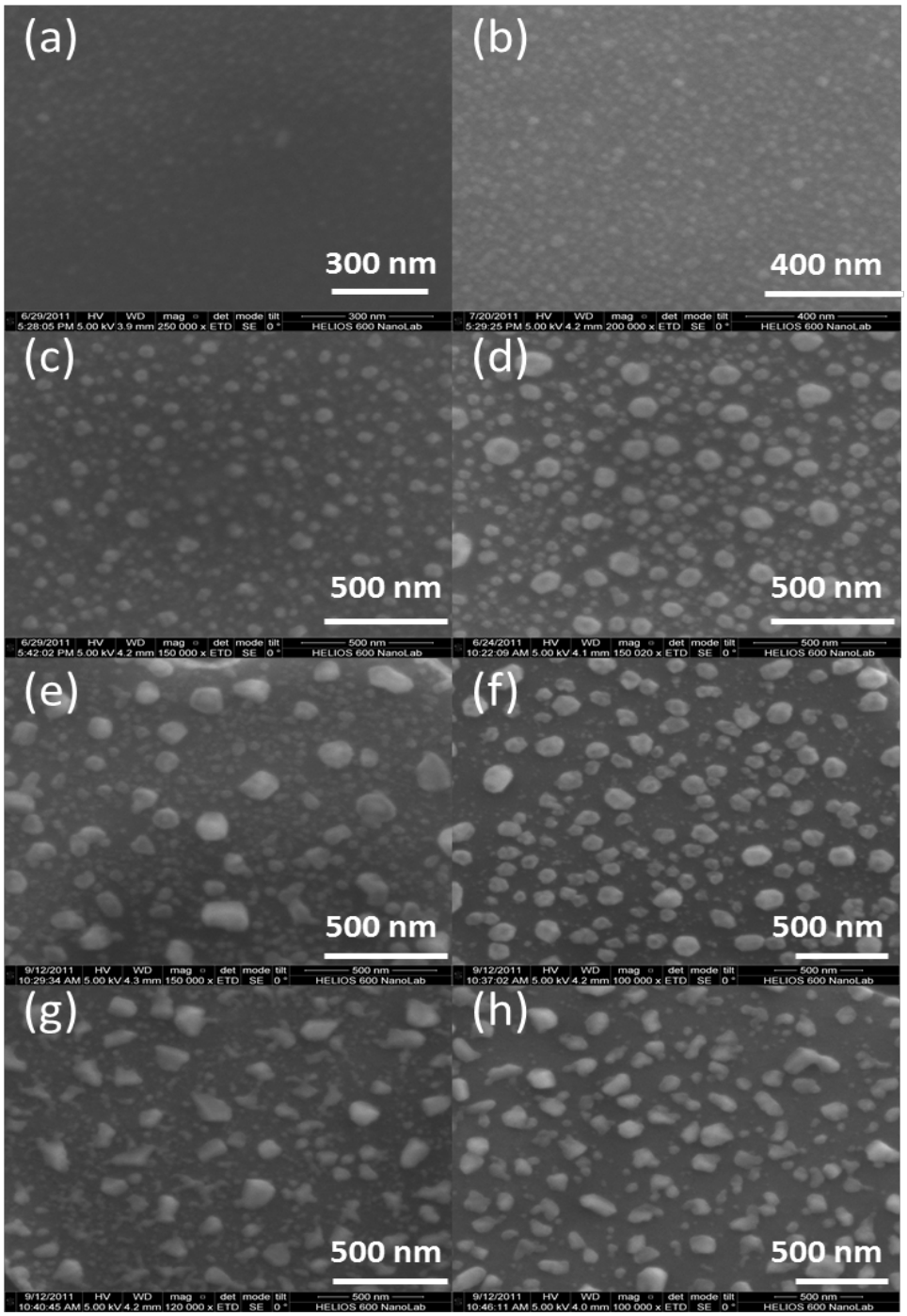

Figure 2.2. Representative SEM micrographs of annealed Fe surfaces with initial Fe thicknesses of (a) 4 nm, (b) 6 nm, (c) 8 nm, (d) 10 nm, (e) 12 nm, (f) 14 nm, (g) 16 nm, and (h) 18 nm.

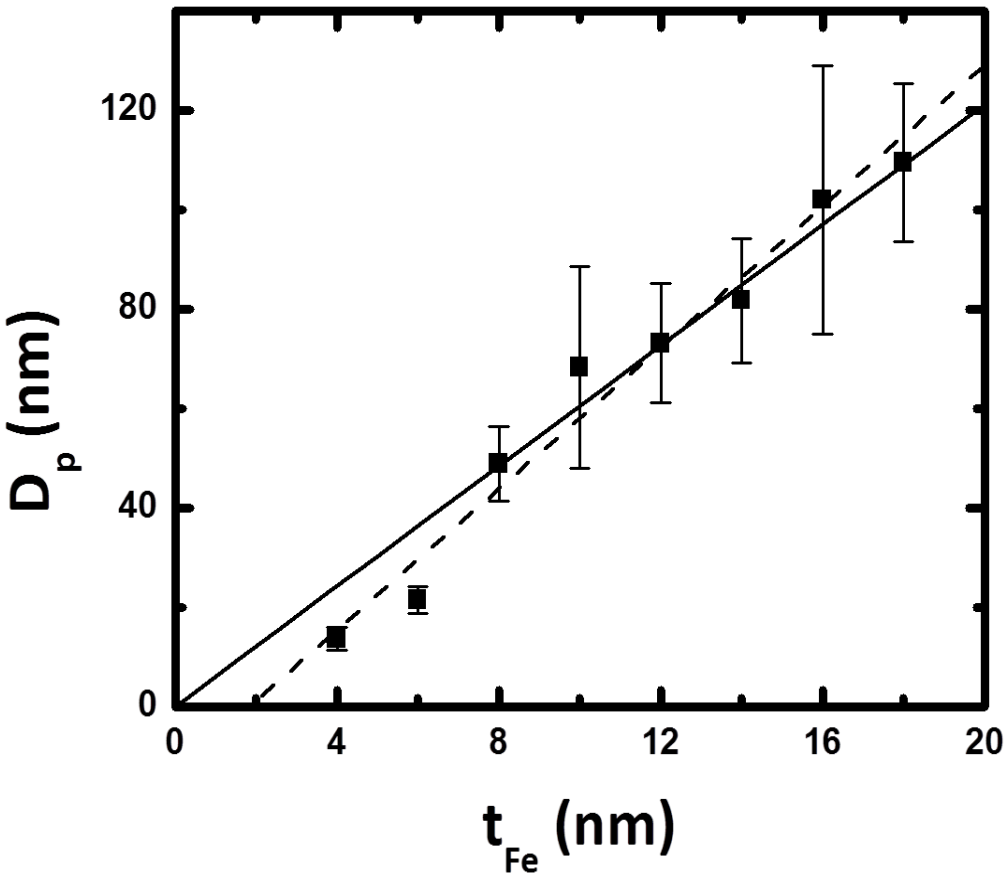

Figure 2.3. Diameter, D_p, of iron nanoparticles as a function of initial Fe film thickness, t_{Fe}. Data points (averages) and error bars (standard deviations) were obtained from three different surfaces annealed under the same conditions – examples of the data used are in Figure 2.2. The fits are: $D_p = 6.06\ t_{Fe}$ (solid line, $R^2 = 0.95$) and $D_p = 7.00\ t_{Fe} - 12.15$ (dashed line, $R^2 = 0.97$).

After studying the size of the Fe catalyst nanoparticles as a function of the initial t_{Fe}, CNTs were grown on patterned Fe nanoparticle films and the diameters of the individual CNTs in these arrays were measured by SEM (see Figure 2.5). In these arrays, it was immediately obvious that there was a lack of integrity in the CNT forests that had been prepared from the thicker (t_{Fe} > 10 nm) catalyst layers (see Figure 2.6). As was the case for the Fe nanoparticle diameters, there was an increase in CNT diameter, D_{CNT}, with increasing t_{Fe}, although the relationship between D_{CNT} and t_{Fe} was not as simple as for D_p vs. t_{Fe}. Here, the data could be well fit empirically to a pair of straight lines, one extending over t_{Fe} = 4 – 14 nm and the other from t_{Fe} = 14 – 18 nm. Previous studies have also shown that thicker catalyst layers lead to thicker, multiwalled CNTs.[27, 28, 32]

Carbon nanotubes grow by one of two different mechanisms in catalytic CVD,[39] and the interaction with the substrate determines which growth pattern is followed. If the catalyst-surface interactions are not too strong, CNT growth may take place with the nanoparticle attached to the top of the nanotube (tip growth). On the other hand, if the catalyst-surface interactions are strong, growth may take place from a particle that remains attached to the substrate (base growth). Transmission electron microscopy (TEM) has been extensively used to characterize CNTs,[40-43] and TEM images taken of the top of our CNT forests suggests that for t_{Fe} = 6 nm (this is the t_{Fe} at which we have grown most of our TLC plates[18, 22, 24]) our growth mechanism is base growth as the metal catalyst particles are not visible near the tips of the nanotubes (see Figure 2.7).

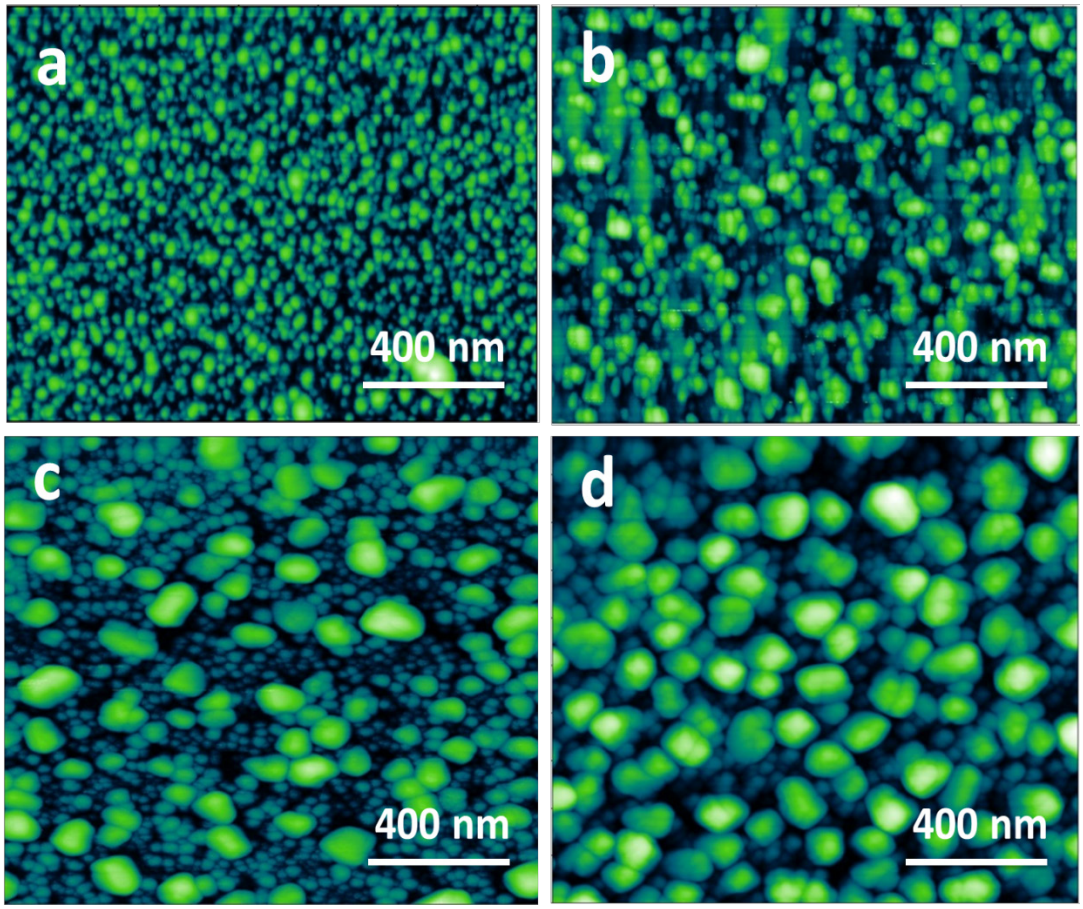

Figure 2.4. AFM images of annealed Fe surfaces that had initial Fe film thicknesses of (a) 4 nm, (b) 8 nm, (c) 12 nm, and (d) 16 nm.

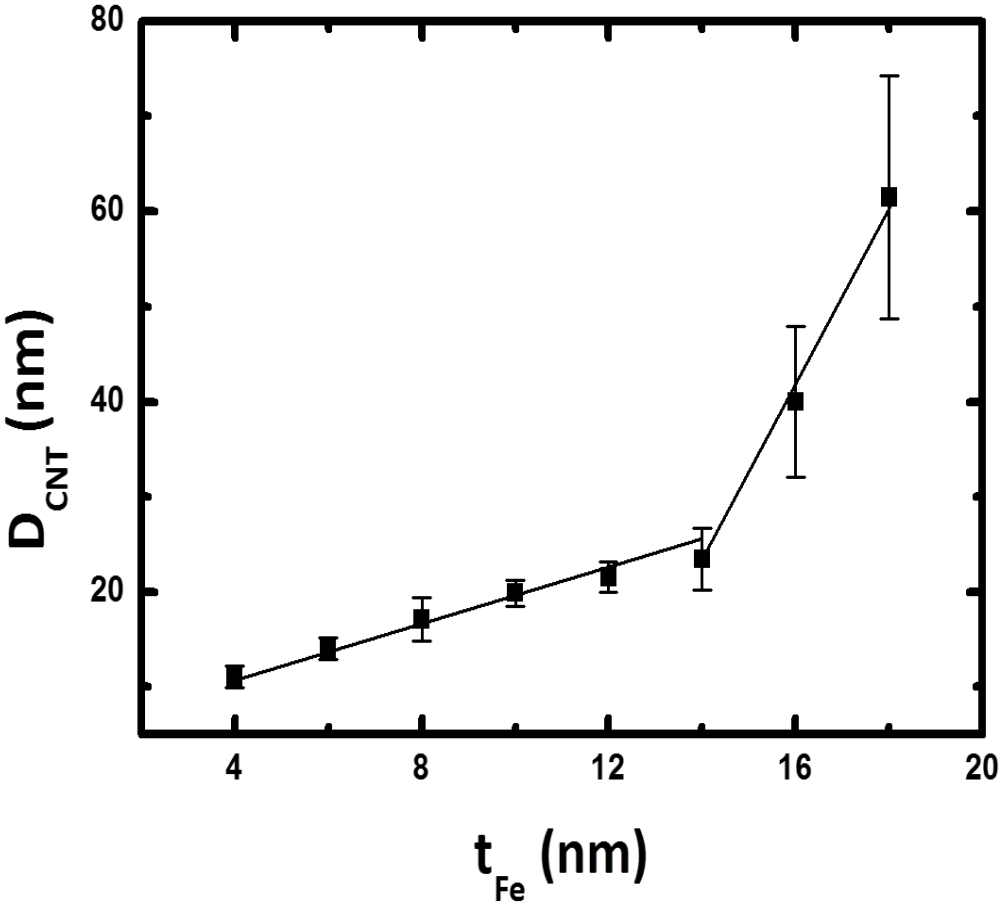

Figure 2.5. Average diameters of CNTs, D_{CNT}, as measured by SEM, as a function of the initial Fe layer thickness, t_{Fe}. Twenty measurements were taken from each of three different images from two different samples. Data points are the averages and error bars are the standard deviations of the data. Fits to lines are (from left to right on the plot): $D_{CNT} = 1.25\ t_{Fe} + 6.59$, $R^2 = 0.98$, and $D_{CNT} = 9.51\ t_{Fe} - 110.52$, $R^2 = 0.99$.

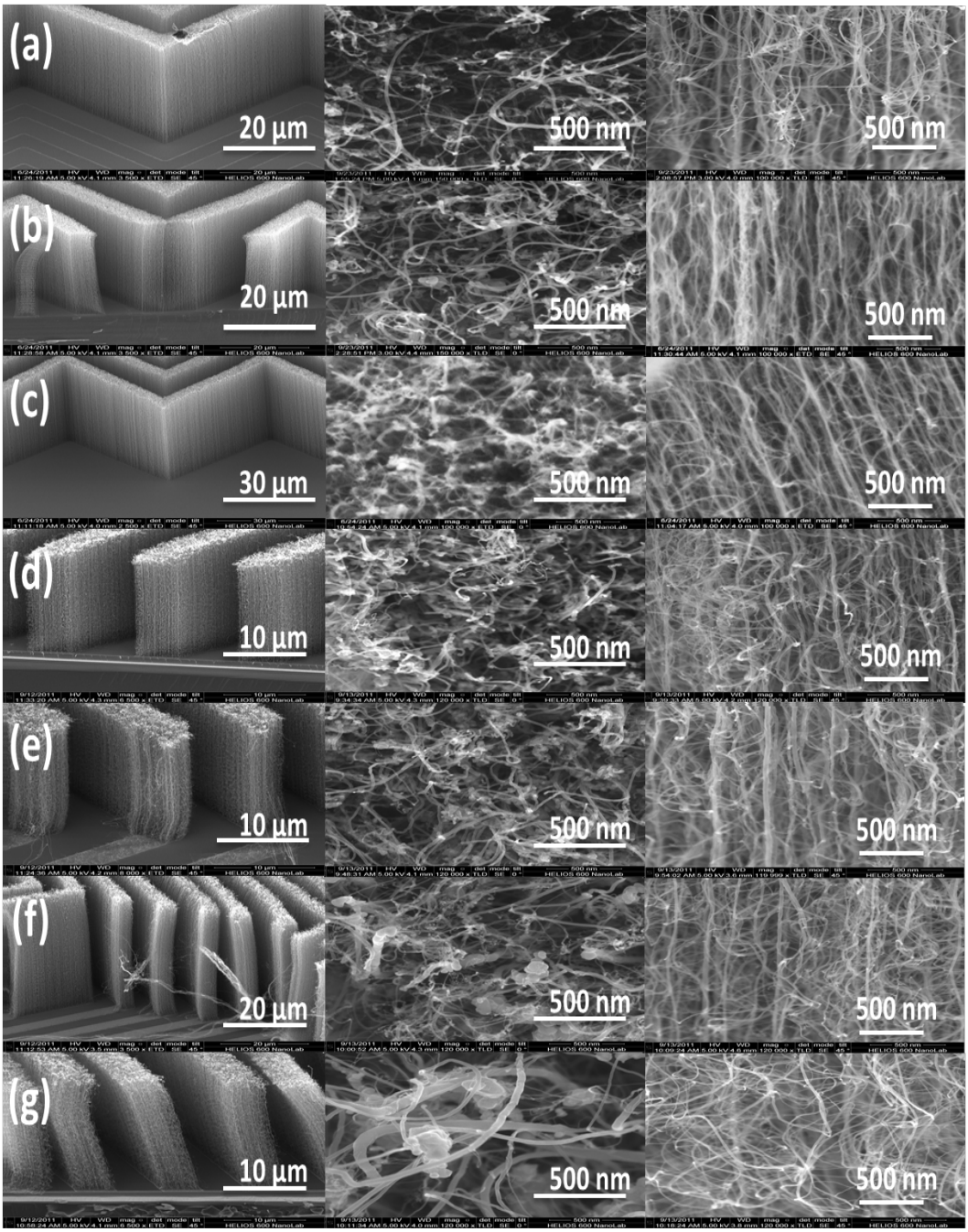

Figure 2.6. SEM micrographs showing side (left), top (middle) and side (right, at higher magnification) views of CNTs grown from initial Fe catalyst thickness of (a) 6 nm, (b) 8 nm, (c) 10 nm, (d) 12 nm, (e) 14 nm, (f) 16 nm, and (g) 18 nm**.**

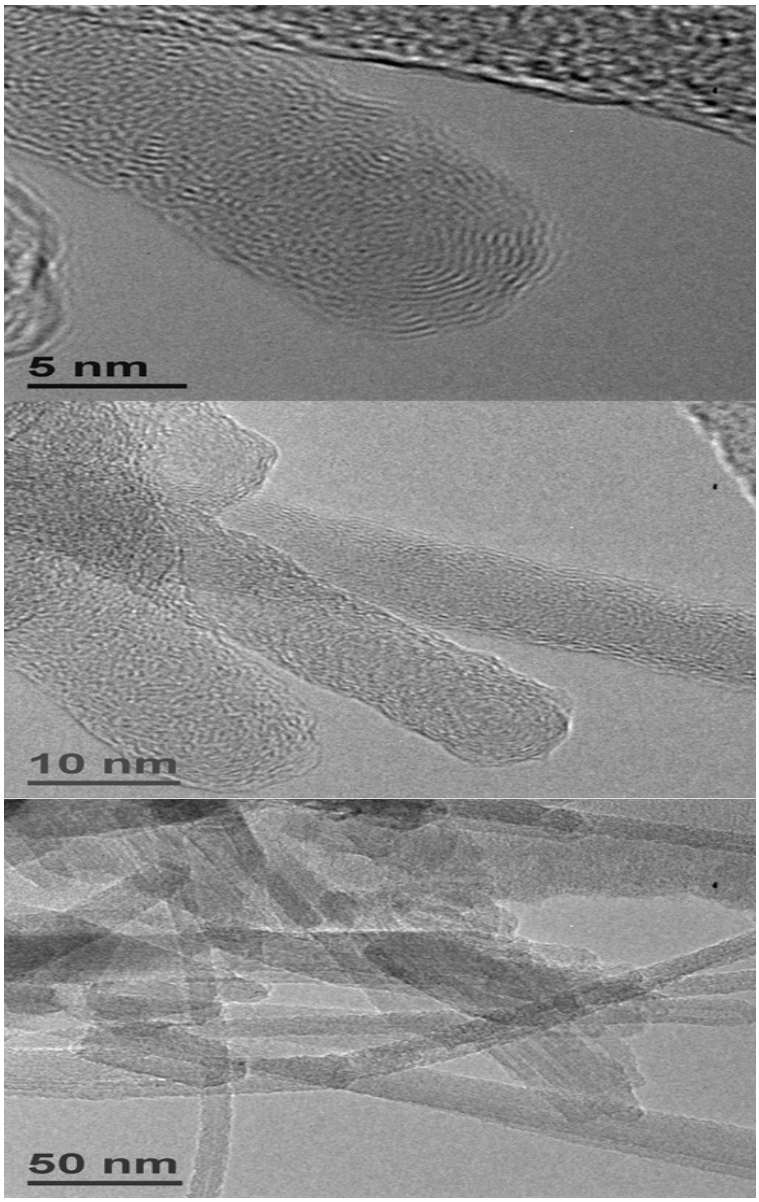

Figure 2.7. TEM images of the tops of CNT forests grown with 6 nm of annealed Fe. Catalyst nanoparticles are not seen, nor are they embedded or inside the tips of the nanotubes, which suggests 'base growth' of CNTs at this t_{Fe}.

As noted previously, our high temperature oxidation process should produce a surface that is all but devoid of the silanol groups that are necessary for normal phase chromatography.[44] Of course, few if any silanols would be expected from the LPCVD of SiH_4, and would only be present as a result of an impurity, e.g., water or O_2, in the system. Accordingly, after LPCVD of Si and subsequent oxidation, TLC plates were hydroxylated in a pH 10.0 bath at room temperature.[26] Diffuse reflectance infrared Fourier transform spectroscopy (DRIFT) has previously been used to study the adsorptive sites/free silanols on silica materials used in high performance liquid chromatography (HPLC). According to Kirkland and coworkers, material showing an Si-OH peak below 3740 cm^{-1} is better for chromatography;[26] Si-OH signals above 3740 cm^{-1} correspond to isolated silanols, which tend to be more acidic and adsorptive than vicinal or associated silanol groups, which appear below 3740 cm^{-1}.[26, 44] Our TLC plate showed a signal at 3742.3 cm^{-1}. Commercial HPTLC (Merck) and TLC (Analtech) plates showed peaks at 3736.8 cm^{-1} and 3738.49 cm^{-1}, respectively (Spectra in Supporting Information.). These results suggested incomplete hydration of our TLC plates. Neverthless, for the purposes of this study (see chromatograms in Supporting Information), the hydroxylation conditions appeared to be adequate to allow us to differentiate between the plates based on their Fe thicknesses. This issue will be the subject of additional study in the future. Like the other plates studied,[45] our TLC plate also showed a broad signal around 3660 cm^{-1}, which was attributed to vicinal or associated silanol groups.

Following infiltration, oxidation, and hydration, TLC was attempted on plates prepared with 4 – 18 nm of iron catalyst. Consistent with the SEM results noted above, TLC plates fabricated with 12, 14, 16 and 18 nm of Fe were mechanically weak and not strong enough and/or dense enough to withstand hydroxylation in ammonium hydroxide, i.e., these plates were destroyed in

this final step of their fabrication and no separations could be performed on them. Separations of a CAMAG test dye mixture were attempted on the remaining plates prepared with 4 – 10 nm of catalyst. The results are shown in Figure 2.8.

Plates prepared with 8 and 10 nm of catalyst showed unacceptable separations/high retention factor (R_F) values. Clearly the best separation, showing baseline separation of dyes and moderate R_F values, was obtained with 6 nm of Fe catalyst, with the highest plate number calculated at 55,110 N/m for the spot with an R_F value of 0.65. The next best separations were found at t_{Fe} = 4 nm.

A possible explanation for the higher R_f values obtained using the t_{Fe} = 8 and 10 nm plates can be found by considering the retention factor, *k*, in HPLC. During a separation, *k* is equal to the number of moles of analyte in the stationary phase, A_S, divided by the number of moles of analyte in the mobile phase, A_M.

(4) $k = As / Am$

Incorporating the volumes of the mobile and stationary phases into this equation allows *k* to be expressed in terms of *K*, the partition coefficient for adsorption of the analyte: $K = [A]_S/[A]_M$, where $[A]_i = A_i/V_i$ for i = M and S:

(5) $$k = \left(A_S / A_M\right) * \left(V_M / V_S\right) * \left(V_S / V_M\right) = K * \left(V_S / V_M\right)$$

Obviously *K* is a constant – one would expect the same surface chemistry from all of the plates. It is also reasonable to expect V_M to be essentially constant in our separations. Thus:

(6) $k \propto V_S$

That is, we expect that if the surface area of our stationary phase decreases, retention will also decrease, i.e., R_F values will increase.

To understand whether a decrease in surface area of the stationary phase should be occurring with increasing t_{Fe}, the following analysis was performed. First, it is observed that the volume of Fe in a certain area, A, of the surface is:

(7) $$V = A * t_{Fe}$$

Now if we assume that this iron is converted into spherical nanoparticles, then the same volume is:

(8) $$V = n\ (4/3)\ \pi\ (D_P/2)^3$$

where n is the number of nanoparticles present in this volume of iron.

Combining Equations (7) and (8) then gives:

(9) $$n/A = t_{Fe} / \left(4/3 * \pi * (D_p/2)^3\right)$$

Thus, measurement of the original Fe thickness, t_{Fe}, and the average diameters of the Fe nanoparticles, D_P, provides an estimate for the areal density (n/A) of nanoparticles at the surface after annealing (Equation 9).

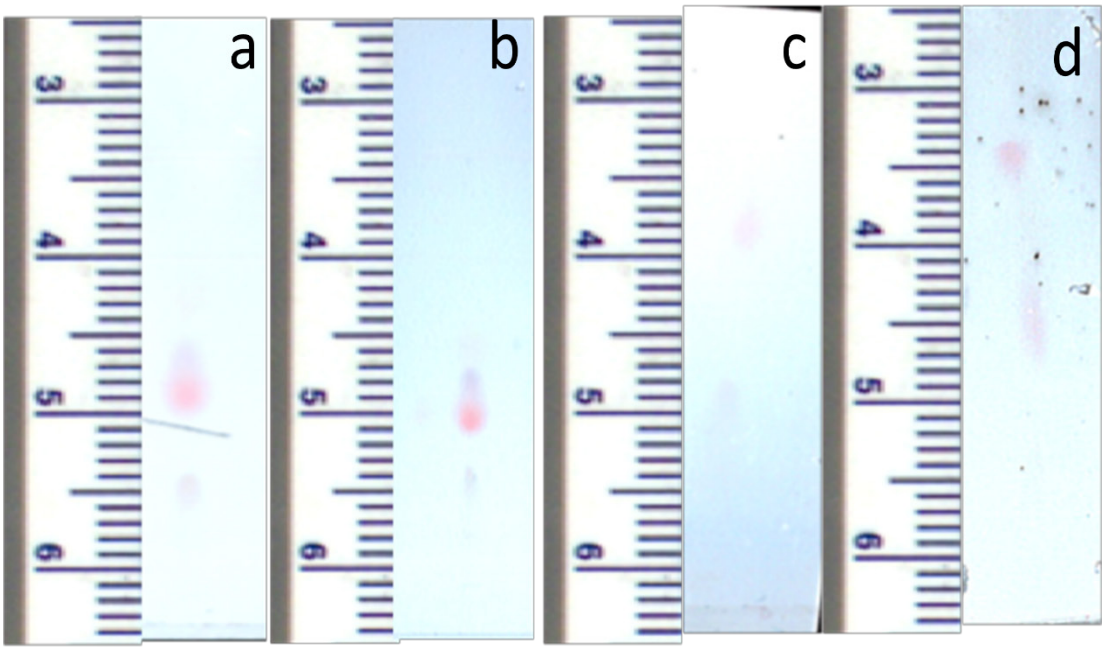

Figure 2.8. Separation of a CAMAG test dye mixture, with toluene as the mobile phase, on TLC plates made with Fe thicknesses of (a) 4 nm, (b) 6 nm, (c) 8 nm, and (d) 10 nm.

In our infiltration we attempt to create silica nanowires of the same diameter, regardless of the diameters of the original CNT template tubes. So if we assume that each nanoparticle leads to the creation of one nanotube, the surface area of our stationary phase will be directly proportional to the density of Fe nanoparticles (n/A) in it. Thus, using Equation 9 and $D_P = 6.06\ t_{Fe}$ (see caption to Figure 2.3), we see that, in general, n/A is directly proportional to $1/t_{Fe}^2$. More particularly, the average number of silica nanowires/μm^2 in each film is estimated as 2990, 1146, 130, and 60 for 4, 6, 8 and 10 nm Fe film thicknesses, respectively. This analysis suggests higher surface areas for the t_{Fe} = 4 and 6 nm TLC plates, compared to the t_{Fe} = 8 and 10 nm plates, and helps provide an explanation for the loss of retention with increasing t_{Fe} based on Equation 6 ($k \alpha V_S$).

To confirm that the SiO_2 nanowires did have nearly the same diameter, CNT forests were grown on patterned Fe nanoparticle surfaces, infiltrated (uniformly coated with Si), and then oxidized to remove the CNTs and convert the Si to SiO_2. BET measurements of the resulting SiO_2 nanowires grown from 6, 10, 14, and 18 nm Fe layers were similar: 21 m^2/g, 19 m^2/g, 27 m^2/g and 21 m^2/g, respectively. Thus, while the surface area per gram of the silica remains the same, the density of nanowires themselves decreases with increasing t_{Fe}. This helps explain the decreased mechanical stability of the arrays with increasing t_{Fe}. These values for surface area are less than 10 percent of the surface areas from Merck HPTLC (320 m^2/g) and Analtech TLC (270 m^2/g) plates, i.e., our silica nanowire material is non-porous. In the future, an effort will be made to increase the surface area, and therefore retention, of our TLC plates.

Finally, an attempt was made to separate a mixture of analgesics (caffeine, phenacetine and propylphenazone) on microfabricated TLC plates prepared using 6 nm of Fe. Two out of three dyes could not be baseline resolved with mobile phases of 4:1 (v/v) toluene: acetonitrile, 6:1 (v/v)

toluene: acetonitrile, or 4:1 (v/v) toluene: acetonitrile (v/v) in which 1.0% (v/v) TEA was added. However, baseline resolution was obtained when 0.1% triethylamine (TEA) was added to the 4:1 (v/v) toluene: acetonitrile mobile phase (see Figure 2.9). TEA is a common additive used to modify the surfaces of adsorbent materials in liquid chromatography.[46, 47] In this case it may have reduced the effects of isolated silanol groups (vide supra). The addition of TEA also changed the selectivity of the separation somewhat and increased the run time.

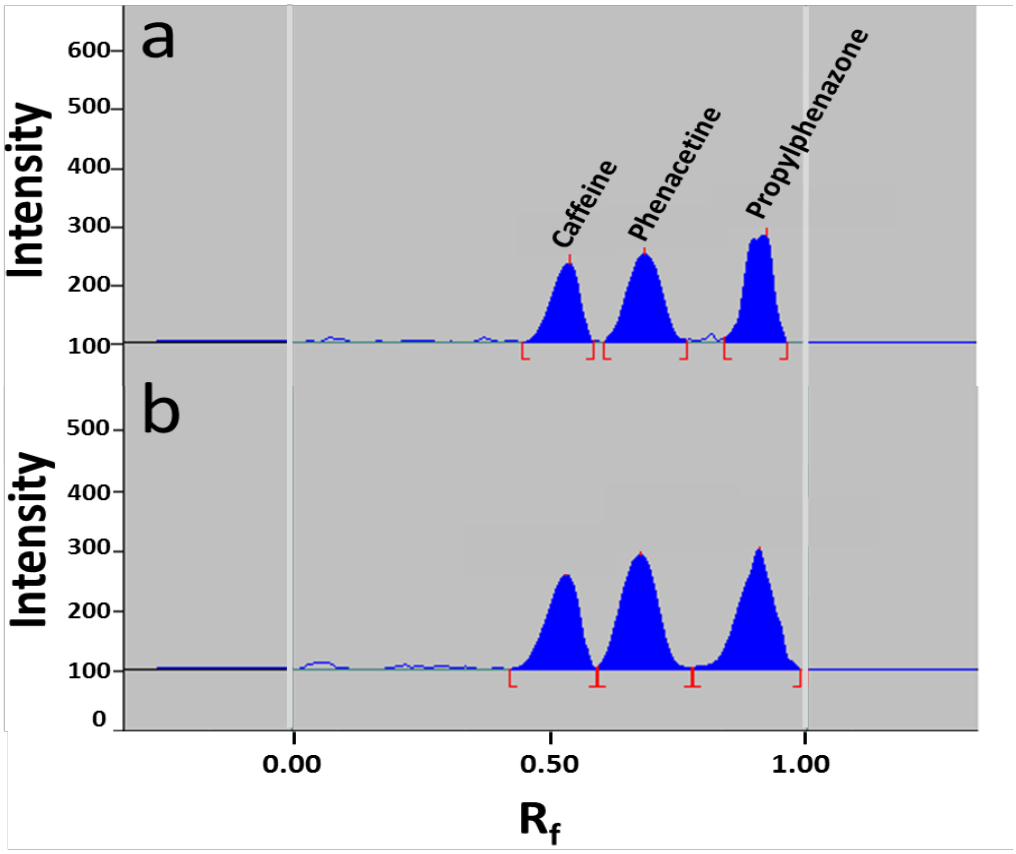

Figure 2.9. Separation of three analgesics (from left to right: caffeine, phenacetine and propylphenazone) using 4:1 toluene:acetonitrile (v/v) with 0.1% TEA with sample volume of (a) 1.8 µL and (b) 3.6 µL. The run time was 3 min 5 s for both plates. The vertical lines on the left and right correspond to the positions of spotting and the solvent front, respectively, where the difference between these points was 3.5 cm on the plates.

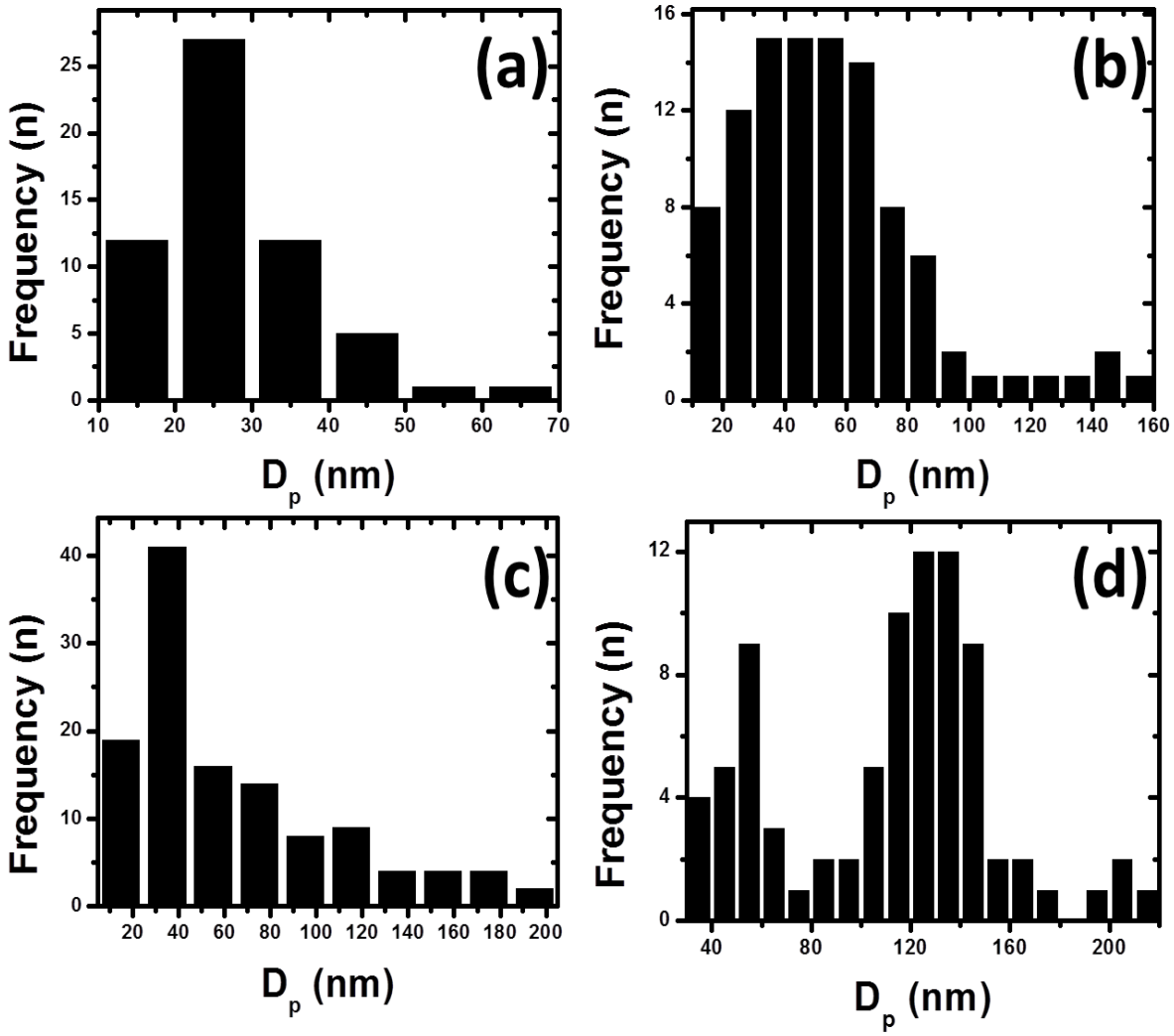

Figure 2.10. Histograms showing distributions of Fe nanoparticles for initial Fe thicknesses of (a) 6 nm, (b) 8 nm, (c) 12 nm and (d) 18 nm

2.5. Conclusion

We have studied the effects of iron thickness, t_{Fe}, on nanoparticle diameter, carbon nanotube diameter, and CNT forest growth/stability in the preparation of microfabricated thin layer chromatography plates. SEM and AFM revealed the formation of Fe nanoparticles after annealing in hydrogen, which became larger with increasing t_{Fe}. SEM showed increasing CNT diameters with increasing t_{Fe}. Nanotube growth at t_{Fe} = 6 nm is base growth, and not tip growth. CNT forests prepared from thicker Fe layers were unstable, and infiltrated/oxidized structures based on these forests were unable to withstand hydroxylation under basic conditions. An analysis based on t_{Fe} and D_P suggests that the surface area of the device goes as $1/t_{Fe}^2$; calculations suggest that the loss of surface area for TLC plates made with thicker Fe layers is a result of fewer, thicker CNTs, although the coated CNTs had similar surface areas. Best TLC separations of a test dye mixture were obtained with plates prepared with 6 or 4 nm of catalyst.

2.6. References

1. L. W. Bezuidenhout and M. J. Brett, J. Chromatogr., A 1183 (1-2), 179-185 (2008).
2. A. P. Boichenko, The Open Surface Science Journal 1, 40-45 (2009).
3. A. M. Frolova, O. Y. Konovalova, L. P. Loginova, A. V. Bulgakova and A. P. Boichenko, J Sep Sci 34 (16-17), 2352-2361 (2011).
4. R. Bakry, G. K. Bonn, D. Mair and F. Svec, Anal Chem 79 (2), 486-493 (2007).
5. I. Urbanova and F. Svec, J Sep Sci 34 (16-17), 2345-2351 (2011).
6. S. R. Jim, M. T. Taschuk, G. E. Morlock, L. W. Bezuidenhout, W. Schwack and M. J. Brett, Anal Chem 82 (12), 5349-5356 (2010).
7. J. E. Clark and S. V. Olesik, Anal Chem 81 (10), 4121-4129 (2009).
8. J. E. Clark and S. V. Olesik, J. Chromatogr., A 1217 (27), 4655-4662 (2010).
9. J. R. Whitney, S. Sarkar, J. F. Zhang, D. Thao, T. Young, M. K. Manson, T. A. Campbell, A. A. Puretzky, C. M. Rouleau, K. L. More, D. B. Geohegan, C. G. Rylander, H. C. Dorn and M. N. Rylander, Laser. Surg. Med. 43 (1), 43-51 (2011).
10. J. D. Whittaker, M. Brink, G. A. Husseini, M. R. Linford and R. C. Davis, Applied Physics Letters 83 (25), 5307-5309 (2003).
11. S. Prakash, M. Malhotra, W. Shao, C. Tomaro-Duchesneau and S. Abbasi, Adv. Drug Delivery Rev. 63 (14-15), 1340-1351 (2011).
12. P. Hojati-Talemi, M. A. Gibson, D. East and G. P. Simon, Appl. Phys. Lett. 99 (19), 194104 - 194104-194103 (2011).
13. S. Iijima, Nature 354 (6348), 56-58 (1991).

14. P. C. Chen, Y. Fu, R. Aminirad, C. Wang, J. L. Zhang, K. Wang, K. Galatsis and C. W. Zhou, Nano Lett. 11 (12), 5301-5308 (2011).

15. Y. C. Jung, J. H. Kim, T. Hayashi, Y. A. Kim, M. Endo, M. Terrones and M. S. Dresselhaus, Macromol Rapid Comm 33 (8), 628-634 (2012).

16. J. F. Yuan, H. C. Gao and C. B. Ching, Toxicol. Lett. 207 (3), 213-221 (2011).

17. A. V. Herrera-Herrera, M. A. Gonzalez-Curbelo, J. Hernandez-Borges and M. A. Rodriguez-Delgado, Anal Chim Acta 734, 1-30 (2012).

18. J. Song, D. S. Jensen, D. N. Hutchison, B. Turner, T. Wood, A. Dadson, M. A. Vail, M. R. Linford, R. R. Vanfleet and R. C. Davis, Adv. Funct. Mater. 21 (6), 1132-1139 (2011).

19. S. Esconjauregui, B. C. Bayer, M. Fouquet, C. T. Wirth, C. Ducati, S. Hofmann and J. Robertson, Appl. Phys. Lett. 95 (17), 173115 - 173115-173113 (2009).

20. S. Esconjauregui, M. Fouquet, B. C. Bayer, C. Ducati, R. Smajda, S. Hofmann and J. Robertson, ACS Nano 4 (12), 7431-7436 (2010).

21. D. Hausmann, J. Becker, S. L. Wang and R. G. Gordon, Science 298 (5592), 402-406 (2002).

22. D. S. Jensen, S. S. Kanyal, V. Gupta, M. A. Vail, A. E. Dadson, M. Engelhard, R. Vanfleet, R. C. Davis and M. R. Linford, J Chromatogr A 1257, 195-203 (2012).

23. F. Zhang, K. Sautter, A. M. Larsen, D. A. Findley, R. C. Davis, H. Samha and M. R. Linford, Langmuir 26 (18), 14648-14654 (2010).

24. D. Jensen, S. S. Kanyal, A. J. Miles, R. C. Davis, R. Vanfleet, M. A. Vail, A. E. Dadson and M. R. Linford, Submitted to J. Vac. Sci. Technol., B. (2012).

25. D. Jensen, S. S. Kanyal, N. Madaan, J. M. Hancock, A. E. Dadson, M. A. Vail, R. Vanfleet, V. Shutthanandan, Z. Zhu, M. H. Engle and M. R. Linford, Submitted to Surf. Interface. Anal. (2012).

26. J. Kohler and J. J. Kirkland, J. Chromatogr., A 385, 125-150 (1987).

27. A. Rizzo, R. Rossi, M. A. Signore, E. Piscopiello, L. Capodieci, R. Pentassuglia, T. Dikonimos and R. Giorgi, Diam Relat Mater 17 (7-10), 1502-1505 (2008).

28. M. A. Signore, A. Rizzo, R. Rossi, E. Piscopiello, T. Di Luccio, L. Capodieci, T. Dikonimos and R. Giorg, Diam Relat Mater 17 (11), 1936-1942 (2008).

29. I. T. Han, B. K. Kim, H. J. Kim, M. Yang, Y. W. Jin, S. J. Jung, N. Lee, S. K. Kim and J. M. Kim, Chem. Phys. Lett. 400 (1-3), 139-144 (2004).

30. T. Komukai, K. Aoki, H. Furuta, M. Furuta, K. Oura and T. Hirao, Jpn. J. Appl. Phys. 45 (7), 6043-6045 (2006).

31. Y. R. Ma, M. S. Wong, C. H. See, K. W. Cheng, J. C. Wu, Y. Liou and Y. D. Yao, J. Appl. Phys. 97 (10), 7291 - 7293 (2005).

32. K. Moulton, N. Morrill, A. Konneker, B. Jensen, R. Vanfleet, D. Allred and R. Davis, J. Micromech. Microeng. 22 (2012).

33. L. T. Zhuravlev, Colloids Surf., A 173 (1-3), 1-38 (2000).

34. J. Nawrocki, J. Chromatogr., A 779 (1-2), 29-71 (1997).

35. L. T. Zhuravlev, React. Kinet. Catal. Lett. 50 (1-2), 15-25 (1993).

36. L. T. Zuravlev, A. A. Agzamkhodzhaev, A. V. Kiselev and K. Y. Shengeliya, Colloid journal of the USSR 36 (6), 1036-1039 (1974).

37. P. M. Parthangal, R. E. Cavicchi and M. R. Zachariah, Nanotechnology 18 (18), 185605 (2007).

38. J. M. Vargas, E. Lima, L. M. Socolovsky, M. Knobel, D. Zanchet and R. D. Zysler, J. Nanosci. Nanotechnol. 7 (9), 3313-3317 (2007).

39. N. Bajwa, X. S. Li, P. M. Ajayan and R. Vajtai, J. Nanosci. Nanotechnol. 8 (11), 6054-6064 (2008).

40. C. Branca, F. Frusteri, V. Magazu and A. Mangione, J. Phys. Chem. B 108 (11), 3469-3473 (2004).

41. M. Fujimoto, Y. Sugiyama, Y. Inoue, E. Muneyuki and H. Haneda, J. Electron Microsc. 55 (3), 143-149 (2006).

42. C. Muller, D. Golberg, A. Leonhardt, S. Hampel and B. Buechner, Phys. Status Solidi A 203 (6), 1064-1068 (2006).

43. M. Nakajima, F. Arai and T. Fukuda, Ieee T Nanotechnol 5 (3), 243-248 (2006).

44. M. Mauss and H. Engelhardt, J. Chromatogr., A 371, 235-242 (1986).

45. A. Ramirez, B. L. Lopez and L. Sierra, J. Phys. Chem. B 107 (35), 9275-9280 (2003).

46. M. Reta and P. W. Carr, J. Chromatogr., A 855 (1), 121-127 (1999).

47. M. Andersson, U. K. Hultin and A. Sokolowski, Chromatographia 48 (11-12), 770-776 (1998).

3. Chapter: Deposition of Aluminum-Free Silica onto Patterned Carbon Nanotube Forests in the Preparation of Microfabricated Thin-Layer Chromatography Plates

3.1. Abstract

We describe the direct, conformal, atomic layer deposition (ALD) of silica onto carbon nanotubes (CNTs) in the microfabrication of thin-layer chromatography (TLC) plates. As before, these plates were prepared with zig-zag hedge and channel microstructures, with high aspect ratio, porous hedges. After ALD, scanning electron microscopy (SEM) showed an increase in the radius of the CNTs of 8–40 nm. X-ray photoelectron spectroscopy (XPS) showed that the plates were composed almost entirely of silicon and oxygen, without contamination of metals or other elements that might compromise chromatographic performance, e.g., aluminum. Time-of-flight secondary ion mass spectrometry confirmed the extremely low level of aluminum in the plates. The final TLC layer thickness was ca. 50 μm. Separations of a test mixture of dyes from CAMAG (Muttenz, Switzerland) on an uncoated silica plate under traditional, normal phase conditions gave efficiencies of 40,000–140,000 plates m^{-1} with migration distances ranging from 2 to 36 mm. A separation of two fluorescent dyes, eosin Y disodium salt and sulforhodamine B, on an amino silane-coated plate gave efficiencies of ca. 170,000 and 200,000 plates m^{-1}, with hR_F values of 76 and 88, respectively. Run times on these new plates were much faster than on conventional TLC plates.

3.2. Introduction

Silica has long been the material of primary interest in thin-layer chromatography (TLC) and high-performance liquid chromatography (HPLC). A conventional TLC plate consists of a thin layer of porous silica particles in a polymeric or inorganic binder. This basic design has changed little during the past few decades. Of late, various research groups have shown interest in developing TLC plates with new materials and fabrication techniques. These include monolithic silica [1], glancing angle deposition (GLAD),[2-4] polymer monoliths,[5-8] and electrospun polymers.[9, 10] Our group has also been active in this area, reporting TLC plates with high efficiencies and short run times prepared from microfabricated, patterned, and infiltrated carbon nanotube (CNT) forests.[11-14] In general, these plates are prepared as follows. A photoresist is spin coated onto a silicon wafer. A contact mask is then placed directly onto the resist-covered substrate. The resist is then exposed to light through the mask, which changes its solubility in a developing solvent. After removal of the exposed resist, the surface is sequentially vacuum-coated with ultrathin films of alumina and iron. The remaining resist is then removed, leaving a substrate patterned with Al_2O_3 and Fe. The substrates are annealed in a reducing environment to form iron nanoparticles, from which CNT forests are grown. The CNTs are then coated with an inorganic material that is suitable for chromatography, the CNTs are removed at elevated temperature in an oxidizing environment, and the plates are hydrated. Photolithography has been widely used in semiconductor chip manufacturing[15, 16] and in microfluidics[17-20] including modern drug delivery.[17, 21-23]

Our first attempt to microfabricate a TLC plate employed the conformal deposition of silicon onto CNTs via low-pressure chemical vapor deposition (LPCVD) of silane (SiH_4), where

the oxidation/removal of the CNTs beneath the silicon led to their removal and the oxidation of the silicon to silica. Unfortunately, the volume expansion of Si to SiO_2 that occurred in this process distorted the features of the device and led to irreproducible results. In our second attempt, the CNTs were coated with a thin layer of carbon, a sheath of alumina deposited by atomic layer deposition (ALD), and a layer of silica that was deposited in a fast (pseudo) ALD process [11] (ψ-ALD, a.k.a. alternating layer deposition). In this scheme, it was believed that the carbon layer would increase the number of defects on the CNTs to allow improved nucleation of alumina compared to its deposition on untreated CNTs. X-ray photoelectron spectroscopy (XPS) confirmed the presence of additional oxygen in this carbon layer. This Al_2O_3 layer then became the substrate for the ψ-ALD deposition of silica. In a third preparation, CNTs were first treated with ozone to introduce oxygen into them.[12] These substrates could then be directly coated with silica via ψ-ALD. These second and third preparations allowed the controlled, conformal growth of an inorganic material onto CNTs without the volume expansion and feature distortion of the first approach. However, residual aluminum from the catalyst needed for the ψ-ALD was present in the stationary phases of these TLC plates after their fabrication. This contaminant appeared to cause considerable peak tailing of analytes. Fortunately, this tailing could be suppressed with a basic modifier (triethylamine) in the mobile phase. Accordingly, a bonded phase consisting of an amino silane was prepared on these TLC plates.[24] The resulting stationary phases yielded high quality separations without the need for the basic modifier. These second and third approaches to making our TLC plates were clearly an advance over the first, but the need to cover strongly active surface sites with amines is disadvantageous. It complicates the synthesis of the plates and limits their potential acceptance – normal phase (pure) silica is by far the most common TLC stationary phase.

In addition to an exploration of different microfabrication schemes, we have reported the detailed characterization of the materials in our TLC plates [13, 25-29] and the effects of Fe layer thickness on nanoparticle size and CNT forest growth.[30]

Herein, we describe the preparation of all silica TLC plates prepared by the true ALD of pure, aluminum-free silica onto patterned carbon nanotube forests. ALD is advantageous because it gives extremely conformal and uniform coatings.[31, 32] (True) ALD is based on the alternating reactions of gas phase species at a surface that generally deposit rather small quantities of material with each step. That is, a first gas phase species will be introduced to a substrate. It will react quickly, in a self-limiting fashion, and deposit up to a monolayer of material. After its removal, a second gas phase reagent is added. It will similarly react with the surface. One of the unique features of ALD is that the first reaction primes the surface for the second reaction, and the second reaction then primes the surface for the first reaction. Thus, ALD allows thin films to be built up in an ABAB type fashion. This ALD approach is an advance over our previous attempts, whereas our third fabrication process required two steps to coat the CNTs with silica: treatment with ozone followed by ψ-ALD; this latest, fourth, approach requires only one step: ALD. This procedure does not employ a catalyst, so there is no chance of a material like aluminum being deposited into the stationary phase. Thus, while creation of a bonded phase via silanization is an option on these plates, it is not necessary. As expected, these plates work well in normal phase mode, quickly and effectively separating a test dye mixture. For comparison to our previous work, they were also coated with an amino silane bonded phase, and two fluorescent dyes were again separated with high efficiency.

3.3. Experimental

3.3.1. Microfabrication of TLC Plates

TLC plates were microfabricated using the methods described previously up through the growth of patterned CNT forests.[11-13, 30] The mask used to make the plates in this study had zig-zag features that produced 3-µm wide hedges, 4.24-µm channel widths, and 50 µm channels as shown in Figure 3.1. The final size of the finished TLC plate patterned with these structures was 1.2 × 6 cm.

3.3.2. ALD of Silica

ALD of SiO_2 was performed at Beneq (Vantaa, Finland) in a Beneq TFS 200 ALD system. The deposition temperature was 325°C. The precursors were AP LTO 330 (Air Products, Allentown, PA, USA) and O_3 from an ozone generator producing 4 g/h at 100 g/Nm^3. The pulsing parameters were: Si precursor pulse time: 1.4 s, Si precursor purge time: 30 s, O_3 pulse time: 2 s, and O_3 purge time: 30 s. Witness silicon substrates were also coated during the SiO_2 depositions. They gave film thicknesses of 20, 30, 40, 50, and 60 nm, as confirmed with a Sentech SE 400adv ellipsometer (Berlin, Germany).

3.3.3. Removal of CNTs and Surface Hydroxylation

Silica-coated TLC plates were placed in a preheated (200°C) furnace (Thermolyne 6000 Furnace, Dubuque, IA), and the temperature was ramped at 1°C min^{-1} to 600°C. This temperature was maintained for 17 h followed by cooling to 200°C in the air. In addition to the desirable effect of removing the CNTs, this elevated temperature results in the undesirable loss of surface silanol groups that are essential for good chromatography.[33-35], [36] For surface hydroxylation/population

with surface silanols, the plates were immersed in a 150-ppm HF solution at room temperature for 24 h after which they were rinsed with deionized water and dried at 120°C. Warning: HF is very toxic and users should be properly trained before attempting to use it.

3.3.4. XPS and SEM Analysis of TLC Plates

X-ray photoelectron spectroscopy (XPS) [37] was performed with an SSX-100 spectrometer (Service Physics Inc., OR) equipped with an Al Kα X-ray source and a hemispherical detector. SEM images of the SiO_2 coated CNTs were taken with an FEI scanning electron microscope (Helios Nanolab 600, Hillsboro, OR).

3.3.5. Separation of a CAMAG Test Dye Mixture

A test dye solution containing six dyes dissolved in toluene: oracet violet 2R, ariabel red 28.9, Sudan blue II, dimethyl yellow, oracet red G, and indophenol was obtained from CAMAG (Muttenz, Switzerland) (see CAMAG catalog at http://www.maneko.cz/data/aktuality/TLC1011.pdf). It was diluted in hexanes to 1% and 3% of its original concentration. Microfabricated TLC plates were spotted with 1 µL of each of these solutions as 3-mm long bands using a Linomat 5 spotter (CAMAG, Muttenz, Switzerland). The band was located 5 mm above the bottom edge of the plate, dried at 120°C for one min, and developed in a twin-trough chamber (CAMAG, Muttenz, Switzerland) that had been presaturated with the vapors of the developing solvent (*t*-butylbenzene) for 10 min. After conditioning the plate for 2 min in the developing chamber in the presence of the developing solvent, *t*-butylbenzene (3 mL) was added to the bottom of the TLC plate. Development then took place over 40 mm from the point of application of the analyte.

3.3.6. Amino Silane Functionalization and Separation of Florescent Dyes

TLC plates were amino functionalized by immersing them in a 1% (*v*/*v*) solution of 3-aminopropyltriethoxysilane (>98%, Sigma-Aldrich) in water-saturated toluene at 70°C for 10 min. The plates were removed from this solution and immediately rinsed thrice with methanol (>99%, Sigma-Aldrich) and then deionized water, and finally dried at 120 °C.[24] For TLC, 0.5 µL of a solution of two fluorescent dyes (eosin Y disodium salt [85%, Sigma-Aldrich] and sulforhodamine B [75%, Sigma-Aldrich]) at ca. 0.5 µM each in methanol were spotted using the Linomat 5. Again, the width of the analyte band (from left to right across the plate) was 3 mm, and the center of the band was 5 mm above the bottom of the plate. After spotting, the plates were dried on a hot plate at 120°C for 1 min and then placed in a twin-trough chamber (CAMAG, Muttenz, Switzerland). Development took place with 1:70:30 LiCl–methanol–isopropanol (m/v/v) in the same manner that the CAMAG test dye mixture was separated.

3.3.7. Visualization of Separated Dyes, R_F, N, and H_{obs}

After development, the plates were exposed to short wavelength, 254 nm, light from a mercury vapor tube (UVP, Upland, CA), and the resulting fluorescence from the analytes was captured with a digital camera (Canon Powershot S95, Canon USA, Inc., Lake Success, NY).

3.3.8. Image and Data Analysis

Analyses of images captured with SEM and by digital camera were performed in ImageJ (version 1.42, NIH, USA). The retardation factors were calculated from:

$$R_{\mathrm{F}} = \frac{Z_{\mathrm{s}}}{Z_{\mathrm{sol}}} \qquad (1)$$

where Z_s is the analyte migration distance from the point of application and Z_{sol} is the solvent front migration distance also from the point of analyte application. Efficiencies or numbers of theoretical plates were calculated from:

$$N = 16\left(\frac{Z_s}{W}\right)^2 \tag{2}$$

where W is the width of the analyte band. Observed plate heights and variances were calculated using an equation described by Poole *et al*[38]:

$$H_{obs} = \frac{\sigma^2_{chrom}}{R_F\left(Z_f - Z_o\right)} \tag{3}$$

where Z_o represents the distance between the solvent entry position and the position of the applied sample spot, and Z_f represents the distance the solvent travels from its entry position. That is, $Z_{sol} = Z_f - Z_o$, and Eq. (3) reduces to:

$$H_{obs} = \frac{\sigma^2_{chrom}}{R_F Z_{sol}} \tag{4}$$

However, for R_F, as defined above, Eq. (4) becomes:

$$H_{obs} = \frac{\sigma^2_{chrom}}{Z_s} \tag{5}$$

In other words, H_{obs} is the quotient of the corrected variance, σ^2_{chrom} (see below), of the band and its migration distance.

From Poole et al. [38], the variance in the band, σ^2_{chrom}, was taken as:

$$\sigma^2_{chrom} = \sigma^2_{obs} - \sigma^2_{SA} - \sigma^2_{den} \tag{6}$$

where σ^2_{obs} is the variance of the separated (developed) analyte band, σ^2_{SA} is the variance of the band at its point of application, and σ^2_{den} is the variance of the densitometer used. Here, $\sigma^2_{den} = 0$ (no densitometer was used). This is not, of course, to say that there is no error in the analysis of our digital images, but σ^2_{den} will nonetheless be taken as zero here. All of the band widths, before and after development, were measured five times in their images with ImageJ, and the corresponding averages were divided by four to give σ^2_{obs} or σ^2_{SA} . In practice, σ^2_{SA} was ca. 0.047 mm^2 for the CAMAG test mixture and 0.050 mm^2 for the mixture of fluorescent dyes.

3.4. Results and Discussion

The silica in our second and third generation TLC plates was contaminated with aluminum that was presumably from the catalyst used in its ψ-ALD deposition. The presence of this species appeared to compromise the chromatographic performance of the resulting TLC plates and mandated the use of a basic additive or aminosilane stationary phase. Thus, it seemed appropriate to find a method for depositing SiO_2 without an aluminum catalyst. Atomic layer deposition (ALD, not ψ-ALD) of silica is well known, and it should not introduce any aluminum into the plates. Accordingly, ALD of SiO_2 was attempted with commercially viable equipment. The particular chemistry chosen here used ozone as one of the half reactants. In our third generation preparation of microfabricated TLC plates, ozone had been used to prime the CNTs for subsequent deposition of an inorganic material. It was again expected that ozone would facilitate good adhesion between the CNTs and a SiO_2 coating.

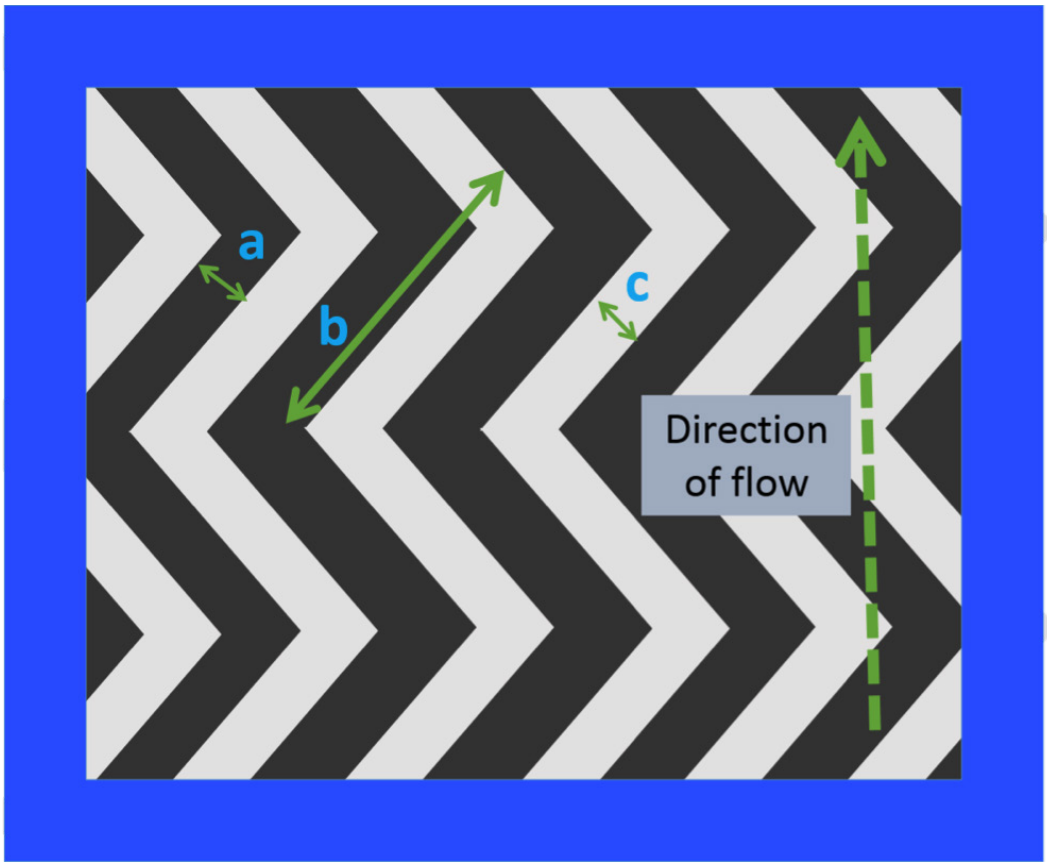

Figure 3.1. Representation of the features on the plates used in this work. (a) hedge width: 3µm, (b) hedge length: 50 µm, and (c) channel width: 4.24 µm.

Figure 3.2 shows SEM micrographs of CNTs coated with different thicknesses of ALD silica. In each case, the SiO_2 is conformally deposited around the CNTs in a manner similar to our previous depositions.[11, 12] The composition of these thin films was confirmed. XPS (Figure 3.3) showed silicon, oxygen, a trace amount of carbon (virtually any material that is exposed to the atmosphere will show some adventitious carbon by XPS), and none of the aluminum that was present after the ψ-ALD depositions. Time-of-flight secondary ion mass spectrometry (ToF–SIMS) further confirmed the SiO_2 deposition, showing significant signals corresponding to Si^+, SiO^+, and $SiOH^+$ (Figure 3.4). ToF–SIMS also revealed the expected adventitious hydrocarbon contamination. However, other gross contaminants were not present, e.g., ToF–SIMS is very sensitive to PDMS, but the signals from this common contaminant (*m/z* 73, 147, 207, and 221) were very small (see Figure 3.4A).[39] Figure 3.4B shows an expanded view of the *m/z* 27 region. Two spectral regions are compared here. The upper region is from a TLC plate prepared by the ψ-ALD deposition of SiO_2 after ozone priming.[12] This spectrum clearly shows a significant Al^+ peak that is larger than the common $C_2H_3^+$ peak attributable to hydrocarbon contamination. The bottom region is from a TLC plate prepared by the true ALD deposition of SiO_2. It shows essentially none of the aluminum present in the ψ-ALD deposition. Because of the well-known matrix effect of ToF–SIMS, it would be difficult to quantify the exact amount of aluminum that is present in these samples. However, it is well known that XPS is typically sensitive to 0.1–1% of an element in the near surface region of a material and that ToF–SIMS is often orders of magnitude more sensitive than XPS. Therefore, it is reasonable to argue that only very low levels of aluminum are present in these new plates.

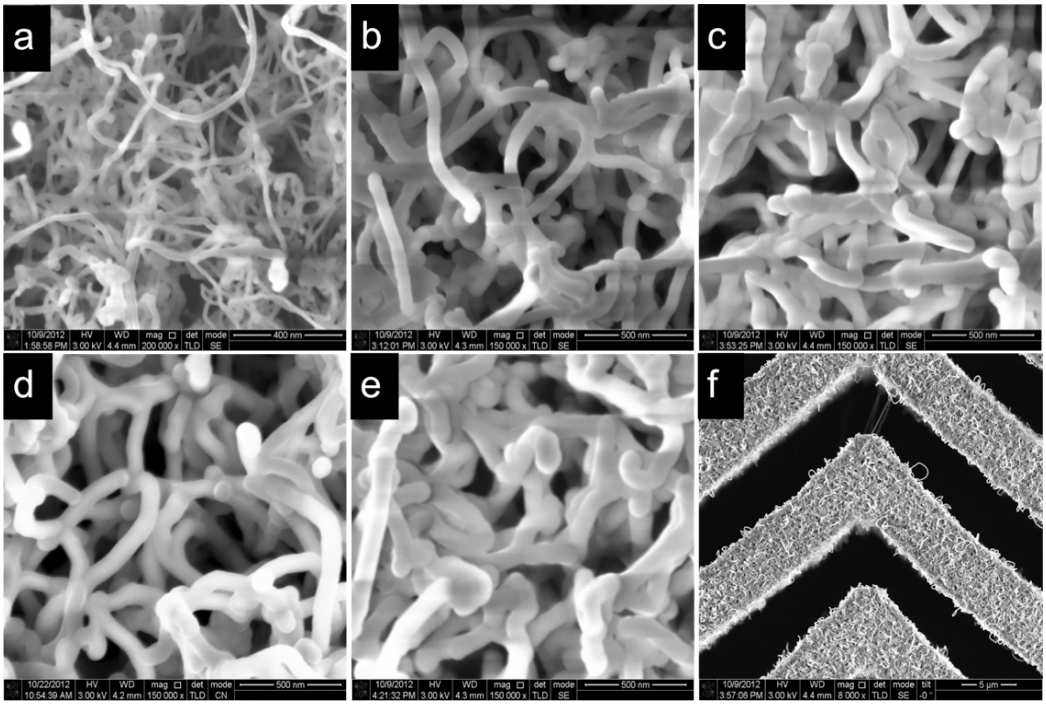

Figure 3.2. SiO_2-coated CNTs prepared in the presence of witness silicon wafers that showed SiO_2 thicknesses of (a) 20 nm, (b) 30 nm, (c) 40 nm, (d) 50 nm, and (e) 60 nm. (f) Top view of a coated CNT microstructure.

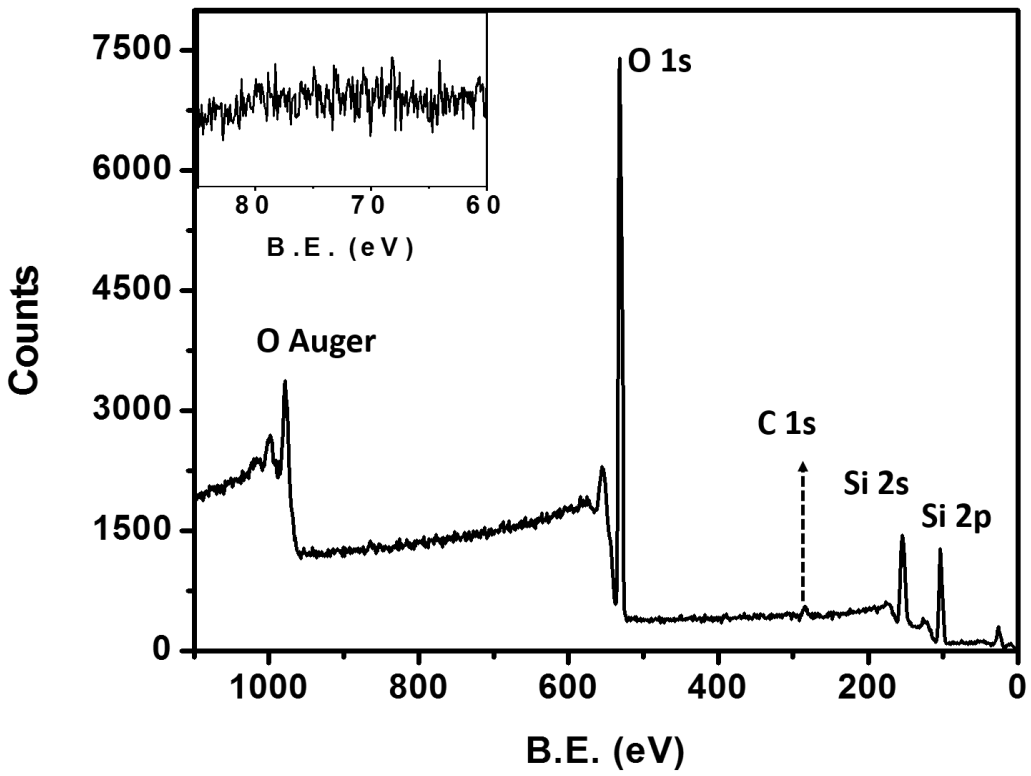

Figure 3.3. XPS survey scan of a silica TLC plate showing primarily O and Si. No aluminum is present in the sample, i.e., no Al 2p signal at ca. 73 eV (see narrow scan in inset).

ALD depositions were confirmed in two ways: (i) by ellipsometry of the SiO_2 layers deposited onto planar substrates (determined to be 20, 30, 40, 50, and 60 nm on witness silicon wafers) and (ii) by the average diameters of the CNTs, as determined by 10 SEM measurements taken on each of two different SEM images (a total of 20 measurements). Clearly, one would not expect the thickness of the planar layer and the diameter of the corresponding coated CNTs to be the same. One is the diameter of a feature that starts at finite thickness and then grows radially, and the other is a thickness on a flat substrate. Figure 3.5 is a plot of the thicknesses of the ALD SiO_2 on planar silicon vs. the average diameter of the coated CNTs. These data suggest that the diameters of the coated CNTs scale in a linear fashion with the thickness of the SiO_2 layer on the planar substrate. Figure 3.5 shows that there is reasonable linear fit to all the data (see the solid line). However, a linear fit to the four points corresponding to the thicker depositions yields a line with an intercept (11.8) that is very close to the thickness of the uncoated CNTs (12 nm). The fact that the first point does not quite fall on this line may be an induction of an initiation period in the nucleation and growth of the SiO_2 on the CNTs that show up in the measurement of the thinner coating to a greater degree than the thicker ones. Much less of an induction period, if any, would be expected on the planar substrates. In general, the thicknesses of the coated CNTs are about 1.5 times greater than that of the film on the corresponding witness shard. The scatter in the data prevents stronger conclusions from being drawn about it. After ALD of SiO_2, the plates were heated to burn out the CNTs. The plates were then hydroxylated by treatment with dilute HF to improve their chromatographic performance.

To evaluate the chromatographic efficiencies of these new, normal phase, silica TLC plates, a separation of a CAMAG test mixture of six dyes was attempted using *t*-butylbenzene as

the mobile phase. The separated compounds were best observed via fluorescence detection with excitation at 254 nm. Figure 3.6 shows that, in the absence of a bonded phase, the dyes could be separated over the full length of the plate without any tailing, which was not previously achievable.[14] The efficiencies for this separation (3.1) indicate high quality chromatography that is comparable to the results we obtained earlier with the bonded amino silane.[11, 12] The negative value of H_{obs} for the first bands indicates focusing of the band by the mobile phase. The run time for this separation was short: 1.25 min as compared to 6–10 min for a conventional TLC plate.

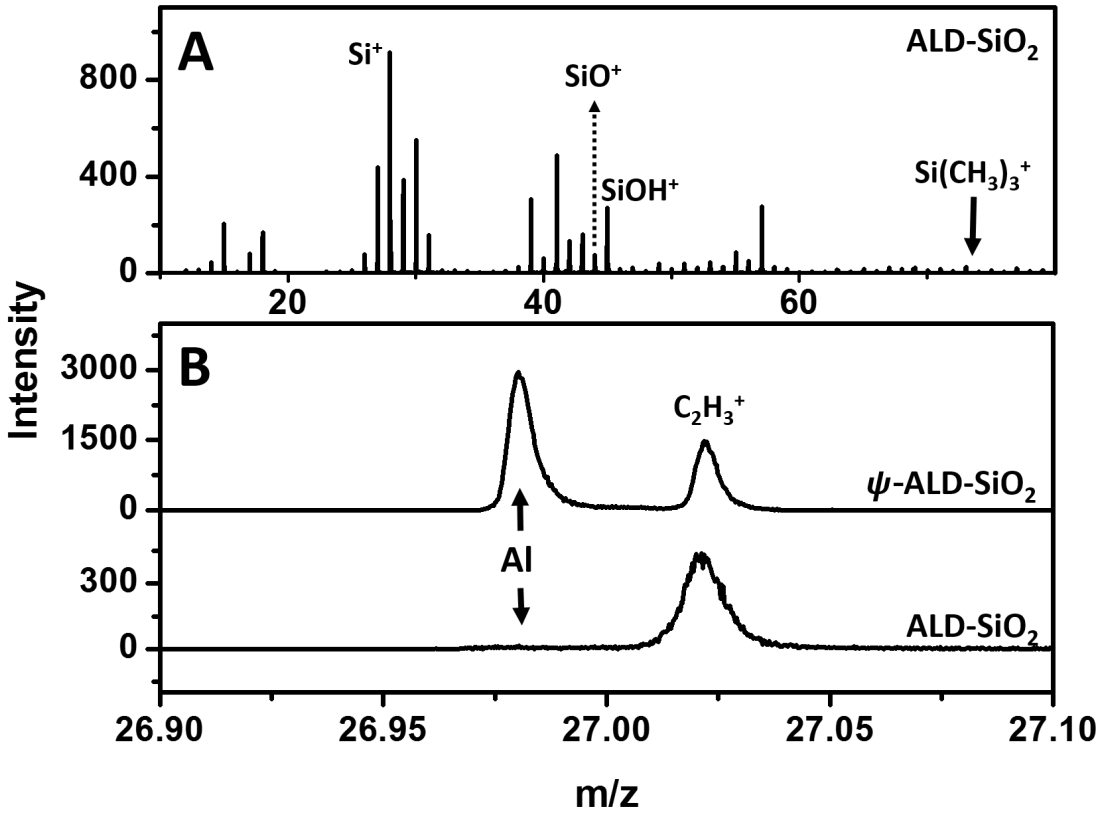

Figure 3.4. (A) ToF-SIMS spectrum of a TLC plate prepared by ALD of SiO_2. (B) Expanded views of the m/z 27 regions from TLC plates prepared by ψ-ALD of SiO_2 (top spectrum) and true ALD of SiO_2 (bottom spectrum).

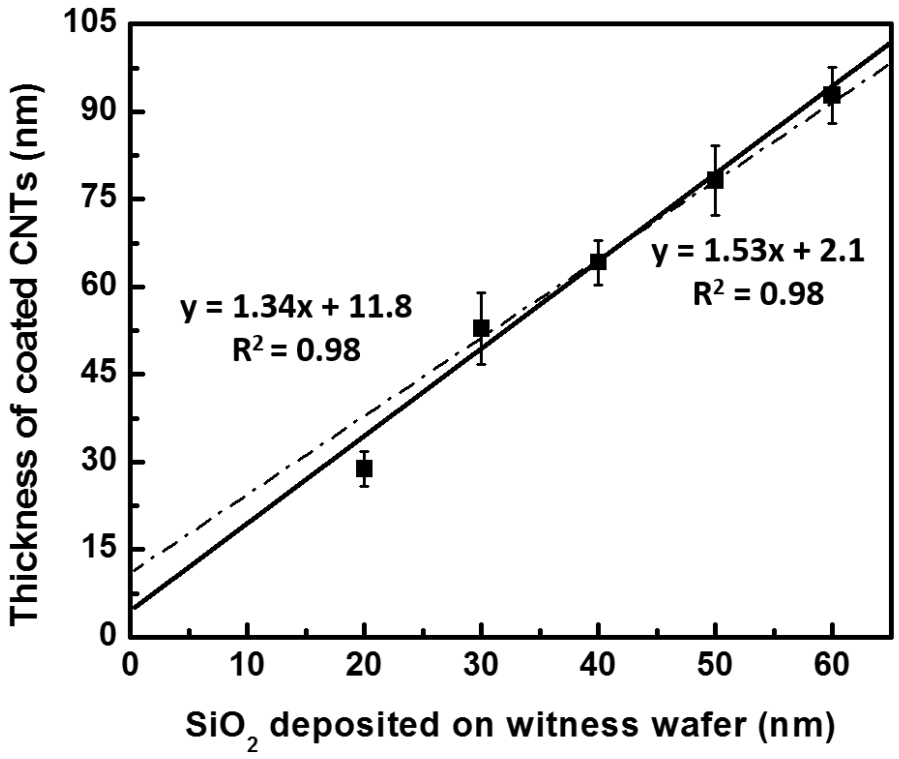

Figure 3.5. Plot of the diameters of coated CNTs, as measured by SEM, vs. the SiO_2 thicknesses of corresponding planar witness silicon shards. Equations are linear fits of all the data (solid line) and the fit that excludes the first data point corresponding to the 20 nm SiO_2 thickness on a witness shard (dashed line). The errors in the slopes and intercepts of the dashed and solid fit lines in the figure are 0.05 and 2.5, and 0.12 and 5.0, respectively.

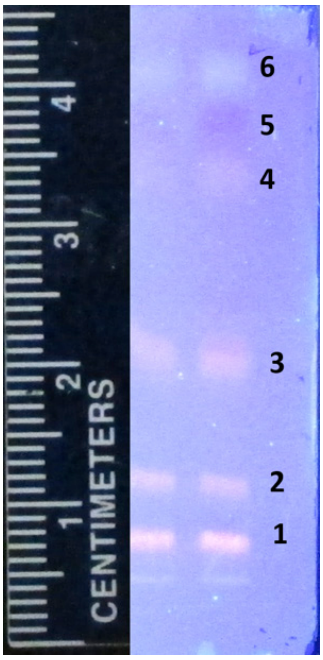

Figure 3.6. Normal phase separation of a CAMAG test dye mixture on an ALD silica-coated TLC plate. The thickness of the silica on the corresponding planar witness samples was 40 nm. The left and right tracks correspond to 1% and 3% dilutions of the standard test dye mixture.

Table 3.1. Migration distances (mm), retardation factors (R_F), efficiencies (plates m^{-1}), values of H_{obs} (μm), and variances of the bands, σ^2_{obs}, (mm^2) in Figure 3.6. RSD of measurements varied from 22-32%

Band	1	2	3	4	5	6
Migration distance	2.62 ± 0.03	6.54 ± 0.16	15.22 ± 0.07	28.99 ± 0.18	32.16 ± 0.15	35.71 ± 0.07
R_F	0.06 ± 0.001	0.16 ± 0.004	0.38 ± 0.002	0.72 ± 0.005	0.80 ± 0.004	0.90 ± 0.002
Plates m^{-1}	39,900	128,000	133,000	126,000	127,000	139,000
H_{obs}	-1.20	0.83	4.68	6.56	3.50	6.14
Variance of band	0.044	0.053	0.12	0.24	0.16	0.27

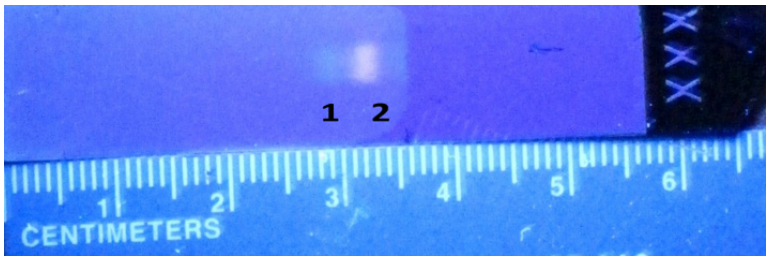

Figure 3.7. Baseline Separations of two flourescent dyes on a microfabricated TLC plate with an amino bonded phase.

Table 3.2. Migration distances (mm), retardation factors (R_F), efficiencies (plates m^{-1}), values of H_{obs} (μm), and variances of the bands (mm^2) in Figure 3.7.

	eosin Y disodium salt	sulforhodamine-B
Migration distance (mm)	26.5	30.8
R_F	0.76 ± 0.09	0.88 ± 0.06
Plates m^{-1}	199,000	170,000
H_{obs} (μm)	3.24	4.26
Variance of band	0.14	0.18

An amino bonded phase was deposited on our new TLC plates in the same way that the bonded phase was prepared in our second and third generation TLC plates .[11, 12] Two fluorescent dyes could be baseline separated in 2.5 min on this plate (see Figure 3.7). The retention factors and numbers of theoretical plates for this separation, which are again high, are given in 3.2. In the future, we will determine the loading capacities of our plates.

3.5. Conclusion

True ALD of silica was performed directly onto carbon nanotube scaffolds. The depositions were conformal. This is the simplest deposition of an inorganic material onto CNTs we have reported to date. The increase in feature diameters varies approximately linearly with the thickness of the SiO_2 deposited onto planar witness substrates. No aluminum is present by XPS. ToF–SIMS confirms an extremely low level of this element. A normal phase, baseline separation of a test mixture of dyes from CAMAG was demonstrated with efficiencies of ca. 40,000–140,000 N m^{-1}. An amino bonded phase was created on this material, and two fluorescent dyes were separated with high efficiency on it.

3.6. Acknowledgment

This work was funded by Diamond Analytics, a US Synthetic Company (Orem, UT).

3.7. References

1. *A. P. Boichenko*, The Open Surface Science Journal **1**, 40-45 (2009).
2. S. R. Jim, A. J. Oko, M. T. Taschuk and M. J. Brett, Journal of Chromatography A **1218** (40), 7203-7210 (2011).
3. S. R. Jim, M. T. Taschuk, G. E. Morlock, L. W. Bezuidenhout, W. Schwack and M. J. Brett, Anal Chem **82** (12), 5349-5356 (2010).
4. A. J. Oko, S. R. Jim, M. T. Taschuk and M. J. Brett, Journal of Chromatography A **1218** (19), 2661-2667 (2011).
5. S. Eeltink, F. Svec and J. M. J. Frechet, Electrophoresis **27** (21), 4249-4256 (2006).
6. Y. H. Han, P. Levkin, I. Abarientos, H. W. Liu, F. Svec and J. M. J. Frechet, Analytical Chemistry **82** (6), 2520-2528 (2010).
7. R. Bakry, G. K. Bonn, D. Mair and F. Svec, Anal Chem **79** (2), 486-493 (2007).
8. I. Urbanova and F. Svec, J Sep Sci **34** (16-17), 2345-2351 (2011).
9. C. L. Shao, H. Kim, J. Gong and D. Lee, Nanotechnology **13** (5), 635-637 (2002).
10. J. E. Clark and S. V. Olesik, J. Chromatogr., A **1217** (27), 4655-4662 (2010).
11. D. S. Jensen, S. S. Kanyal, V. Gupta, M. A. Vail, A. E. Dadson, M. Engelhard, R. Vanfleet, R. C. Davis and M. R. Linford, Journal of Chromatography A **1257**, 195-203 (2012).
12. D. S. Jensen, S. S. Kanyal, N. Madaan, A. J. Miles, R. C. Davis, R. Vanfleet, M. A. Vail, A. E. Dadson and M. R. Linford, J Vac Sci Technol B **31** (3) 031803(1)- 031803(8) (2013).
13. D. S. Jensen, S. S. Kanyal, N. Madaan, J. M. Hancock, A. E. Dadson, M. A. Vail, R. Vanfleet, V. Shutthanandan, Z. H. Zhu, M. H. Engelhard and M. R. Linford, Surf. Interface Anal. **45** (8), 1273-1282 (2013).

14. J. Song, D. S. Jensen, D. N. Hutchison, B. Turner, T. Wood, A. Dadson, M. A. Vail, M. R. Linford, R. R. Vanfleet and R. C. Davis, Adv Funct Mater **21** (6), 1132-1139 (2011).

15. H. Ishikawa, Ifip Trans A **12**, 674-682 (1992).

16. A. Hierlemann, O. Brand, C. Hagleitner and H. Baltes, P Ieee **91** (6), 839-863 (2003).

17. M. S. Talary, J. P. H. Burt and R. Pethig, Parasitology **117**, S191-S203 (1998).

18. A. V. Govindarajan, S. Ramachandran, G. D. Vigil, P. Yager and K. F. Bohringer, Lab Chip **12** (1), 174-181 (2012).

19. H. Becker and L. E. Locascio, Talanta **56** (2), 267-287 (2002).

20. B. A. Peeni, M. L. Lee, A. R. Hawkins and A. T. Woolley, Electrophoresis **27** (24), 4888-4895 (2006).

21. H. R. Li, Y. Yu, S. F. Dana, B. Li, C. Y. Lee and L. F. Kang, J Drug Target **21** (7), 611-629 (2013).

22. P. DelNero, Y. H. Song and C. Fischbach, Biomed Microdevices **15** (4), 583-593 (2013).

23. E. Nuxoll, Adv Drug Deliver Rev **65** (11-12), 1611-1625 (2013).

24. F. Zhang, K. Sautter, A. M. Larsen, D. A. Findley, R. C. Davis, H. Samha and M. R. Linford, Langmuir **26** (18), 14648-14654 (2010).

25. N. Madaan, S. S. Kanyal, D. S. Jensen, M. A. Vail, M. Engelhard and M. R. Linford, surface Science Spectra **20**, 49-54 (2013).

26. D. S. Jensen, S. S. Kanyal, N. Madaan, M. A. Vail, A. E. Dadson, M. Engelhard and M. R. Linford, Surface Science Spectra **20**, 36-42 (2013).

27. N. Madaan, S. S. Kanyal, D. S. Jensen, M. A. Vail, M. Engelhard and M. R. Linford, Surface Science Spectra **20**, 43-48 (2013).

28. N. Madaan, S. S. Kanyal, D. S. Jensen, M. A. Vail, M. Engelhard and M. R. Linford, Surface Science Spectra **20**, 55-61 (2013).

29. D. S. Jensen, S. S. Kanyal, N. Madaan, M. A. Vail, M. Engelhard and M. R. Linford, Surface Science Spectra **20**, 62-67 (2013).

30. S. S. Kanyal, D. S. Jensen, A. J. Miles, A. E. Dadson, M. A. Vail, R. E. Olsen, S. Fabien, J. Nichols, R. Vanfleet, R. Davis and M. R. Linford, J. Vac. Sci Technol. B **31** (3), 031203 (2013).

31. T. Hatanpaa, M. Ritala and M. Leskela, Coordin Chem Rev **257** (23-24), 3297-3322 (2013).

32. D. J. H. Emslie, P. Chadha and J. S. Price, Coordin Chem Rev **257** (23-24), 3282-3296 (2013).

33. M. Mauss and H. Engelhardt, J. Chromatogr., A **371**, 235-242 (1986).

34. L. T. Zhuravlev, Colloids Surf., A **173** (1-3), 1-38 (2000).

35. F. Grossmann, V. Ehwald, C. D. von Hohenesche and K. K. Unger, Journal of Chromatography A **910** (2), 223-236 (2001).

36. L. T. Zhuravlev, React. Kinet. Catal. Lett. **50** (1-2), 15-25 (1993).

37. V. Gupta, H. Ganegoda, M. Engelhard, J. Terry and M. R. Linford, J. Chem. Educ. **91** (2), 232-238 (2013).

38. S. K. Poole and C. F. Poole, J Chromatogr A **1218** (19), 2648-2660 (2011).

39. L. Yang, N. Shirahata, G. Saini, F. Zhang, L. Pei, M. C. Asplund, D. G. Kurth, K. Ariga, K. Sautter, T. Nakanishi, V. Smentkowski and M. R. Linford, Langmuir **25** (10), 5674-5683 (2009).

4. Chapter: Hydroxylation of the Silica in Microfabricated Thin Layer Chromatography Plates as Probed by Time-of-Flight Secondary Ion Mass Spectrometry and Diffuse Reflectance Infrared Fourier Transform Spectroscopy

4.1. Abstract

Microfabricated, silica thin layer chromatography (TLC) plates have previously been prepared on patterned carbon nanotube (CNT) forests. The high temperatures used in their fabrication reduce the number of hydroxyl groups on their surfaces. Fortunately, silica can be rehydroxylated. In diffuse reflectance infrared Fourier transform spectroscopy (DRIFT), a silanol peak below 3740 cm^{-1} indicates a well hydroxylated silica surface that is fit for chromatography. Hydroxylations of our materials with HF are so effective that it is not possible to discern the position of this peak. In contrast, this signal is discernable when the plates are treated with NH_4OH. To find a more convenient method for studying the surfaces of TLC plates, time-of-flight secondary ion mass spectroscopy (ToF-SIMS) was considered. ToF-SIMS is advantageous because multiple microfabricated TLC plates must be scraped to obtain enough silica for one DRIFT analysis, while static SIMS can be performed on very small regions (500 x 500 μm^2 or less) of individual plates. Ratios of the $SiOH^+$ and Si^+ ToF-SIMS signals for microfabricated TLC plates correlated well with the ca. 3740 cm^{-1} silanol peaks from DRIFT. Thus, SIMS allows direct analysis of all of our treated and untreated plates, including those hydroxylated with HF. The best hydroxylation condition for HF, which was better than any studied for NH_4OH, was around 150 ppm at room temperature. The best hydroxylation condition for NH_4OH was 50 ºC for 72 h. ToF-SIMS vs. DRIFT results of commercial TLC plates were also obtained and evaluated.

4.2. Introduction

A conventional thin layer chromatography (TLC) plate consists of a thin, uniform layer of porous silica particles on a planar support. In general, these particles are held to each other and to the substrate with a binder. Some plates also have a fluorescent indicator. This basic structure has not changed substantially in decades. Recently, however, there have been efforts to apply newer technologies and materials to TLC. These have included monolithic silica,[1, 2] electrospun polymer fibers[3, 4] monolithic porous polymer layers,[5, 6] and vacuum deposition of glancing angle deposition (GLAD) structures.[7, 8] Some of us have also been active in this area, microfabricating TLC plates based on infiltrated, patterned carbon nanotube (CNT) forests,[9-12] and characterizing the materials in them.[13-19] This microfabrication is a binder-free approach that potentially offers a great deal of flexibility with regards to feature heights and dimensions. In general, the efficiencies of our plates match or exceed those of commercial HPTLC plates. Their capacities appear to be similar. However, it is our short run times that are perhaps the most distinguishing feature of our plates at present – ca. ½ - 1/3 of those of commercial plates.

Because of its unique surface and material properties, silica has long been the material of primary interest in thin layer chromatography (TLC). At its surface, silica typically shows adsorbed water, siloxane (Si-O-Si) moieties, and vicinal, geminal, and isolated silanol groups.[20] However, the chemistry of silica changes as it is heated. As its temperature is raised, water is increasingly desorbed from its surface. Above 200 ºC, dehydroxylation occurs as a result of condensation between adjacent silanol groups.[21] This process increases the number of isolated silanols at the silica surface, which are detrimental to good chromatography. Heating to ca. 400 ºC results in loss of ca. half of silica's surface silanols, and additional heating causes even greater

surface dehydroxylation. At 1000 ºC only ca. 2% of a silica surface is covered with silanol groups.[20-22]

Silanol groups on silica have been studied by a variety of techniques, including thermogravimetry, solid-state NMR, and diffuse reflectance infrared Fourier transform spectroscopy (DRIFT).[23, 24, 25, 26] In the case of DRIFT, a silanol peak position above 3740 cm^{-1} indicates the presence of isolated silanol groups, which can interact strongly with analytes, while a peak position below this value corresponds to a silica material that is good for chromatography.[27] In general, one can follow the hydroxylation or dehydroxylation of silica with this peak position. It is well known that NH_4OH and HF can be used to hydroxylate the silica used for high performance liquid chromatography (HPLC).[27]

We wished to understand whether the surfaces of the silica nanostructures in our microfabricated TLC plates were well suited for chromatography. FTIR/DRIFT is readily available in many laboratories, including ours, and thus it seemed like the logical tool for this study. However, we found two problems in our efforts to apply DRIFT. First, to obtain enough material for each analysis, it was necessary to scrape at least ten microfabricated TLC plates. Currently, it takes us more than a small amount of effort to make these plates, so DRIFT is clearly not the most convenient technique for us to apply. Second, DRIFT analysis of our *HF* treated TLC plates failed. That is, the 3740 cm^{-1} peak decreased in intensity and became so diffuse that its position could not be accurately determined. We hypothesized that the diffuse nature of this peak was due to effective surface hydroxylation, and it has previously been reported that HF very effectively hydroxylates silica.[27] Accordingly, we looked for another analytical tool that might provide us with additional information about our materials. We do not have ready access to

thermogravimetry and solid-state NMR, and these techniques would again require us to scrape plates – they are destructive. Accordingly, we investigated a surface mass spectrometry tool that would be essentially nondestructive: time-of-flight secondary ion mass spectrometry (ToF-SIMS). ToF-SIMS is a powerful tool for surface and material characterization that is exquisitely sensitive to surface chemistry. For the analysis of our TLC materials, ToF-SIMS could examine very small areas (500 μm x 500 μm or less) at the edges or corners of our plates that are not used in a separation. In addition, ToF-SIMS only samples a small fraction of a monolayer of material from a sample. Thus, ToF-SIMS can be performed on a single plate in an essentially non-destructive manner. We have previously used ToF-SIMS to analyze separated analytes on TLC plates.[28] Finally, we note that X-ray photoelectron spectroscopy (XPS) has also been considered as a surface analytical tool for the quantification of surface silanol groups on silica surfaces. However, SIMS has much higher surface sensitivity, and it is more chemically specific. D'Souza et al. reported that quantifying the silanol concentration at a silica surface by deconvolution of the O 1s and/or Si 2p signals was not possible.[29] Wood et al. also noted that XPS is not well suited for this task.[30]

The microfabricated TLC plates used in this study were prepared by the low-pressure chemical vapor deposition (LPCVD) of silicon onto CNT scaffolds, which was followed by the high temperature (ca. 1000 °C) oxidation of the silicon to silica.[9] This high temperature step removes the CNT scaffolds, leaving white plates upon which analytes can be identified. However, as noted previously, this process also makes a subsequent surface hydroxylation step necessary. Our first attempt at hydroxylation was with NH_4OH at pH 10 for 18 h.[10] No characterization of the hydroxylation state of the resulting plates was reported, and arguably this characterization was unnecessary in this study. A reasonable literature procedure had been followed, and the plates were

covered with a bonded phase before they were used (an amino silane).[31] Our second use of surface hydroxylation was very similar to the first – the same hydroxylation conditions followed by an amino bonded phase.[11] These same hydroxylation conditions were again followed for plates made via LPCVD silicon[9] that were part of a study on the thickness of the iron catalyst used in CNT growth.[32] For this study, no bonded phase was employed, and some surface characterization by DRIFT was reported. Here, our hydroxylated plates showed a silanol peak at 3742.3 cm^{-1}, which suggested incomplete surface hydroxylation, while two commercial TLC plates had peaks at 3736.8 and 3738.5 cm^{-1}. In our most recent report, we used HF – the literature suggests that it is a more effective hydroxylation agent than NH_4OH.[33] For this work, we used our best guess from the literature: 150 ppm HF for 24 h at room temperature.[34] Good, normal phase chromatography took place with these plates. Unfortunately, however, we were unable to prepare enough TLC plates so that a DRIFT analysis could be performed. In the much more complete study reported herein, microfabricated TLC plates were treated with different concentrations of NH_4OH or HF under different experimental conditions. Here, we also report ToF-SIMS vs. DRIFT results obtained from three commercial TLC plates.

We have previously performed SIMS on the materials in our microfabricated TLC plates, including the silica.[14, 35] Other researchers have also been interested in the SIMS of silica. Halfpenny et al. reported the surface modification of silica by irradiation with ultraviolet light followed by analysis with ToF-SIMS.[36] D'Souza et al. determined silanol concentrations on amorphous silica glass surfaces.[37] Wood et al. studied the surface silanol concentrations of low surface area synthetic quartz.[38] All of these researchers recognized the importance of the $SiOH^+/Si^+$ ratio in their ToF-SIMS analyses, and D'Souza et al. also used FTIR in their work.

4.3. Experimental

4.3.1. Fabrication of TLC plates

The TLC plates used in this study were microfabricated by the LPCVD of silicon according to our previously described method.[9] In this preparation, the CNT scaffolds were removed from the plates by air oxidation at 1000 °C for 24 h.

4.3.2. Hydroxylation with NH_4OH

A pH 10.0 solution of NH_4OH (Macron Chemicals, PA) was prepared in deionized water. Hydroxylations were performed with this solution in thick-walled pressure vessels (see Table 4.1 for reaction times and temperatures). *Warning: The combination of the temperatures, pressures, and pH values employed in this process is potentially dangerous.* After each hydroxylation, plates were rinsed with deionized water for 3 min and then dried in an oven at 120 °C for 24 h.

4.3.3. Hydroxylation with HF

Concentrated HF (40%, Sigma-Aldrich, St. Louis, MO) was used to prepare 100, 150, 200, and 400 ppm solutions of HF. Six plates were hydroxylated in each of these solutions for 24 h at room temperature. The plates were then removed and washed with water for 3 min, and finally dried in an oven for 24 h at 120 °C. *Warning: HF is toxic. Prior to using this reagent, individuals should be fully trained, and follow all appropriate safety procedures!*

4.3.4. DRIFT analysis

DRIFT spectra (512 scans) were collected at 4 cm^{-1} resolution using a Thermo Fisher Nicolet 6700 FT-IR spectrometer. These spectra are shown here with Kubelka-Munk units.

4.3.5. Dehydroxylation of commercially available TLC plates

Three commercially available TLC plates from EMD (Damstadt, Germany): HPTLC Silica Gel 60, HPTLC Silica Gel $NH_2F_{254}S$, and Lichrosphere TLC plates were heated to 120 ºC, 300 ºC, 500 ºC, 700 ºC, or 900 ºC for 10 h after which they were analyzed by DRIFT and ToF-SIMS. Microfabricated TLC plates were similarly heated and analyzed after hydroxylation with NH_4OH.

4.3.6. ToF-SIMS

Samples (ca. 1 x 1 cm) of microfabricated and commercial TLC plates were analyzed with an ION-TOF IV instrument (ION-TOF, Münster, Germany). Data were collected in positive and negative ion modes in a ultra-high vacuum chamber with a base pressure of ca. 1 x 10^{-9} Torr. The instrument was equipped with a gallium (Ga^+) liquid metal ion gun. An electron flood gun supplying pulsed, low energy electrons was used for charge compensation. The spectra were collected from a 500 µm x 500 µm scan area. The beam current was 1.8 – 2.5 pA for a total ion dose of $1.3x10^{12}$ – $1.8x10^{12}$ ions/cm^2, which should place our measurements within the static limit of the technique. A single commercial TLC plate provided enough material for the FTIR and ToF-SIMS studies. As noted, multiple (ca. 10) microfabricated TLC plates needed to be scraped to obtain enough material for these analyses. One FTIR analysis was performed on each powder sample. Two positive ion and two negative ion ToF-SIMS analyses were also performed on each sample. $SiOH^+/Si^+$ ratios were calculated from these positive ion spectra. The average value of the two measurements, with its corresponding percent relative standard deviation (%RSD), was then calculated for the sets of data points labeled A, C, D, and E in Figure 4.2. With the exception of two samples, which showed large %RSDs (22.4% and 38.6%), all of the other analyses had %RSD values between 0.05% and

12.0%. If the outliers were included, the average and median values of the %RSD values were 7.6% and 5.5%, respectively. If the outliers were omitted, the average and median values of the %RSD values were 5.0% and 4.2%, respectively.

4.4. Results and Discussion

1.4.1. FTIR Analysis

The high temperature treatment of silica induces the following condensation reaction between associated silanol (SiOH) groups to form siloxane (SiOSi) moieties:[20, 25, 26, 39-44]

(1) $SiOH + SiOH \rightarrow SiOSi + H_2O$

Clearly, this reaction leads to an increasing number of isolated silanol groups at a silica surface. According to Kirkland, good chromatography is possible on silica that shows a silanol peak position below 3740 cm^{-1}, which occurs for associated and geminal, but not isolated, silanols.[27] In previous efforts to hydroxylate our microfabricated TLC plates with pH 10 NH_4OH (room temperature for 18 h) we were unable to get below this threshold (our silanol peak position was 3742.3 cm^{-1}), which suggested incomplete surface hydroxylation.[13] In contrast, signals below this level were found for commercial TLC plates.

Table 4.1. The four different sets of reaction conditions for silica TLC plate hydroxylation with pH 10 NH_4OH.

Temp. (°C)	Time (h)	Coded Temp.	Coded Time	Silanol Peak Pos. (cm^{-1})
50	18	0	0	3739.9
50	72	0	1	3739.0
100	18	1	0	3739.8
100	72	1	1	3740.5

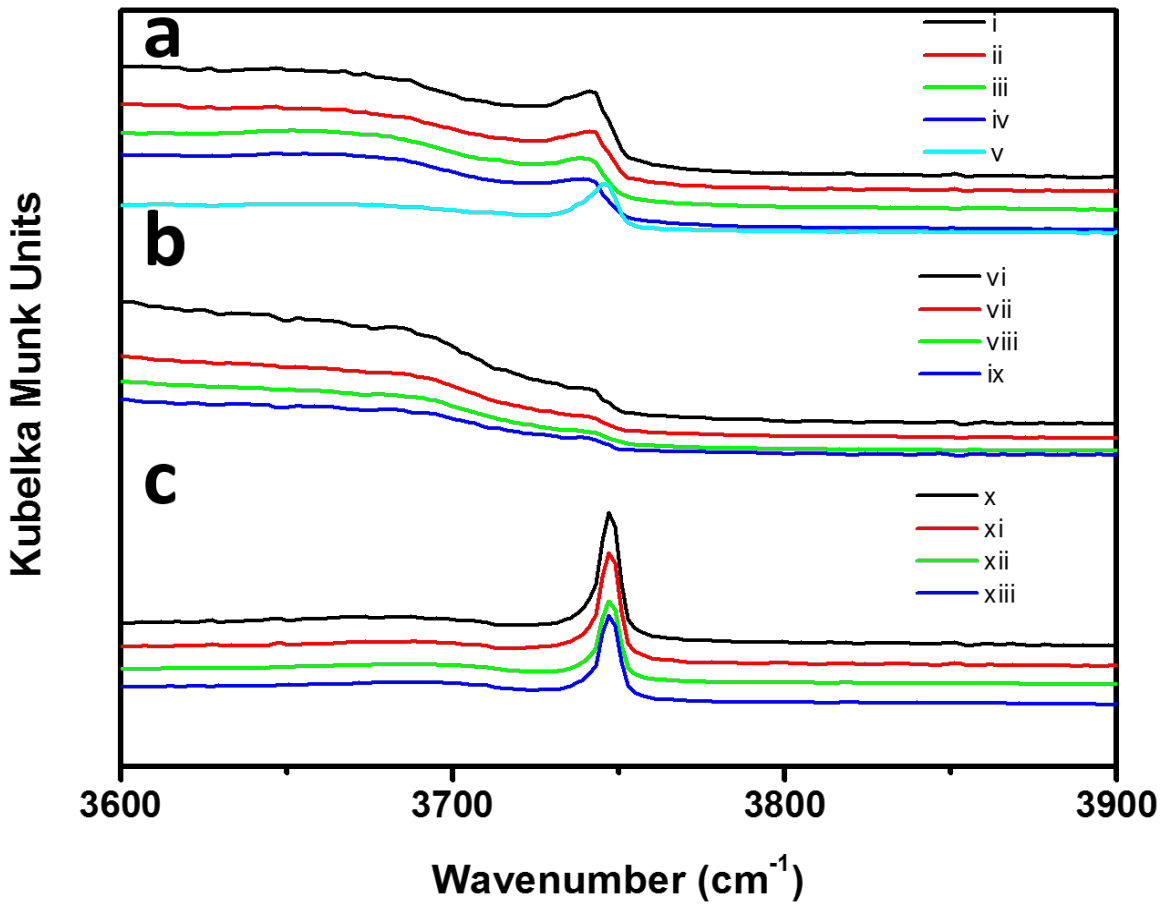

Figure 4.1. DRIFT spectra of microfabricated TLC plates. (a) Plates treated in ammonium hydroxide (NH_4OH) under the following conditions (from top to bottom): (i) 100 ºC, 72 h, (ii) 50 ºC, 18 h, (iii) 100 ºC, 18 h, (iv) 50 ºC, 72 h, and (v) no hydroxylation. (b) Plates treated in hydrofluoric acid (HF) at room temperature for 24 h at the following concentrations (from top to bottom): (vi) 400 ppm, (vii) 200 ppm, (viii) 150 ppm, and (ix) 100 ppm. (c) Plates heated in the air to 800 ºC for 24 h after previous treatment with aqueous HF at 25 ºC (from top to bottom): (x) 400 ppm, (xi) 200 ppm, (xii) 150 ppm, and (xiii) 100 ppm.

Here we have studied different reaction conditions for the NH_4OH and HF treatments of microfabricated TLC plates. For NH_4OH, the four conditions listed in Table 4.1 were explored. The DRIFT spectra from these NH_4OH treated TLC plates are shown in Figure 4.1A. All four of these spectra have silanol peak positions that can be identified. The four conditions in Table 4.1 constitute a two-level, full factorial experimental design. Both the high and the low levels for the temperature variable (50 and 100 °C) were above the level previously studied (room temperature). For the time variable, the low level (18 h) is equal to the amount of time we used previously, and the high level for this variable is four times that amount. For three of these conditions (72 h at 50 °C, 18 h at 50 °C, and 18 h at 100 °C) peak positions below 3740 cm^{-1} were obtained: 3738.9 and 3739.9, and 3739.8 cm^{-1}, respectively. For the 72 h at 100 °C experiment, the microfeatures of the plates were damaged, but the plates could still be scraped and analyzed by FTIR. This plate showed a silanol peak just above the 3740 cm^{-1} threshold (3740.5 cm^{-1}). Using basic matrix algebra and the principles of experimental design[45] the experimental levels were coded (0 for the lower levels, 1 for the higher levels, see Table 4.1), and they were fit to a simple polynomial. The resulting equation for the coded variables is:

(2) silanol peak position (cm^{-1}) = 3739.9 – 0.10*Temp – 1.00*Time + 1.73*Temp*Time

The value of this type of exercise is that it allows one to predict the importance of the different variables and their combination. Thus, in this region of phase space (50 – 100 °C and 18 – 72 h), for the coding scheme created here, and assuming linear relationships, time is a more important

variable than temperature for lowering the silanol peak position, and the combination of time and temperature raises it.

TLC plates were also hydroxylated with 100, 150, 200, and 400 ppm HF for 24 h at room temperature. At 400 ppm, the plates were substantially damaged. Heated HF, i.e., treatment at 50 °C, also damaged the plates, causing delamination of the microfeatures at concentrations as low as 50 ppm. Figure 4.1B shows the DRIFT spectra of microfabricated TLC plates collected after hydroxylation with HF. Here, the peaks around 3740 cm^{-1} are much more diffuse than the peaks corresponding to the NH_4OH treatments. It was inferred from these results that hydroxylation with HF was more effective than with NH_4OH, which would be consistent with Kirkland's findings.[27] An argument in favor of a more diffuse silanol peak from a more hydroxylated surface is that a greater degree of surface hydroxylation will lead to more hydrogen bonding interactions between surface silanols, which will in turn lead to a larger number of possible states for these moieties, and therefore broader peaks. To help confirm this hypothesis, we reasoned that if HF had effectively hydroxylated our TLC plates, it should be possible to reverse this effect by heating. Accordingly, the silica from the HF treated TLC plates was heated to 800 ºC for 24 h. Figure 4.1C shows the DRIFT silanol peaks for these materials. These peaks are now distinct, and their positions, which are all well above 3740 cm^{-1}, can be easily determined.

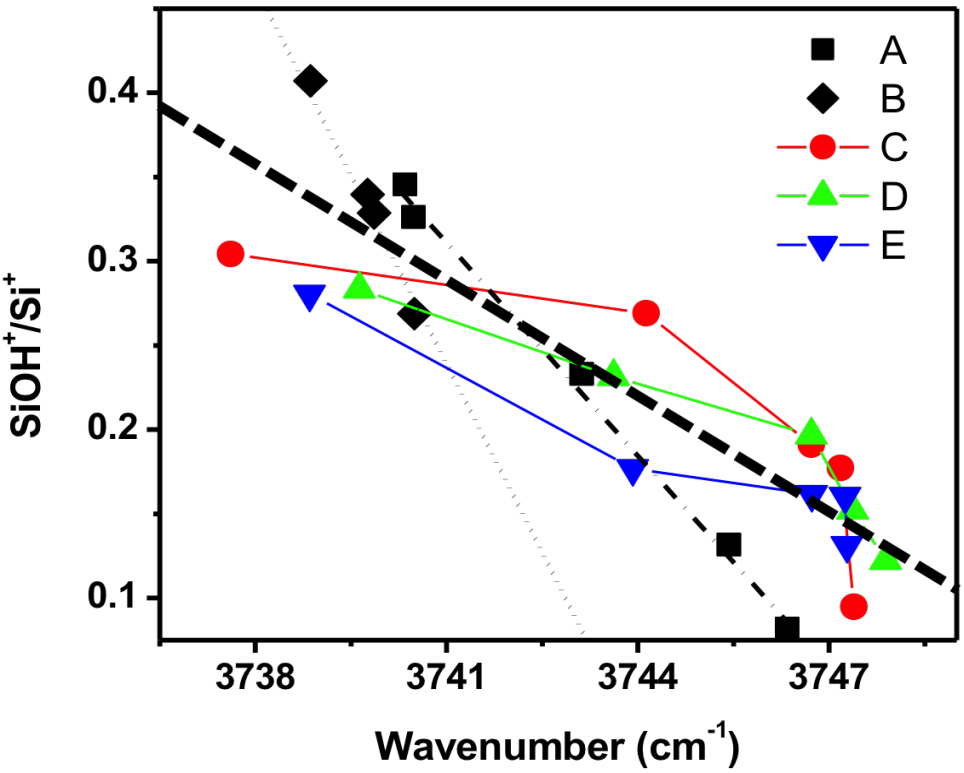

Figure 4.2. Plot of the $SiOH^+/Si^+$ ratio from ToF-SIMS vs. the silanol peak position from DRIFT. A. NH_4OH treated microfabricated TLC plates that were heated (from left to right) to 120, 300, 500, 700, and 800 °C. B. Microfabricated TLC plates that were hydroxylated with pH 10.0 NH_4OH per the conditions in Table 4.1. Commercial HPTLC plates: C. Silica Gel 60, D. Silica Gel $NH_2F_{254}S$, and E. Lichrosphere, treated (from left to right) at 120, 300, 500, 700, and 800 °C. The overall fit to the data (the heavy dashed line) has the equation $y = -0.0227x + 85.19$, $R^2 = 0.791$. See the Experimental for information about the errors in these measurements.

1.4.2. ToF-SIMS Analysis

Because it was not possible to reliably identify the silanol peak positions in DRIFT spectra from HF treated microfabricated TLC plates, it was desirable to find another analytical tool that might give similar information. Accordingly, we investigated time-of-flight secondary ion mass spectrometry (ToF-SIMS), which shows high surface sensitivity. In particular, we looked for a correlation in the DRIFT and ToF-SIMS spectra for: (i) microfabricated TLC plates treated with NH_4OH, (ii) microfabricated TLC plates treated with NH_4OH and then heated to various temperatures to remove a fraction of their silanol groups, and (iii) three different commercial plates that were analyzed after heating. In an examination of the resulting spectra, it was found that the area ratio of the $SiOH^+$ (m/z = 45.00) and Si^+ (m/z = 27.98) peaks ($SiOH^+/Si^+$) in the positive ion ToF-SIMS spectra correlated with the *ca*. 3740 cm^{-1} peak position obtained by DRIFT, where an increase in the $SiOH^+/Si^+$ ratio corresponded to a decrease in the *ca*. 3740 cm^{-1} peak position.

Microfabricated TLC plates treated with NH_4OH showed a linear relationship between their $SiOH^+/Si^+$ ratios obtained by ToF-SIMS and their ca. 3740 cm^{-1} peak positions obtained from DRIFT (see diamonds in Figure 4.2). The four points along this line (from left to right) correspond to the following conditions: 50 °C, 72h; 100 °C, 18h; 50 °C, 18h; and 100 °C, 72h, respectively. The fit line to the resulting data (y = -0.0842x + 315.26) showed an R^2 value of 0.994. $SiOH^+/Si^+$ ratios were also obtained for microfabricated TLC plates treated with NH_4OH (pH 10, 25 °C, 18 h) and then heated to 120, 300, 500, 700, and 800 °C. The plot of the $SiOH^+/Si^+$ ratios vs. DRIFT values for these samples also showed a linear relationship, where these points appear from left to right in Figure 4.2 in order of increasing temperature. These results were as expected – higher temperatures led to lower $SiOH^+/Si^+$ ratios and higher silanol peak positions. The fit line to these

points is y = -0.042x + 157.8 with an R^2 value of 0.99. Interestingly, the linear relationship for these plates is different than the previous one.

Three different types of commercial TLC plates were heated to 120, 300, 500, 700, or 800 °C for 10 h, and then analyzed by DRIFT and ToF-SIMS. After heating to 120 °C, all three types of plates showed silanol peak positions below the 3740 cm^{-1} threshold. After heating to 300 °C, or higher, the silanol peak positions were found above this value. Interestingly, the relationships between the $SiOH^+/Si^+$ ratios and silanol peak positions were *not* linear. It is not entirely clear why this is the case, except that these plates contain a binder, other additives may also be present, and the presence of these chemicals may perturb the surface chemistry of the plates in a way that influences the results of a very surface sensitive technique. Indeed, each type of plate – microfabricated or commercial – has a somewhat different relationship between its $SiOH^+/Si^+$ ratio and its silanol peak position. Nevertheless, the overall trend in all the data from our plates and various commercial plates is clear. The $SiOH^+/Si^+$ ratio decreases with silanol peak position. The heavy, dashed line in Figure 4.2 is the fit for all the data.

Microfabricated TLC plates hydroxylated with 200 ppm, 150 ppm, and 100 ppm HF at room temperature showed $SiOH^+/Si^+$ ratios of 0.53, 0.53, and 0.44, respectively. These are the highest values we found in this study (see Figure 4.2). These results are consistent with our hypothesis, and also literature precedent, that indicate that HF is a very effective hydroxylating agent for silica. The fit line to all the data in Figure 4.2 predicts silanol peak positions of 3729.5, 3729.5, and 3733.5 cm^{-1} for these $SiOH^+/Si^+$ ratios from HF, respectively. These values are well below the 3740 cm^{-1} threshold, and lower than any obtained in this study. Finally, we note again

that good chromatographic performance has been obtained for HF treated, microfabricated TLC plates, which is also consistent with these results.[34]

The results described herein are in good agreement with our latest microfabricated TLC plate preparation and testing. We recently made some new silica-based plates using a deposition chemistry we have not previously reported on. The plates performed poorly after treatment with pH 10 NH_4OH. Their $SiOH^+/Si^+$ ratio by ToF-SIMS was 0.26. Suspecting that their surface chemistry may have been inadequate, the same plates were hydroxylated with HF. Their $SiOH^+/Si^+$ ratio increased to 0.30 and their performance was good.

4.5. Conclusions

The hydroxylation of microfabricated TLC plates with NH_4OH and HF was studied. The best surface hydroxylation obtained with NH_4OH (pH 10) was at 50 ºC for 72 h. The best hydroxylation conditions for HF occurred at either 150 or 200 ppm at room temperature for 24 h. Heated HF was destructive to our materials. NH_4OH and HF treated TLC plates were characterized by DRIFT and ToF-SIMS. In the case of the NH_4OH treatment of freshly prepared plates, we obtained a linear correlation between the ratio of the $SiOH^+$ and Si^+ peaks by ToF-SIMS ($SiOH^+/Si^+$) and the signal of the silanol peak by DRIFT. A linear correlation was also obtained between these figures of merit in an experiment in which NH_4OH treated microfabricated TLC plates were heated to progressively higher temperatures. These correlations suggested that ToF-SIMS could be used to predict the silanol peak position in DRIFT analyses of silica. HF treated plates were also analyzed by ToF-SIMS. Here, ToF-SIMS provides strong support for our hypothesis that HF is a more effective hydroxylating agent for our TLC plates than NH_4OH. At a

minimum, ToF-SIMS should be an effective means of quality control in the manufacture of microfabricated TLC plates. To the best of our knowledge, this is the first application of SIMS to the problem of understanding silica's hydroxylation state for chromatography.

4.6. Acknowledgments

This work was supported by Diamond Analytics, a U.S. Synthetic Company (Orem, UT). LPCVD deposition of silicon was performed at the University of Utah Nanofab (Salt Lake City, UT).

4.7. References

1. A. M. Frolova, O. Y. Konovalova, L. P. Loginova, A. V. Bulgakova and A. P. Boichenko, J Sep Sci **34** (16-17), 2352-2361 (2011).
2. A. M. Frolova, M. A. Chukhlieb, A. V. Drobot, A. P. Kryshtal, L. P. Loginova and A. P. Boichenko, The Open Surface Science Journal **1** (1), 40-45 (2009).
3. J. E. Clark and S. V. Olesik, Anal Chem **81** (10), 4121-4129 (2009).
4. J. E. Clark and S. V. Olesik, J. Chromatogr., A **1217** (27), 4655-4662 (2010).
5. R. Bakry, G. K. Bonn, D. Mair and F. Svec, Anal Chem **79** (2), 486-493 (2007).
6. I. Urbanova and F. Svec, J Sep Sci **34** (16-17), 2345-2351 (2011).
7. L. W. Bezuidenhout and M. J. Brett, J. Chromatogr., A **1183** (1-2), 179-185 (2008).
8. S. R. Jim, M. T. Taschuk, G. E. Morlock, L. W. Bezuidenhout, W. Schwack and M. J. Brett, Anal Chem **82** (12), 5349-5356 (2010).
9. J. Song, D. S. Jensen, D. N. Hutchison, B. Turner, T. Wood, A. Dadson, M. A. Vail, M. R. Linford, R. R. Vanfleet and R. C. Davis, Adv Funct Mater **21** (6), 1132-1139 (2011).
10. D. S. Jensen, S. S. Kanyal, V. Gupta, M. A. Vail, A. E. Dadson, M. Engelhard, R. Vanfleet, R. C. Davis and M. R. Linford, Journal of Chromatography A **1257**, 195-203 (2012).
11. D. S. Jensen, S. S. Kanyal, N. Madaan, A. J. Miles, R. C. Davis, R. Vanfleet, M. A. Vail, A. E. Dadson and M. R. Linford, J Vac Sci Technol B **31** (3) (2013).
12. S. S. Kanyal, D. S. Jensen, A. E. Dadson, R. R. Vanfleet, R. C. Davis and M. R. Linford, J. Plan. Chrom. **27** (3), 151-156 (2014).

13. S. S. Kanyal, D. S. Jensen, A. J. Miles, A. E. Dadson, M. A. Vail, R. E. Olsen, S. Fabien, J. Nichols, R. Vanfleet, R. Davis and M. R. Linford, J. Vac. Sci Technol. B **31** (3), 031203 (2013).

14. D. S. Jensen, S. S. Kanyal, N. Madaan, J. M. Hancock, A. E. Dadson, M. A. Vail, R. Vanfleet, V. Shutthanandan, Z. H. Zhu, M. H. Engelhard and M. R. Linford, Surf. Interface Anal. **45** (8), 1273-1282 (2013).

15. D. S. Jensen, S. S. Kanyal, N. Madaan, M. A. Vail, A. E. Dadson, M. Engelhard and M. R. Linford, Surface Science Spectra **20**, 36-42 (2013).

16. N. Madaan, S. S. Kanyal, D. S. Jensen, M. A. Vail, M. Engelhard and M. R. Linford, Surface Science Spectra **20**, 43-48 (2013).

17. N. Madaan, S. S. Kanyal, D. S. Jensen, M. A. Vail, M. Engelhard and M. R. Linford, surface Science Spectra **20**, 49-54 (2013).

18. N. Madaan, S. S. Kanyal, D. S. Jensen, M. A. Vail, M. Engelhard and M. R. Linford, Surface Science Spectra **20**, 55-61 (2013).

19. D. S. Jensen, S. S. Kanyal, N. Madaan, M. A. Vail, M. Engelhard and M. R. Linford, Surface Science Spectra **20**, 62-67 (2013).

20. L. T. Zhuravlev, Colloids Surf., A **173** (1-3), 1-38 (2000).

21. L. T. Zhuravlev, React. Kinet. Catal. Lett. **50** (1-2), 15-25 (1993).

22. P. G. Righetti, C. Gelfi, R. Sebastiano and A. Citterio, Journal of Chromatography A **1053** (1-2), 15-26 (2004).

23. R. F. de Farias and C. Airoldi, J Therm Anal Calorim **53** (3), 751-756 (1998).

24. S. Ek, A. Root, M. Peussa and L. Niinisto, Thermochim Acta **379** (1-2), 201-212 (2001).

25. A. Ramirez, B. L. Lopez and L. Sierra, Journal of Physical Chemistry B **107** (35), 9275-9280 (2003).

26. M. Mauss and H. Engelhardt, J. Chromatogr., A **371**, 235-242 (1986).

27. J. Kohler and J. J. Kirkland, J. Chromatogr., A **385**, 125-150 (1987).

28. A. A. Parent, T. M. Anderson, D. J. Michaelis, G. L. Jiang, P. B. Savage and M. R. Linford, Appl Surf Sci **252** (19), 6746-6749 (2006).

29. A. S. D'Souza, C. G. Pantano and K. M. R. Kallury, J Vac Sci Technol. A **15** (3) (1997).

30. B. J. Wood, R. N. Lamb and C. L. Raston, Surf Inter Anal **23**, 680-688 (1995).

31. F. Zhang, K. Sautter, A. M. Larsen, D. A. Findley, R. C. Davis, H. Samha and M. R. Linford, Langmuir **26** (18), 14648-14654 (2010).

32. S. S. Kanyal, D. S. Jensen, A. J. Miles, A. E. Dadson, M. A. Vail, R. Olsen, F. Scorza, J. Nichols, R. R. Vanfleet, R. C. Davis and M. R. Linford, J Vac Sci Technol B **31** (3) (2013).

33. J. Kohler and J. J. Kirkland, J Chromatogr **385**, 125-150 (1987).

34. S. Kanyal, D. Jensen, A. Dadson, R. Vanfleet, R. Davis and M. Linford, JPC - Journal of Planar Chromatography - Modern TLC **27** (3), 151-156 (2014).

35. G. L. Jiang, F. Rivera, S. S. Kanyal, R. C. Davis, R. Vanfleet, B. M. Lunt, V. Shutthanandan and M. R. Linford, Opt Eng **50** (1) (2011).

36. D. R. Halfpenny, D. M. Kane, R. N. Lamb and B. Gong, Appl Phys a-Mater **71** (2), 147-151 (2000).

37. A. S. D'Souza, C. G. Pantano and K. M. R. Kallury, Journal of Vacuum Science & Technology a-Vacuum Surfaces and Films **15** (3), 526-531 (1997).

38. B. J. Wood, R. N. Lamb and C. L. Raston, Surf. Interface Anal. **23** (10), 680-688 (1995).

39. L. T. Zhuravlev, Colloid Surface A **74** (1), 71-90 (1993).

40. J. Nawrocki, J. Chromatogr., A **779** (1-2), 29-71 (1997).

41. L. T. Zuravlev, A. A. Agzamkhodzhaev, A. V. Kiselev and K. Y. Shengeliya, Colloid journal of the USSR **36** (6), 1036-1039 (1974).

42. A. A. Christy and P. K. Egeberg, Analyst **130** (5), 738-744 (2005).

43. S. Shioji, M. Hanada, Y. Hayashi, K. Tokami and H. Yamamoto, Adv Powder Technol **18** (4), 467-483 (2007).

44. I. S. Chuang and G. E. Maciel, Journal of Physical Chemistry B **101** (16), 3052-3064 (1997).

45. R. G. Brereton, *Chemometrics: data analysis for the laboratory and chemical plant*. (John Wiley & Sons, 2003).

5. Chapter: Microfabricated Thin-layer Chromatography Plates Prepared via the Low-Pressure Chemical Vapor Deposition of Silicon Nitride

5.1. Abstract

We demonstrate the microfabrication of thin layer chromatography (TLC) plates through the conformal deposition of silicon nitride by low-pressure chemical vapor deposition (LPCVD) onto patterned, carbon nanotube (CNT) scaffolds. After removal of the CNTs and hydroxylation, the resulting normal phase TLC plates show no expansion/distortion of their microfeatures and are robust. Efficiencies of 25,000 plates m^{-1} to 170,000 plates m^{-1} are obtained in the separation of a CAMAG (Muttenz, Switzerland) test dye mixture. Two fluorescent dyes: rhodamine and basic blue 7 could also be well separated with efficiencies from 25,000 plates m^{-1} to 170,000 plates m^{-1}.

5.2. Introduction

Thin layer chromatography (TLC) is a form of liquid chromatography that enjoys a number of important niches. In general, TLC plates are prepared from a slurry of porous silica particles that is spread over a planar substrate. A low concentration of binder is typically present in these plates that adheres the particles to each other and to the substrate. This general design of the plate has not changed significantly in decades. Recently, several groups have applied unconventional methods and materials to TLC plate manufacture. These have included glancing angle deposition (GLAD),[1-3] monoliths,[4-8] and electrospun polymers.[9-11] The Linford group at BYU has also been interested in exploring new materials for TLC. To this end we have prepared patterned, infiltrated, carbon nanotube (CNT)-templated TLC plates based on a zigzag geometry.[12-16]

We have infiltrated/conformally coated our CNTs with a series of inorganic materials in an effort to find a solution that would meet all of the demands of good TLC and also allow for good manufacturability of the plates. We began with the low-pressure chemical vapor deposition (LPCVD) of silicon.[12] In this process, the silicon adhered conformally and directly to the CNTs, and the depositions were rapid. Nevertheless, in the oxidation step that is required for removing the CNTs to create a white background for detection, the silicon underwent a volume expansion (it was converted to SiO_2). As a result, the features of the TLC plates became distorted and their chromatographic performance suffered. We next investigated a fast, ca. 10 nm/cycle, aluminum catalyzed deposition of silicon dioxide.[17] Unfortunately, this silica did not adhere well to the CNTs (the CNTs are expected to be quite inert) so it became necessary to chemically modify them prior to this deposition. Two approaches for priming the CNTs were investigated. In the first, the CNTs were coated with a few nanometers of carbon, followed by a thin film of alumina that was deposited via atomic layer deposition (ALD).[13] In the second approach, the CNTs were lightly oxidized with ozone.[15] After this limited oxidation, the fast deposition of silica proceeded smoothly. Unfortunately, in both approaches aluminum appeared to be present at the surfaces of our final structures, and its presence compromised the resulting chromatography. Fortunately, the chromatography could be improved by the addition of an additive to the mobile phase (triethylamine), and good separations became possible when the aluminum-contaminated silica structures were coated with an aminosilane. Nevertheless, amino plates are not nearly as widely used as pure silica plates. Accordingly, our next attempt was to make a true normal phase (all silica) TLC plate via the ALD of silica.[18] This effort was successful. The resulting plates showed neither the volume expansion of the silicon LPCVD plates, nor the aluminum contamination of

the plates prepared via the fast deposition of silica. True normal phase separations were possible on these plates. Nevertheless, and in spite of the significance of this proof of concept, ALD is a slow process. That is, while the ALD of silica appeared to make plates that were satisfactory for TLC, the manufacturability of this approach was questionable.

In the study reported in this chapter, I believe that I have overcome all of the major issues associated with our previous methods. That is, I describe the LPCVD of silicon nitride (Si_3N_4) onto our CNTs for the preparation of microfabricated TLC plates. This LPCVD silicon nitride deposits directly onto the CNTs in a conformal manner. Depositions appear to be fast enough to be industrially viable. Industrial equipment is available for this purpose. The resulting plates show a high degree of robustness – they are considerably more robust than the plates prepared by the ALD of silica, although these previous plates were adequate for their purposes. Silicon nitride also has the correct chemistry for normal phase TLC. The silicon-nitrogen bond is subject to hydrolysis, so after silicon nitride has been exposed to the water in the air its surface will be silica, which is the desired material for our TLC plates. In addition, because our plates undergo a high temperature oxidation process to remove the CNTs embedded in them, the nitrogen is actually removed from fairly deeply within the plates, yielding a true normal phase, silicon dioxide material. We were also successful in making these TLC plates fluorescent by depositing zinc oxide (ZnO) into the nanowires via ALD.

5.3. Experimental

5.3.1. Photolithography and deposition of alumina and iron

A positive photoresist (AZ3312) was spin coated over a 4-inch silicon wafer (100), exposed to UV light, developed for 40 s with MIF-300 developer, washed with deionized water for a minute, and dried. A thin film of alumina was then deposited by e-beam evaporation. This alumina layer acts as a barrier to prevent poisoning of the iron catalyst with silicon from the substrate. A thin film of the iron catalyst was then thermally evaporated. Other details of this process have been previously reported.[13, 18]

5.3.2. Carbon nanotube growth

Carbon nanotubes were grown by first annealing the iron films in the presence of hydrogen at 750 °C to form iron nanoparticles. The resulting surfaces were then exposed to a hydrocarbon gas to grow CNTs per our previous reports.[13, 16, 18]

5.3.3. Low-pressure chemical vapor deposition (LPCVD) of silicon nitride

Carbon nanotubes were coated with silicon nitride in an LPCVD system (Canary Furnace, CA) at 435 mTorr and 780 °C. The precursor gases flow rates were 80 sccm for ammonia (NH_3) and 20 sccm for dichlorosilane (DCS). These conditions result in deposition of stoichiometric silicon nitride (Si_3N_4).

5.3.4. Oxidation after Si_3N_4 deposition

TLC plates were heated in the air at 600 °C or 1000 °C for 48 h to remove the CNTs and at least partially convert the silicon nitride into silicon dioxide.

5.3.5. Hydroxylation

As a final step in their preparation, the TLC plates were hydroxylated in aqueous ammonium hydroxide at pH of 10.0 at 50 °C for 48 h.

5.3.6. ToF-SIMS and XPS analysis

ToF-SIMS was performed with an ION-TOF (Münster, Germany) instrument equipped with a Ga^+ ion gun. The analysis area was 500 x 500 μm^2. XPS was performed using an SSX-100 X-ray photoelectron spectrometer, which is serviced by Service Physics (Bend, OR). Survey spectra were acquired at a spot size of 800 x 800 μm^2, a resolution of 4, and a step size of 1 eV. For high resolution narrow scans, a spot size of 500 x 500 μm^2 was used. Other parameters included: resolution: 3, number of scans: 20, and step size: 0.065 eV.

5.3.7. Separation of rhodamine and basic-blue 7

A mixture of rhodamine and basic blue 7, both from Sigma-Aldrich (St. Louis, MO), was prepared in ethanol (2 mg/mL). From this stock solution, a 0.2 µg/µL working solution was prepared, also in ethanol. A 0.5 µL aliquot of each of these two dyes was spotted at the same position on the TLC plate using a Linomat V (CAMAG, Muttenz, Switzerland) as a 3 mm band. After spotting, the plate was dried on a hot plate at 120 °C for 15 s, and cooled to room temperature prior to its equilibration in a saturated twin trough chamber (Camag, Muttenz) for 1 min. It was then developed in a t-butylbenzene mobile phase over 25 mm from the point of analyte application.

5.3.8. Separation and DESI-MSI

Some of the separations of BB7 and rhodamine on Si_3N_4 plates were analyzed by desorption electro-spray ionization mass spectrometry imaging (DESI-MSI). Plates were dried on

a hot plate at 120 °C for 10 s before analysis. DESI-MSI was performed in lane-scanning mode to map the entire TLC plate. The distance between two consecutive lanes was 300 µm and plates were continuously scanned in the X direction in unidirectional scanning mode. Each lane along the X-axis was scanned at 112 µm/s and took 223 seconds to complete. Each step in the Y-axis was set at 300 µm. Methanol was used as the spray solvent at a flow rate of 3 µL/min. The total area scanned was 25 mm x 3.4 mm (85 mm^2) producing an array of 112 x 12 (1344 pixels). The spectral rate and rolling average were set at 1 Hz and 2 respectively. The total analysis time was approximately 45 minutes. The molecular ion images were then generated and represented with a false color intensity scale with the relative ion intensities of the analytes represented by different colors.

5.3.9. Separation of CAMAG test dye

A six-dye test solution from CAMAG (Muttenz, Switzerland) that was dissolved in toluene was further diluted in hexanes to a final concentration of 3% of the original solution that was obtained from the vendor. Microfabricated TLC (M-TLC) plates were spotted with 1.5 µL of this solution as 3 mm long bands using a Linomat V spotter. Separations were then performed as previously described using *t*-butylbenzene (3 mL) as the developing solvent over 35 mm from the point of analyte application.

5.3.10. Separations of a food dye mixture

A mixture of food dyes (1.5 µL) was spotted on M-TLC plates with the Linomat V. A developing chamber (Camag, Muttenz) was saturated with the developing solvent (EtOAc/MeOH/H_2O/AcOH 1.5/0.35/0.20/0.01, v/v/v/v) for 3 min. The M-TLC plate was placed

in the developing chamber, equilibrated for 2 min with the vapors of the developing solvent, and then developed with the same solvent for over a developing distance of 55 mm.

5.3.11. Image and data Analysis

All the analyses of images from SEM and digital camera were performed in ImageJ (version 1.42, NIH, USA). We calculated the retardation factors as described previously[18] from:

$$R_F = \frac{Z_s}{Z_{sol}} \quad (1)$$

Z_S represents analyte migration from the application, Z_{sol} represents solvent front migration distance again from the application point.

Numbers of theoretical plates/Efficiencies were calculated using:

$$N = 16\left(\frac{Z_s}{W}\right)^2 \quad (2)$$

W is the analyte band width. Also, observed plate heights, H_{obs} and variances were calculated by using an equation defined by *Poole et al*:[19]

$$H_{obs} = \frac{\sigma^2_{chrom}}{R_F\left(Z_f - Z_o\right)} \quad (3)$$

Z_o is the distance between the solvent entry position and the position of the applied sample spot, and Z_f represents the distance the solvent travels from its entry position. That is, $Z_{sol} = Z_f - Z_o$, and Eq. (3) reduces to:

$$H_{obs} = \frac{\sigma^2_{chrom}}{R_F Z_{sol}} \quad \text{or} \quad H_{obs} = \frac{\sigma^2_{chrom}}{Z_s} \quad (4)$$

We can define σ^2_{chrom} as described by *Poole* et al,[19] as:

$$\sigma^2_{chrom} = \sigma^2_{obs} - \sigma^2_{SA} - \sigma^2_{den} \quad (6)$$

where, σ^2_{obs} is the variance of the developed/separated analyte band, σ^2_{SA} is the variance of the band at its application point, and σ^2_{den} is the variance of the densitometer used. Also, σ^2_{den} = 0 in this case as no densitometer was used. All of the band widths, before and after development, were measured four times in their images with ImageJ, and the corresponding averages were divided by four to give σ^2_{obs} or σ^2_{SA}. In practice, σ^2_{SA} was ca. 0.047 mm^2 for the CAMAG test mixture.

5.3.12. Separations of a food dye mixture

A mixture of food dyes (1.5 µL) was spotted on M-TLC plates with the Linomat V. A developing chamber (Camag, Muttenz) was saturated with the developing solvent (EtOAc/MeOH/H_2O/AcOH 1.5/0.35/0.20/0.01, v/v/v/v) for 3 min. The M-TLC plate was placed in the developing chamber, equilibrated for 2 min with the vapors of the developing solvent, and then developed with the same solvent for over a developing distance of 55 mm.

5.3.13. Preparation of Fluorescent TLC plates

Fluorescent TLC plates were prepared as described below. see Figure 5.1 shows a schematic depicting the final configuration of the plates.

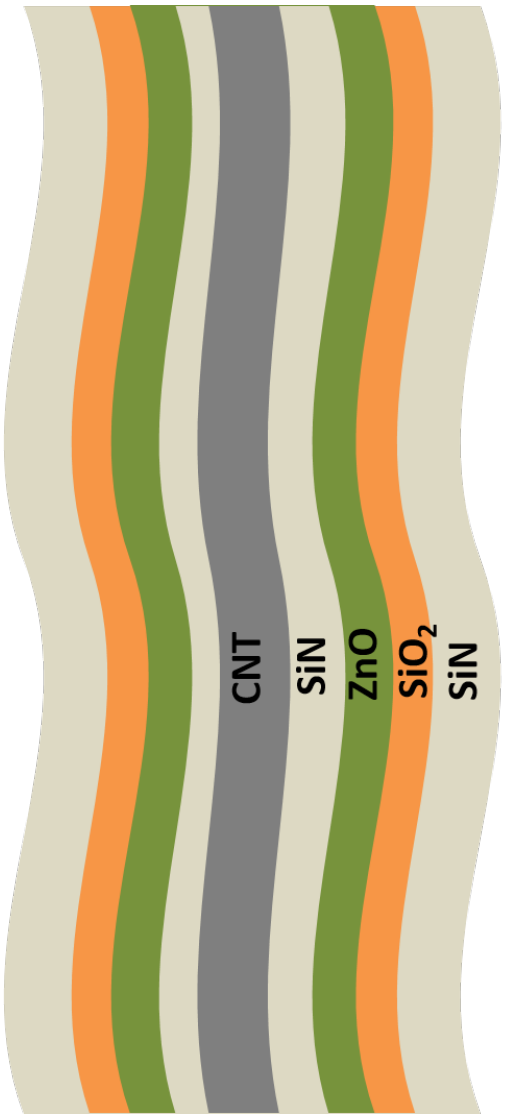

Figure 5.1. Idealized representation of a microfabricated, fluorescent TLC plate.

5.3.14. LPCVD of Si_3N_4 and ALD of ZnO

A thin film of Si_3N_4 (~15 nm) was deposited as described in Figure 5.1. Dimethyl zinc (DMZ) and water were the two ALD precursors for deposition of ZnO. All ALD depositions were done in a Fiji F200 system (Cambridge NanoTech Inc). Figure 5.2a gives the ALD pulse cycle scheme. Further details of this ALD deposition are: DMZ pulse time: 0.1s, purge time 20 s, and H_2O pulse time: 0.1 s, purge time 20 s.

5.3.15. ALD of SiO_2

SiO_2 was deposited via ALD using 3DMAS and O_2 plasma precursors. The parameters used for this process are discussed below (See Figure 5.2b). Further details of this ALD deposition are: 3DMAS pulse time: 0.15s, four times, purge time: 5 s, and O_2 plasma (300 W) pulse time: 20 s, two times, purge time: 5 s.

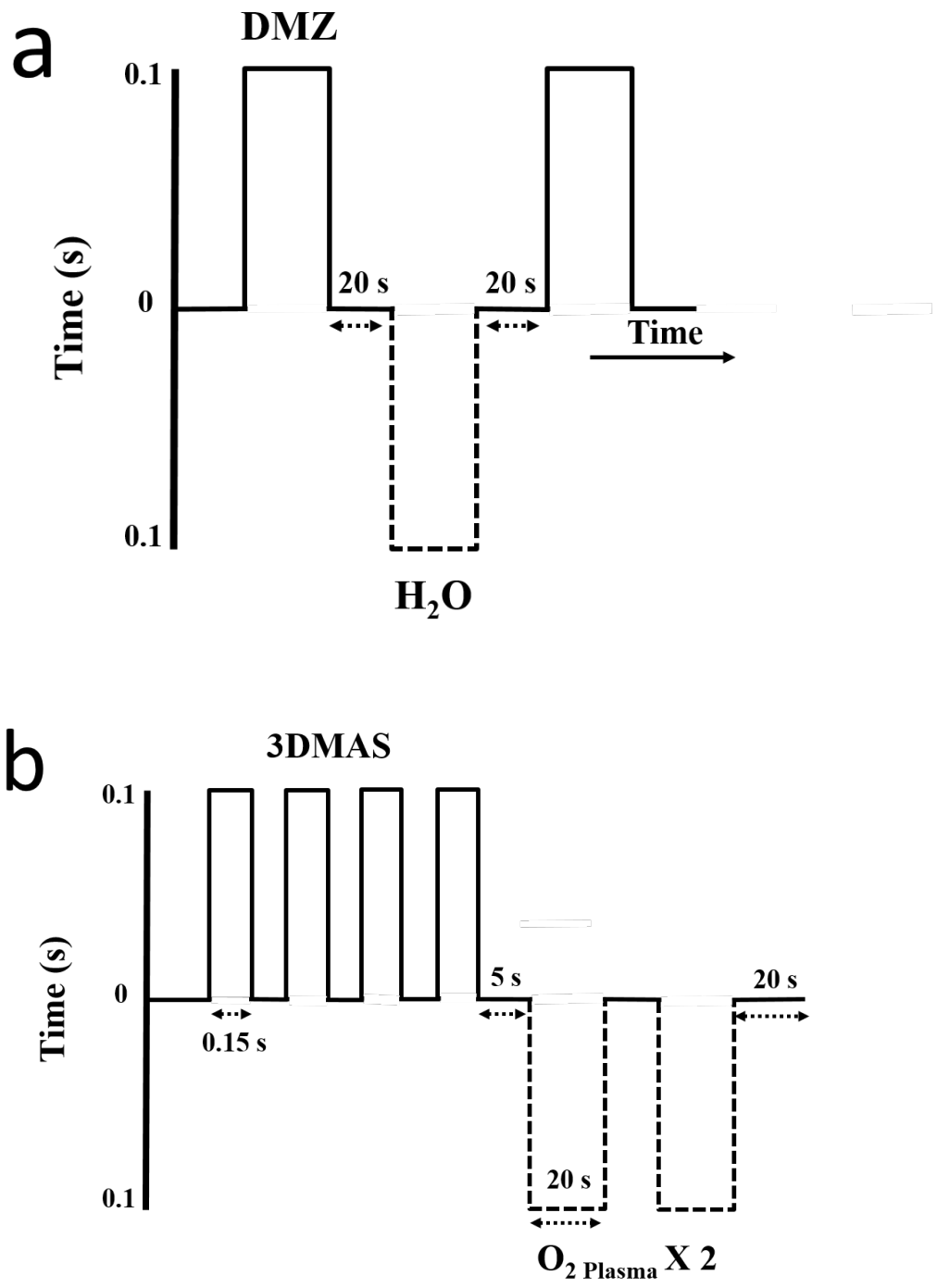

Figure 5.2. Pulse scheme in ALD cycle of films: (a) ZnO (b) SiO_2

5.3.16. *LPCVD of Si_3N_4 over deposited films, oxidation and hydroxylation.*

A thin film (10 nm) of Si_3N_4 was deposited using parameters similar to those described in Section 1.3.3, and then oxidized as described in Sections 1.3.4 and 1.3.5.

5.3.17. *XRD*

X-Ray diffraction (XRD) is a non-destructive tool that probes the crystal structure and d-spacing of materials. A PANalytical X'Pert Pro diffractometer with a Cu X-ray source and a Ge monochromator tuned to the Cu-$K_{\alpha 1}$wavelength (λ = 1.540598 Å) was used to collect X-ray diffraction (XRD) data of SiN/ZnO/SiN film oxidized at 1000 °C. Sample was scanned from 10° to 130° 2θ using a step size of 0.008° at a scan rate of 100 s/step for the X'Celerator detector.

5.3.18. *Separations on fluorescent TLC plates*

Separations of caffeine and amoxicillin were performed on the fluorescent TLC plates. Both compounds were obtained from Sigma Aldrich (St. Louis, MO). A mixture of 1.5 mg/mL of each analyte was prepared in ethanol. The plates were spotted with 3 µL of this solution using the Linomat V 5 mm from the bottom of the TLC plate, and developed by introducing 3 mL of chloroform:methanol:acetic acid (80:15:5 v/v/v) into the development chamber.

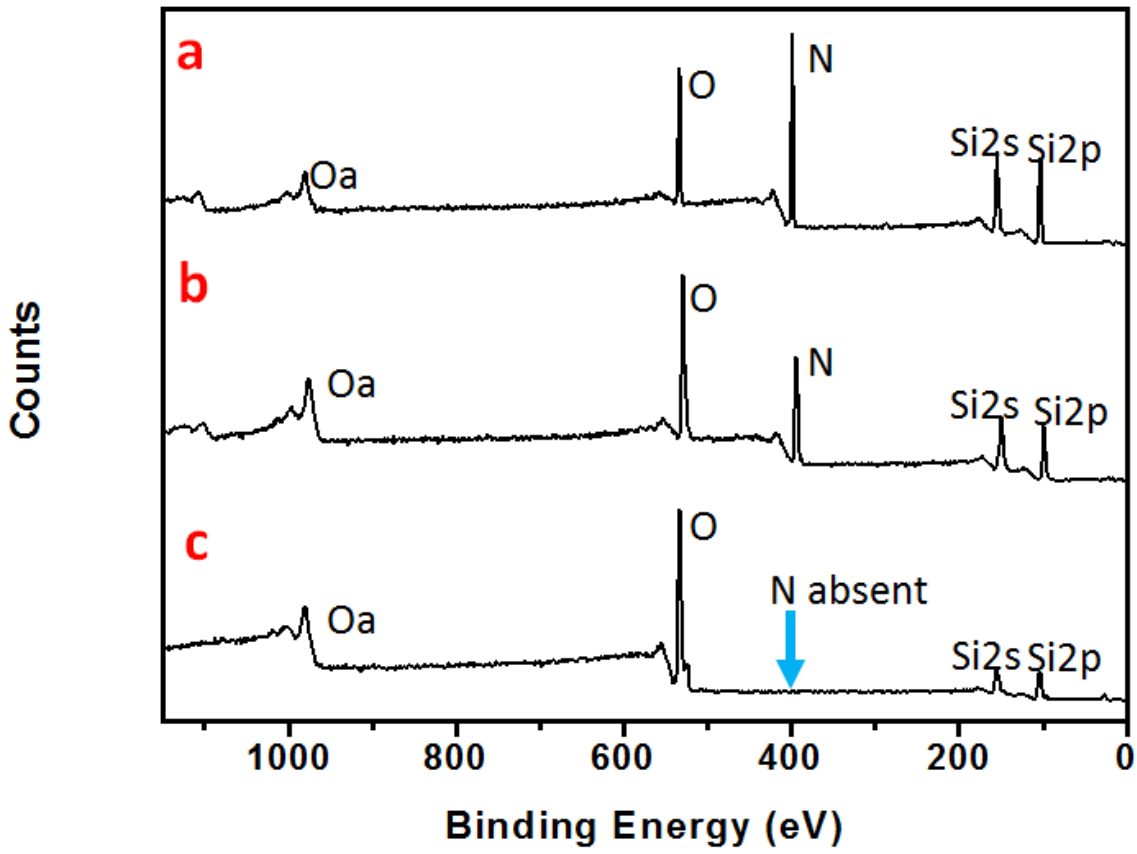

Figure 5.3. XPS survey spectra of microfabricated TLC plates coated with Si_3N_4. (a) After deposition. (b) After oxidation at 600 °C for 48 h, and (c) after oxidation at 1000 °C for 48 h.

5.4. Results

XPS was performed on microfabricated TLC plates coated with Si_3N_4, which revealed strong O, N, and Si signals (Figure 5.3a). The plates were then oxidized at elevated temperature in the air. After oxidation at 600 °C for 48 h, a noticeable decrease in the N 1s signal was observed (see Figure 5.3b). After oxidation at 1000 °C for 48 h, the N 1s signal had disappeared (see also Figure 5.3c), suggesting complete removal of this element. Obviously silicon oxide (not nitride) is the desired material for liquid chromatography, so these transformations are viewed as positive.

SEM micrographs of Si_3N_4 coated CNTs showed uniform deposition of Si_3N_4 onto the CNTs (see Figure 5.4). Witness wafers were also used to monitor the Si_3N_4 deposition, which were found to have 37 nm of Si_3N_4 when measured via a Nanospec 3000 thickness monitor (Nanometrics, CA). After oxidation at 1000 °C feature expansion was not observed (see Figure 5.5). If any distortions in the plates had occurred during oxidation, they would be expected to decrease the efficiencies of the resulting TLC separations. The van Deemter equation is often used to analyze separation efficiency in chromatography:

$$H = A + B/u + Cu$$

where H is the plate height for a separation, A is the eddy diffusion term, which accounts for randomness/irregularity in the channel bed, B represents contributions from longitudinal diffusion, and C represents resistance to mass transfer in the radial direction (in a column, i.e., perpendicular to the direction of flow) in both the mobile and stationary phase. Potentially, all three terms of the van Deemter equation would be raised by irregularities in the stationary phase.

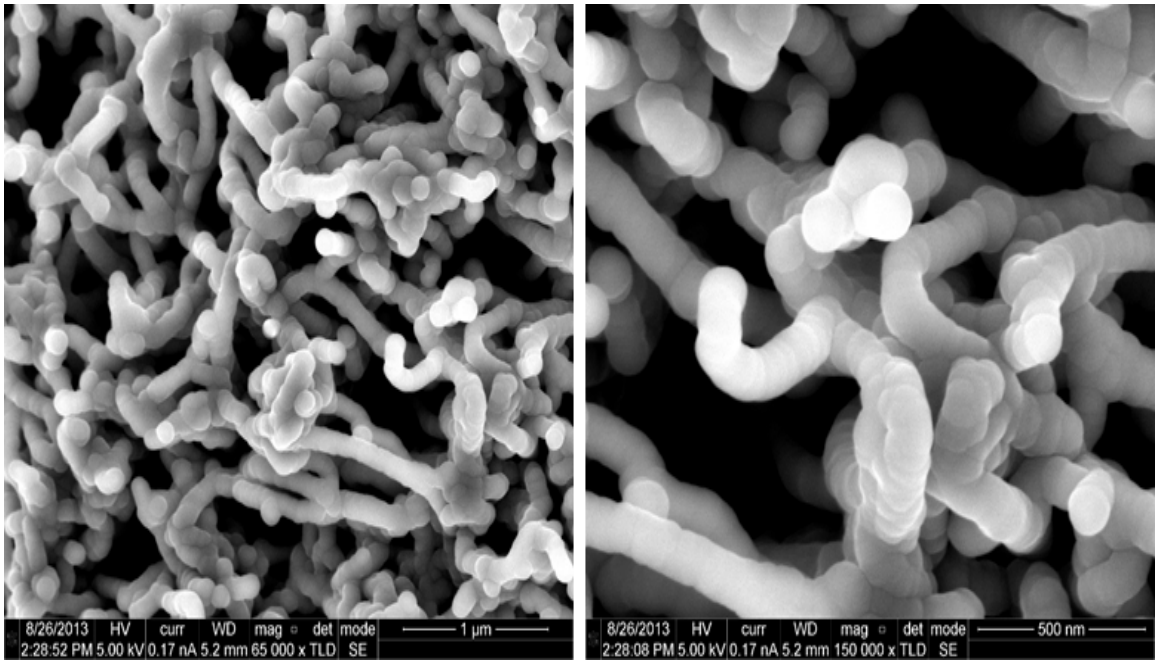

Figure 5.4. SEM micrographs of CNTs coated with Si_3N_4 (before oxidation).

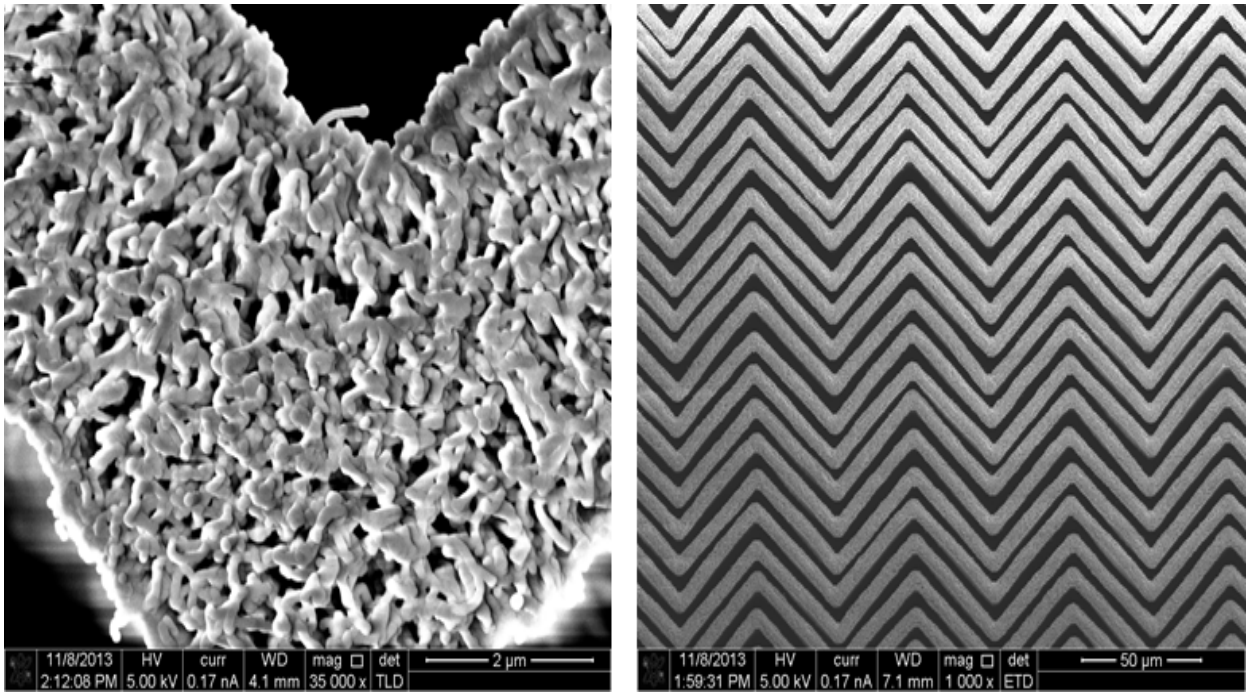

Figure 5.5. SEM micrographs of a microfabricated TLC plate after oxidation at 1000 °C. No expansion or distortions of the features was observed here.

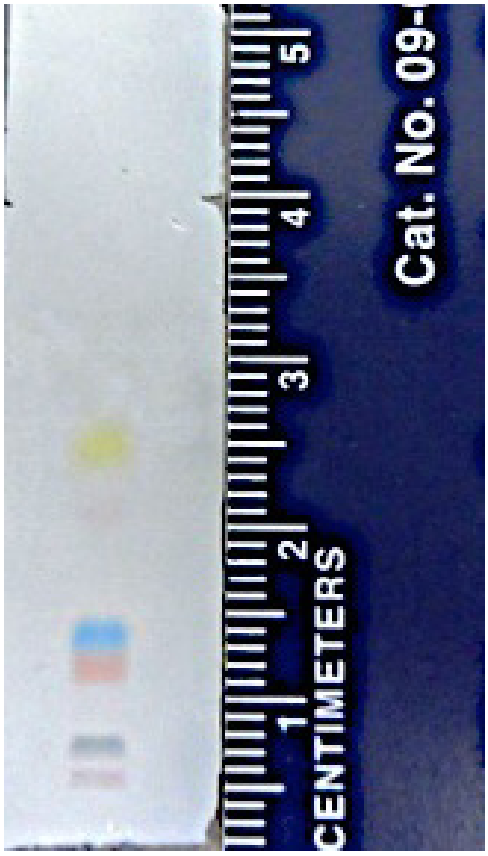

Figure 5.6. Normal phase separation of a CAMAG test dye mixture on a silicon nitride TLC plate. The thickness of the silicon nitride on the corresponding planar witness samples was 37 nm. Development solvent: *t*-butylbenzene. Run time: 3 min 15 sec.

Table 5.1. Migration distances (mm), retardation factors (R_F), efficiencies (plates m^{-1}), values of H_{obs} (μm), and variances, σ^2_{obs}, (mm^2) of the bands in Figure 5.6.

Band	1	2	3	4	5	6
Migration distance	0.41 ± 0.10	2.24 ± 0.06	7.00 ± 0.20	8.77 ± 0.10	16.22 ± 0.19	19.85 ± 0.22
R_F	0.01±0.28	0.06±0.002	0.20±0.006	0.25±0.003	0.46±0.005	0.57±0.006
Plates m^{-1}	24,300	94,300	92,200	82,700	173,000	133,000
H_{obs}	4.39	5.42	9.20	10.70	4.88	6.90
Variance of band	0.12	0.16	0.28	0.32	0.31	0.39

After SEM, separations were attempted on the TLC plates. For example, a CAMAG test mixture of six dyes could be well separated (see Figure 5.6), producing bands that were narrow and tight. Efficiencies for these bands ranged from 28,225 – 171,696 plates/m (see Table 5.1), which is quite high for TLC. These efficiencies were better than those we previously obtained with our normal phase ALD plates.

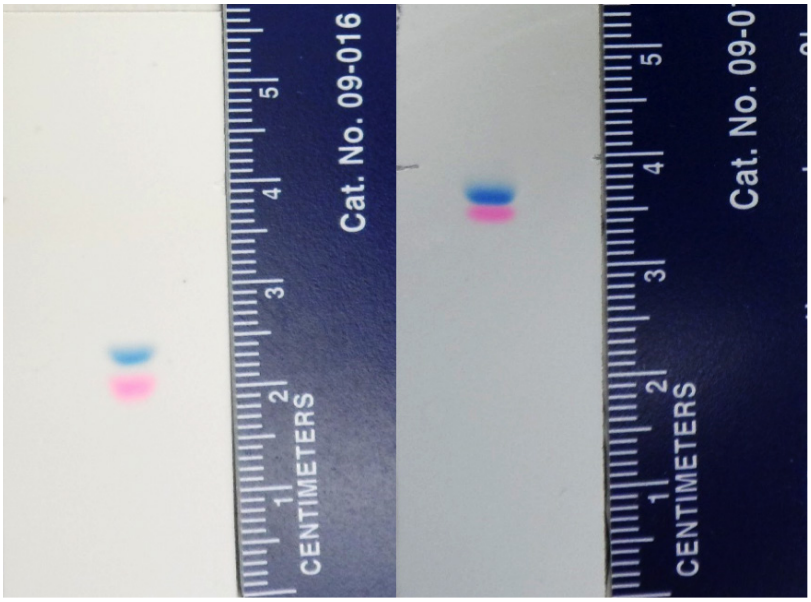

Figure 5.7. Normal phase separation of a BB7 and rhodamine dye mixture on (a) a Merck TLC plate, and (b) M-TLC-plates. Development solvent: EtOAc:MeOH:H_2O (75:15:10). Run times: 1 min 15 s and 3 min 43 s for M-TLC and Merck TLC plates, respectively.

Table 5.2. Migration distances (mm), retardation factors (R_F), efficiencies (plates m^{-1}), values of H_{obs} (μm), and variances of the bands, σ^2_{obs}, (mm^2) in Figure 5.7

	MTLC		HPTLC	
	1	2	1	2
Migration distance	29.80 ± 0.09	31.42 ± 0.18	20.07 ± 0.22	23.18 ± 0.16
R_F	0.85 ± 0.002	0.89 ± 0.005	0.57 ± 0.006	0.66 ± 0.005
Plates m^{-1}	310,000	254,000	219,000	134,000

Figure 5.7 shows a baseline separation of a mixture of rhodamine and BB7 on a microfabricated silicon nitride TLC plate. This separation was compared to a separation of the same analytes on a commercial TLC plate from Merck. Table 5.2 compares the R_F and plate m^{-1} values for the two plates. The run times of the M-TLC plate and the Merck plate were 1 min 28 s and 3 min 58 s respectively. Clearly the M-TLC plate allows separations to be performed more quickly than with commercial materials. Finally, a separation of food dyes showed extremely narrow bands (see Figure 5.8). The quality of this separation points to the robustness and efficacy of these TLC plates.

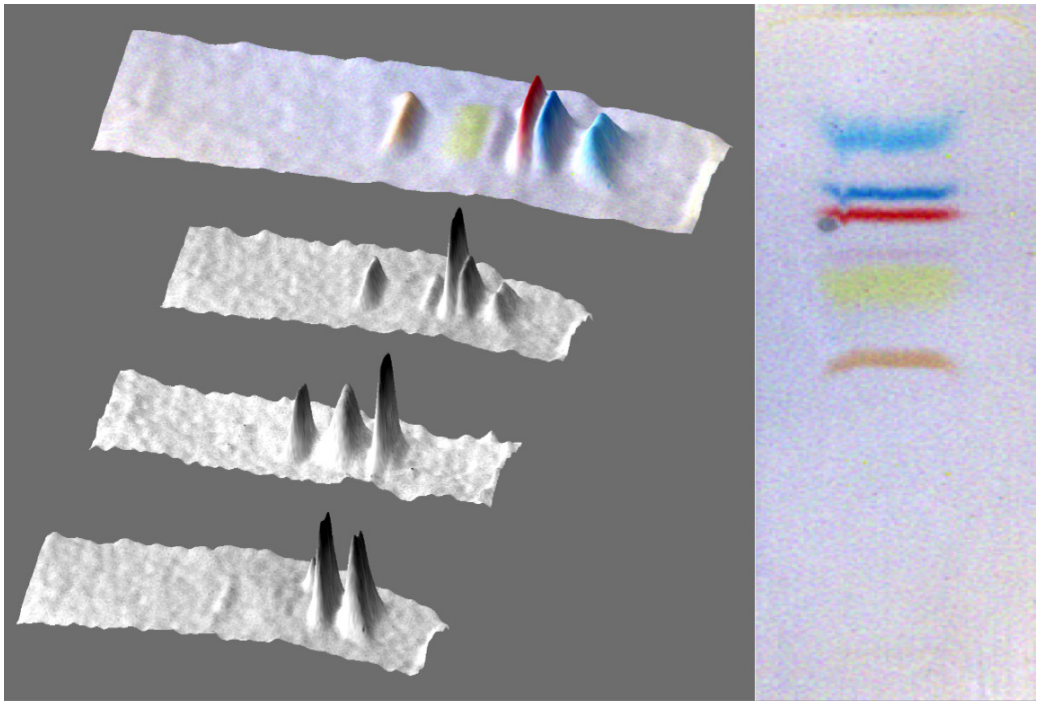

Figure 5.8. Normal phase separation of a mixture of food dyes on a microfabricated TLC plate that was initially coated with silicon nitride. Development solvent: EtOAc/MeOH/H_2O/AcOH (1.5/0.35/0.20/0.01 v/v/v/v). Left: multiple wavelength scans. Right: chromatogram.

Part of this current effort to prepare silicon nitride-based TLC plates was to make them fluorescent. This was achieved by depositing a very thin film of ZnO into the plates using ALD with dimethylzinc and water as precursors. Due to the large surface areas of our CNTs, more than usual dose of precursor was employed and various conditions and parameters, including dose pulse times and multiple pulses of the same precursor, were tried. It was evident that high doses of the precursor resulted in the deposition of Zn/ZnO nanoparticles, as shown in the TEM images in Figure 5.9. The formation of zinc metal was observed by Libera *et al.* in their ALD deposition of ZnO onto high surface area silica. After the attempted deposition of ZnO, silicon nitride was deposited on the plates to cover the fluorescent material.

Silicon nitride plates coated with ZnO by ALD showed some fluorescence at their edges (see Figure 5.10a). However, Figure 5.10b shows that the direct deposition of silicon nitride over this ZnO layer results in a quenching of this fluorescence. A possible explanation for this is a reaction between a byproduct of the LPCVD process (HCl) and the ZnO. Accordingly, a thin barrier layer of SiO_2 was deposited over the ZnO. Figure 5.11 shows a fully fluorescent TLC plate that was made by depositing additional Si_3N_4 over the ZnO/SiO_2. It should be emphasized that these results were not obtained every time, and that further exploration of these deposition conditions is needed. To characterize the oxidized, fluorescent TLC plates, XRD was performed (Figure 5.12). Interestingly, the XRD pattern matched that of zinc silicate (Zn_2SiO_4). It is of significance that Zn_2SiO_4 particles are used as a fluorescent indictor in commercially available TLC plates.

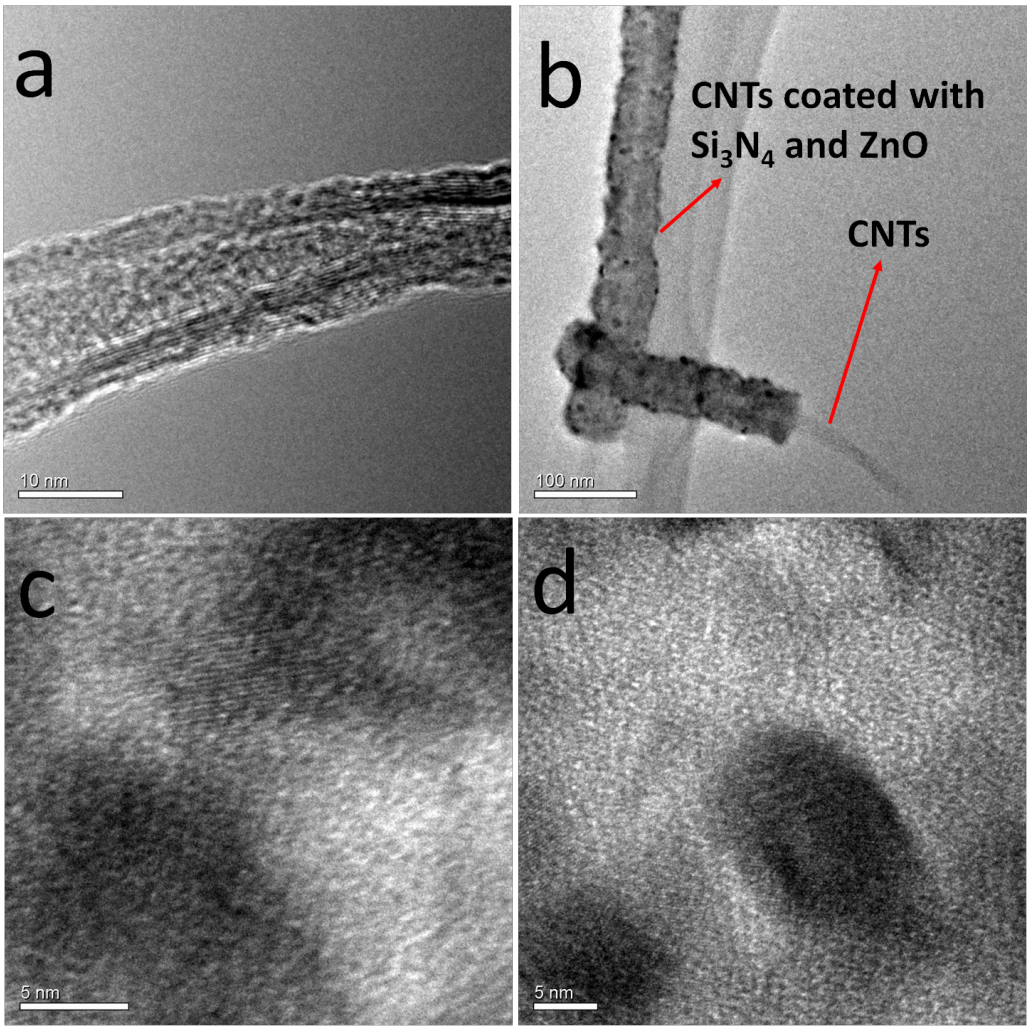

Figure 5.9. TEM images of ZnO coated CNTs showing crystals of Zn/ZnO deposited at high Zn precursor concentration.

Figure 5.10. TLC plates made by depositing (a) Si_3N_4/ZnO (fluorescent at its edge) and (b) Si_3N_4/ZnO/Si_3N_4 (not fluorescent).

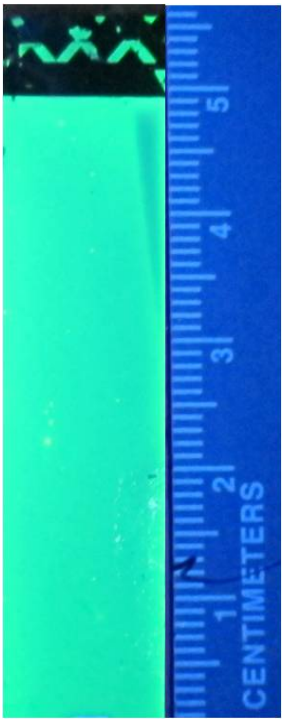

Figure 5.11. A fluorescent silicon nitride TLC plates prepared by depositing $Si_3N_4/ZnO/SiO_2/Si_3N_4$.

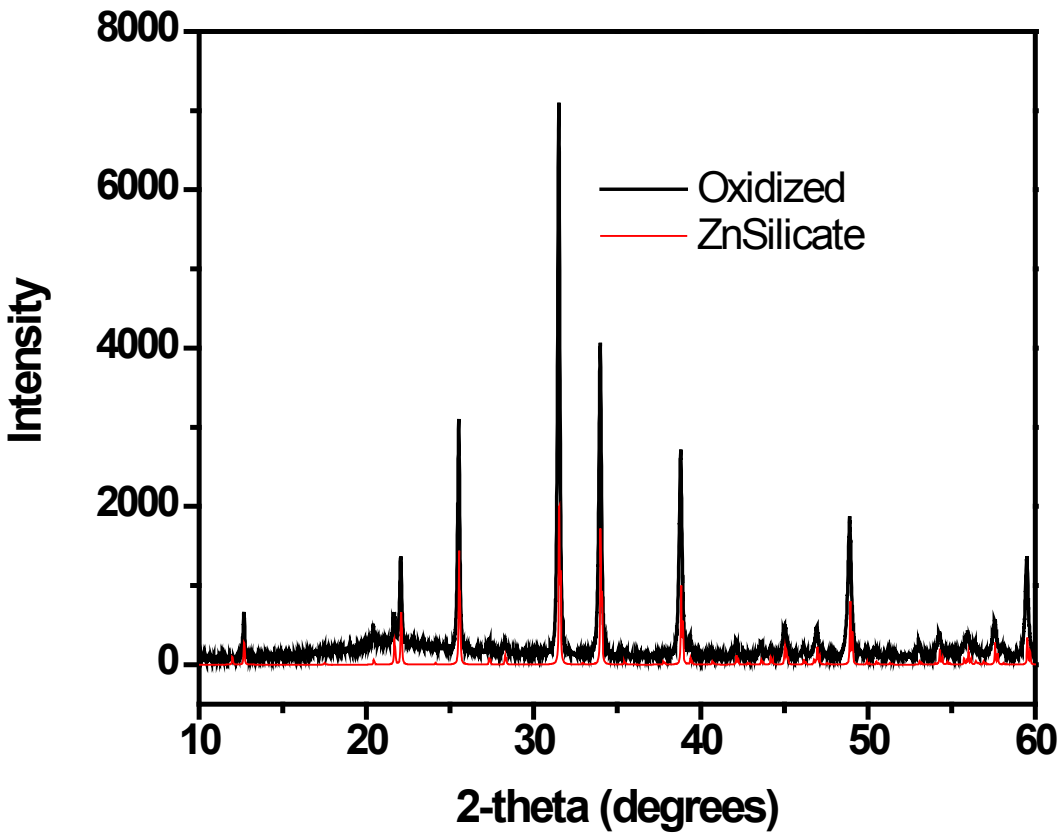

Figure 5.12. XRD spectra of an oxidized TLC plate made by depositing Si_3N_4/ZnO onto CNTs, compared to the spectrum of zinc silicate from an online database.

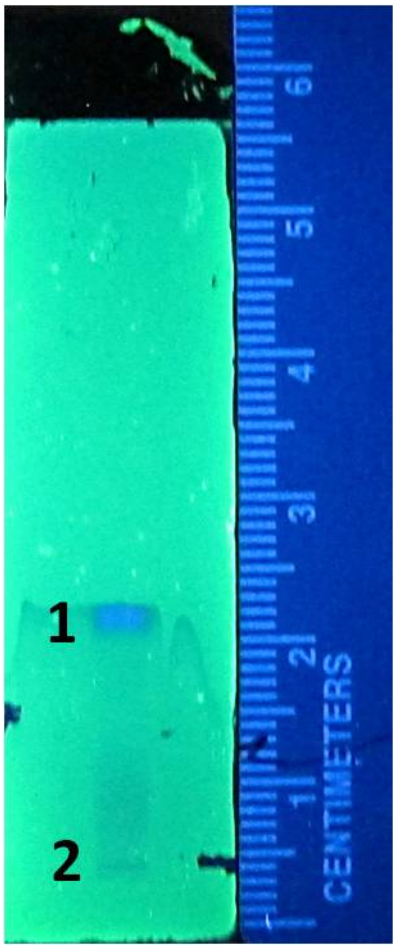

Figure 5.13. Separations of caffeine (1) and phenacetin (2) on a fluorescent, microfabricated TLC plate. Development solvent: chloroform:methanol:acetic acid (80:15:5, v/v/v). The analyte solution consisted of 1.5 mg/mL each of caffeine and phenacetin in ethanol respectively. Development time: 0:50 min.

Separations were attmpted on fluorescent TLC plates. To wit, a mixture of caffeine (1) and amoxicillin (2) could be well separated and detected against a green background, as shown in Figure 5.13. The TLC plates made with this method were robust and could be used with additional detection methods like DESI-MSI.

Figure 5.14 shows the optical image of a developed M-TLC plate prior to DESI analysis (part A), the selected m/z selected mass spectrometric image of BB7 and rhodamine B (part B and C, respectively), the direction of the scan (part D), and relative intensity graphs from two spots on the M-TLC plate for the dyes (part E and F). The molecular ion images generated were represented with a false color intensity scale with relative ion intensities of the analytes represented by different color intensities. A red color in the images represents the highest intensity ions and black represents the lowest intensity ions.

5.5. Conclusions

Normal phase TLC plates were prepared by depositing Si_3N_4 onto CNTs and then removing the CNTs by oxidation. Separations of a CAMAG test dye mixture, two other dyes, and a mixture of food dyes are shown. Efforts were made to prepare fluorescent plates to enable detection on them. This was achieved by conformally coating silicon nitride nanotubes with ZnO via atomic layer deposition. The oxidation of the TLC plates converts the ZnO to zinc silicate as determined by XRD. The plates showed green fluorescence when observed under UV light at 254 nm. A mixture of caffeine and amoxicillin could be separated and detected against the green fluorescent background. DESI was possible on these plates.

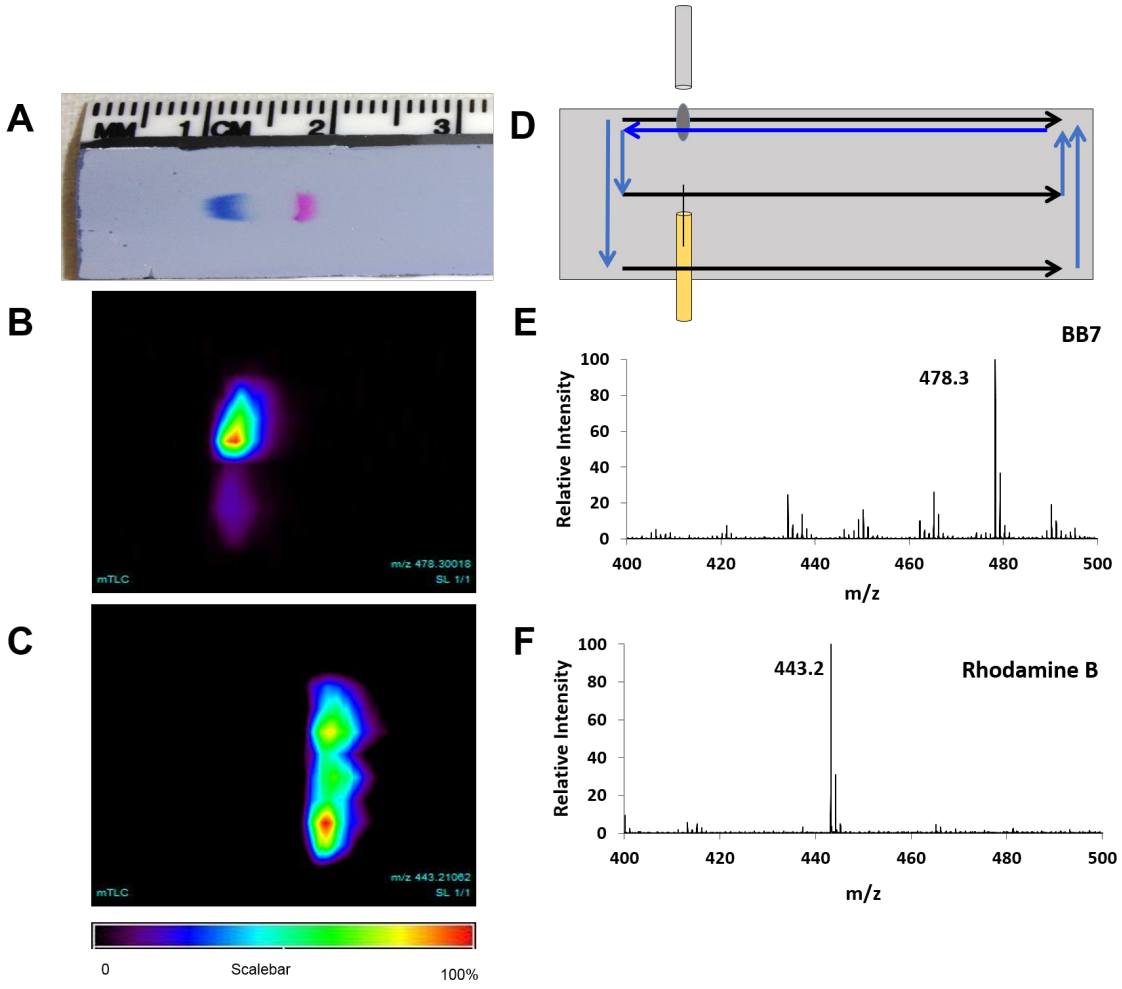

Figure 5.14. Detection with DESI-MSI of a separated mixture of analytes on an M-TLC plate. Concentration of analytes spotted: basic blue 7 (0.2 µg/µL) and rhodamine B (0.2 µg/µL). Spotting volume: 3 µL each. M-TLC mobile phase: t-butylbenzene. Elution distance: 25 mm. Spray solvent: methanol. Solvent flow rate: 3 µL/min. (A) Optical image of developed M-TLC plate. The blue spot and the red spot on the TLC plate are BB7 and rhodamine B, respectively. (B) Molecular ion image of the BB7 dye recorded by DESI. (C) Molecular ion image of rhodamine B recorded by DESI. (D) Black arrows followed by blue arrows show the route of the probe during the automated lane scanning of the TLC plate. (E) Relative intensity graph of the BB7 dye from a spot on the TLC plate. (F) Relative intensity graph of rhodamine B dye from a spot on the TLC plate. Images A, B and C have the same orientation.

5.6. References

1. L. W. Bezuidenhout and M. J. Brett, J. Chromatogr., A **1183** (1-2), 179-185 (2008).
2. S. R. Jim, A. J. Oko, M. T. Taschuk and M. J. Brett, Journal of Chromatography A **1218** (40), 7203-7210 (2011).
3. A. J. Oko, S. R. Jim, M. T. Taschuk and M. J. Brett, Journal of Chromatography A **1218** (19), 2661-2667 (2011).
4. A. M. Frolova, O. Y. Konovalova, L. P. Loginova, A. V. Bulgakova and A. P. Boichenko, J Sep Sci **34** (16-17), 2352-2361 (2011).
5. *A. P. Boichenko*, The Open Surface Science Journal **1**, 40-45 (2009).
6. S. Eeltink, F. Svec and J. M. J. Frechet, Electrophoresis **27** (21), 4249-4256 (2006).
7. R. Bakry, G. K. Bonn, D. Mair and F. Svec, Anal Chem **79** (2), 486-493 (2007).
8. I. Urbanova and F. Svec, J Sep Sci **34** (16-17), 2345-2351 (2011).
9. J. E. Clark and S. V. Olesik, Anal Chem **81** (10), 4121-4129 (2009).
10. C. L. Shao, H. Kim, J. Gong and D. Lee, Nanotechnology **13** (5), 635-637 (2002).
11. J. E. Clark and S. V. Olesik, J. Chromatogr., A **1217** (27), 4655-4662 (2010).
12. J. Song, D. S. Jensen, D. N. Hutchison, B. Turner, T. Wood, A. Dadson, M. A. Vail, M. R. Linford, R. R. Vanfleet and R. C. Davis, Adv Funct Mater **21** (6), 1132-1139 (2011).
13. D. S. Jensen, S. S. Kanyal, V. Gupta, M. A. Vail, A. E. Dadson, M. Engelhard, R. Vanfleet, R. C. Davis and M. R. Linford, Journal of Chromatography A **1257**, 195-203 (2012).
14. S. S. Kanyal, D. S. Jensen, A. J. Miles, A. E. Dadson, M. A. Vail, R. E. Olsen, S. Fabien, J. Nichols, R. Vanfleet, R. Davis and M. R. Linford, J. Vac. Sci Technol. B **31** (3), 031203 (2013).

15. D. S. Jensen, S. S. Kanyal, N. Madaan, A. J. Miles, R. C. Davis, R. Vanfleet, M. A. Vail, A. E. Dadson and M. R. Linford, J Vac Sci Technol B **31** (3), 031203 (2013).

16. D. S. Jensen, S. S. Kanyal, N. Madaan, J. M. Hancock, A. E. Dadson, M. A. Vail, R. Vanfleet, V. Shutthanandan, Z. H. Zhu, M. H. Engelhard and M. R. Linford, Surf. Interface Anal. **45** (8), 1273-1282 (2013).

17. D. Hausmann, J. Becker, S. L. Wang and R. G. Gordon, Science **298** (5592), 402-406 (2002).

18. S. S. Kanyal, D. S. Jensen, A. E. Dadson, R. R. Vanfleet, R. C. Davis and M. R. Linford, J. Plan. Chrom. **27** (3), 151-156 (2014).

19. S. K. Poole and C. F. Poole, J Chromatogr A **1218** (19), 2648-2660 (2011).

6. Chapter: ToF-SIMS of Silicon (100)/SiO_2

6.1. Abstract

We report the time-of-flight secondary ion mass spectrometry (ToF-SIMS) of Si (100)/SiO_2. Both positive and negative ion spectra were obtained using a cluster ion source (Bi_3^{2+} primary ions at 50 keV). Si^+ is the base peak in positive ion mode. The negative ion spectrum shows signals characteristic of the native oxide: SiO_2^-, SiO_2H^-, SiO_3^-, and SiO_3H^-.

6.2. Introduction

Silicon wafers are used extensively in various industries for fabrication of integrated circuits, biomedical devices, solar cells, micromachinets, etc.[1-5] Silicon is also used heavily in research laboratories. ToF-SIMS is a powerful tool for examining the composition and chemical states of surfaces. In essence, SIMS functions by generating and detecting the secondary ions formed by sputtering. ToF-SIMS was performed on silicon wafers in both positive and negative ion modes using Bi_3^{2+} cluster ions. Si^+ was the strongest signal (base peak) in positive ion mode (see Figure 6.1). The positive ion spectrum also showed a series peaks attributable to hydrocarbon contamination on the surface, i.e., CH_x^+, $C_2H_x^+$, $C_3H_x^+$, $C_4H_x^+$, etc., and a noticeable peak corresponding to ammonium (NH_4^+). The positive ion spectrum showed that the sample was free of contamination from metals such as aluminum (Al^+), calcium (Ca^+), and iron (Fe^+), although sodium (Na^+) and a small amount of potassium (K^+) were present. The expected peaks corresponding to silicon, i.e., $^{28}Si^+$, $^{29}Si^+$, and $^{30}Si^+$ were observed. The negative ion SIMS spectrum showed signals from the native oxide: SiO_2^-, SiO_2H^-, SiO_3^-, and SiO_3H^- as well as signals

from other contaminants, e.g.,fluorine (F^-), chlorine (Cl^-), CN^-, CNO^-, and sulphates (see Figure 6.3). The Si silicon substrate described herein is an essential part of the materials created in the preparation of microfabricated thin layer chromatography (TLC) plates.[7-11] Indeed, submissions to Surface Science Spectra have been made on the XPS and SIMS characterization of the key materials in this microfabrication, including the silicon substrate,[12] an alumina barrier layer on the Si/SiO_2 substrate,[13, 14] the Fe film on the alumina layer,[15, 16] the Fe film after annealing in H_2 to create Fe nanoparticles[17, 18] and the carbon nanotube forest grown on the Fe nanoparticles.[19, 20]

6.3. Instrument setting

a. Manufacturer : ION-TOF

b. Model : ToF-SIMS V

c. Analyzer mode : positive and negative

d. Analyzer description : time of flight (ToF)

e. Detector description : MCP

f. Ion Source : Pulsed

g. Ion Pulse Width (ns) : 8.6

h. Ion Pulse Rate (kHz): 10

i. DC Beam current (nA) : 20

j. Pulsed beam current (pA) : 0.01

k. Current measurement : Faraday Cup

l. Energy Acceptance Window (eV) : 20

m. Post-acceleration Voltage (kV) : 10

n. Beam raster width X (μm) : 200

o. Beam raster width Y (μm) : 200

p. Beam incident angle : 45 degree

q. Specimen Normal to Analyzer (θ, in deg) : 45

r. Sputter species : Bi

s. Sputter species charge : 2+

t. Net Beam Voltage : 50 keV

6.4. Acknowledgement

We thank Diamond Analytics, a US Synthetic company (Orem, UT), for funding this current study. Also, a part of this research was performed at EMSL (Environmental Molecular Sciences Laboratory) located at Pacific Northwest National Laboratory.

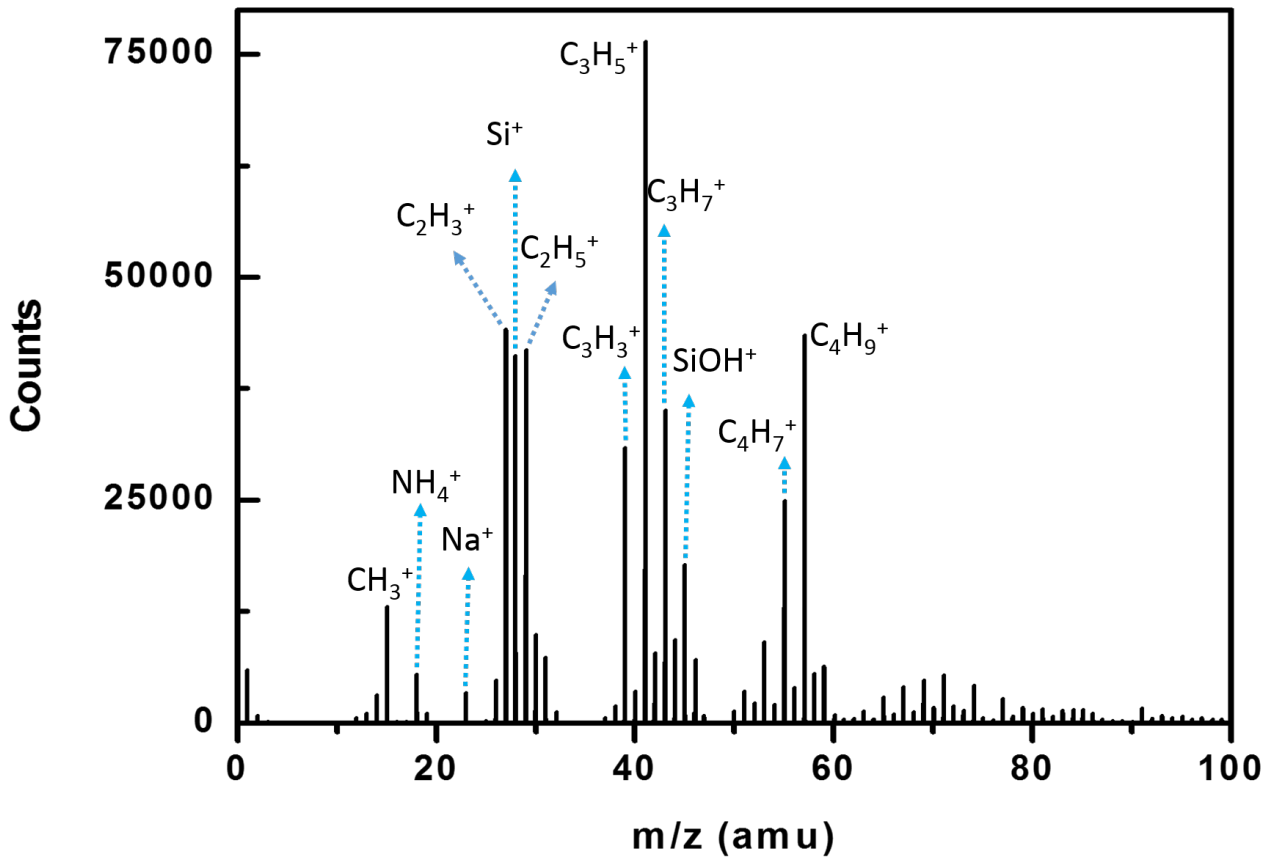

Figure 6.1. ToF-SIMS spectrum of Silicon wafer in positive mode (m/z 0-100).

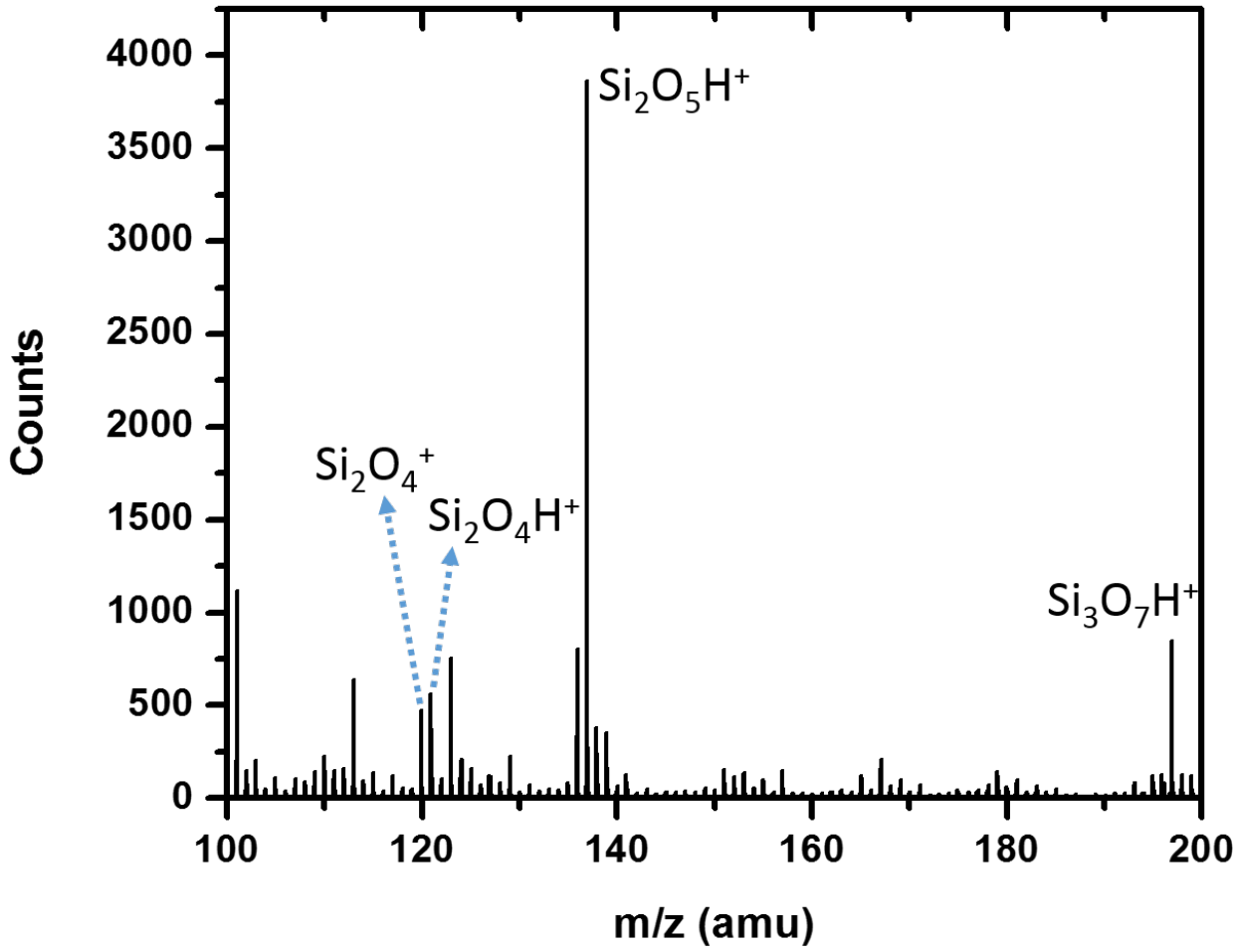

Figure 6.2. ToF-SIMS spectrum of Silicon wafer in positive mode (m/z 100-200).

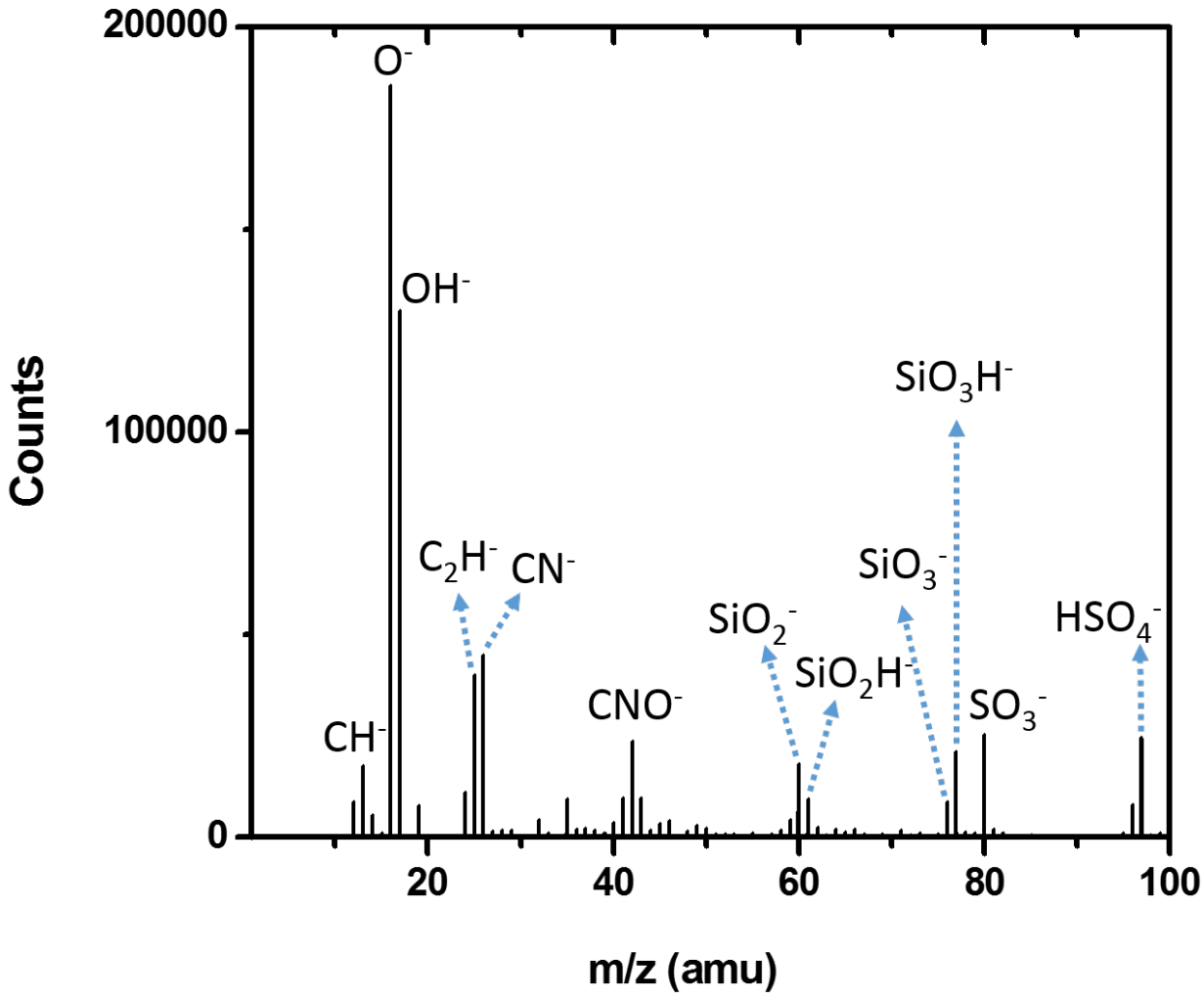

Figure 6.3. ToF-SIMS spectrum of Silicon wafer in negative mode.

6.5. References

1. C. Kopp, S. Bernabe, B. Ben Bakir, J. M. Fedeli, R. Orobtchouk, F. Schrank, H. Porte, L. Zimmermann and T. Tekin, Ieee J Sel Top Quant **17** (3), 498-509 (2011).
2. T. Liu, Z. Y. Dong, Y. W. Zhao, J. Wang, T. Chen, H. Xie, J. Li, H. J. Ni and D. X. Huo, J Cryst Growth **351** (1), 19-22 (2012).
3. M. J. R. Heck, H. W. Chen, A. W. Fang, B. R. Koch, D. Liang, H. Park, M. N. Sysak and J. E. Bowers, Ieee J Sel Top Quant **17** (2), 333-346 (2011).
4. J. M. Weisse, C. H. Lee, D. R. Kim and X. L. Zheng, Nano Letters **12** (6), 3339-3343 (2012).
5. A. S. Fiorillo, Ieee T Nanotechnol **11** (4), 654-656 (2012).
6. L. Yang, Y. Y. Lua, G. L. Jiang, B. J. Tyler and M. R. Linford, Analytical Chemistry **77** (14), 4654-4661 (2005).
7. D. S. Jensen, S. S. Kanyal, V. Gupta, M. A. Vail, A. E. Dadson, M. Engelhard, R. Vanfleet, R. C. Davis and M. R. Linford, Journal of Chromatography A **1257**, 195-203 (2012).
8. D. S. Jensen, S. S. Kanyal, N. Madaan, A. J. Miles, R. C. Davis, R. Vanfleet, M. A. Vail, A. E. Dadson and M. R. Linford, J Vac Sci Technol B **31** (3), 031203 (2013).
9. D. S. Jensen, S. S. Kanyal, N. Madaan, J. M. Hancock, A. E. Dadson, M. A. Vail, R. Vanfleet, V. Shutthanandan, Z. H. Zhu, M. H. Engelhard and M. R. Linford, Surf. Interface Anal. **45** (8), 1273-1282 (2013).
10. S. S. Kanyal, D. S. Jensen, A. J. Miles, A. E. Dadson, M. A. Vail, R. E. Olsen, S. Fabien, J. Nichols, R. Vanfleet, R. Davis and M. R. Linford, J. Vac. Sci Technol. B **31** (3), 031203 (2013).

11. J. Song, D. S. Jensen, D. N. Hutchison, B. Turner, T. Wood, A. Dadson, M. A. Vail, M. R. Linford, R. R. Vanfleet and R. C. Davis, Adv Funct Mater **21** (6), 1132-1139 (2011).

12. D. S. Jensen, S. S. Kanyal, N. Madaan, M. A. Vail, A. E. Dadson, M. Engelhard and M. R. Linford, Surface Science Spectra **20**, 36-42 (2013).

13. N. Madaan, S. S. Kanyal, D. S. Jensen, M. A. Vail, M. Engelhard and M. R. Linford, Surface Science Spectra **20**, 43-48 (2013).

14. S. S. Kanyal, D. S. Jensen, Z. Zihua and M. R. Linford, Surface Science Spectra (2014).

15. N. Madaan, S. S. Kanyal, D. S. Jensen, M. A. Vail, M. Engelhard and M. R. Linford, surface Science Spectra **20**, 49-54 (2013).

16. S. S. Kanyal, D. S. Jensen, Z. Zihua and M. R. Linford, Surface Science Spectra (2014).

17. N. Madaan, S. S. Kanyal, D. S. Jensen, M. A. Vail, M. Engelhard and M. R. Linford, Surface Science Spectra **20**, 55-61 (2013).

18. S. S. Kanyal, D. S. Jensen, Z. Zihua and M. R. Linford, Surface Science Spectra (2014).

19. D. S. Jensen, S. S. Kanyal, N. Madaan, M. A. Vail, M. Engelhard and M. R. Linford, Surface Science Spectra **20**, 62-67 (2013).

20. S. S. Kanyal, D. S. Jensen, Z. Zihua and M. R. Linford, Surface Science Spectra (2014).

7. Chapter: ToF-SIMS of Al_2O_3 e-Beam Evaporated onto Silicon (100)/SiO_2

7.1. Abstract

We report the positive and negative ion ToF-SIMS characterization of a thin film of e-beam evaporated alumina on a silicon substrate using Bi_3^{2+} primary ions at 50 keV, where this film prevents poisoning of an Fe catalyst in carbon nanotube (CNT) growth. The positive ion spectrum showed a strong Al^+ signal, while the negative ion spectrum showed strong peaks due to AlO^- , O, and OH^-.

7.2. Introduction

Alumina (Al_2O_3) is an important material for the semiconductor industry.[1-4] It also acts as a barrier layer to prevent silicide formation (poisoning) in carbon nanotube (CNT) forest growth from transition metal particles on silicon substrates.[5, 6] Herein we show the characterization of a ca. 35 nm e-beam evaporated alumina-on-silicon film by positive and negative ion time-of-flight secondary ion mass spectrometry (ToF-SIMS) using Bi_3^{2+} primary ions. The positive ion mode shows a strong Al^+ signal and $Al_xO_yH_z$ (see Figure 7.1-7.2). The negative ion spectrum shows significant AlO^-, O^-, OH^-, AlO_2^- and $Al_xO_yH_z^-$ signals (see Figure 7.3-7.4). The alumina layer described herein is an essential part of the materials deposited in the preparation of microfabricated thin layer chromatography (TLC) plates.[7-11] Indeed, submissions to Surface Science Spectra have been made on the XPS and SIMS characterization of the key materials in this microfabrication, including the silicon substrate,[12, 13] an alumina barrier layer on the Si/SiO_2 substrate (this submission and a corresponding XPS submission),[14] an Fe film on the alumina layer,[15, 16] the Fe

film after annealing in H_2 to create Fe nanoparticles[17, 18] and the carbon nanotube forest grown on the Fe nanoparticles.[19, 20]

7.3. Instrument setting

Refer to section 6.3.

7.4. Acknowledgement

We thank Diamond Analytics, a US Synthetic company (Orem, UT), for funding this current study. Also, a part of this research was performed at EMSL (Environmental Molecular Sciences Laboratory) located at Pacific Northwest National Laboratory.

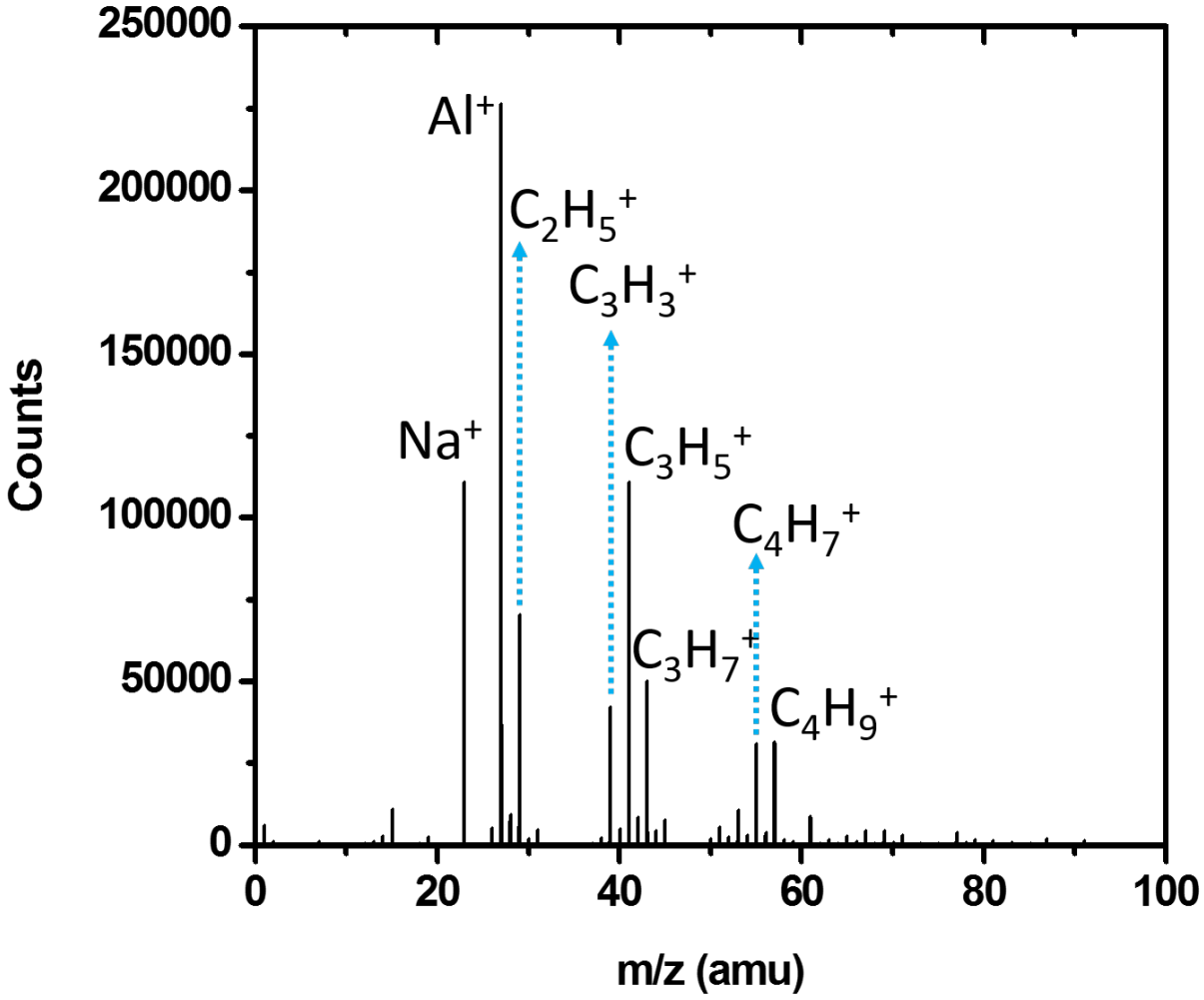

Figure 7.1. ToF-SIMS spectrum of $Si/SiO_2/Al_2O_3$ stack in positive mode (m/z 0-100).

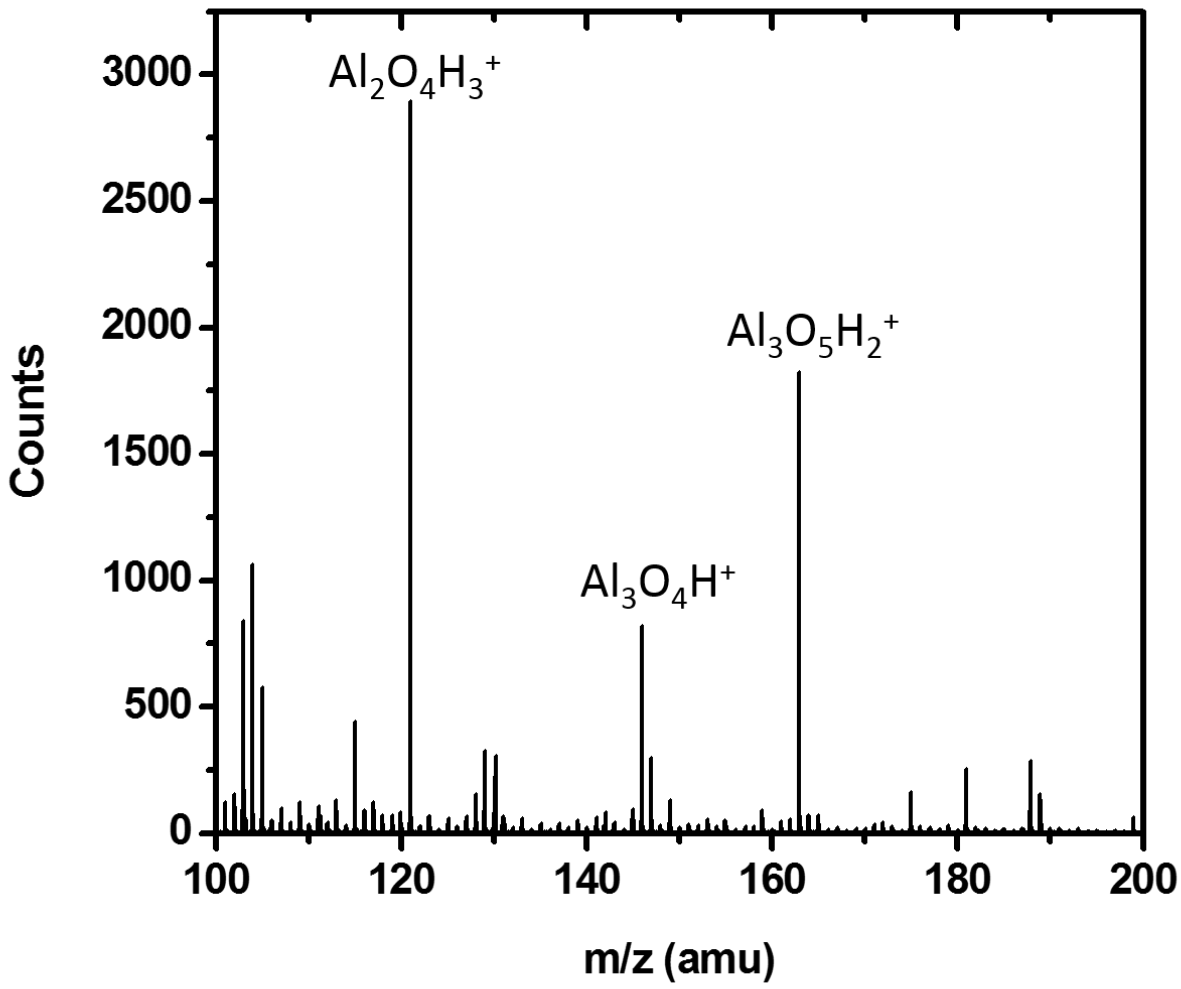

Figure 7.2. ToF-SIMS spectrum of $Si/SiO_2/Al_2O_3$ stack in positive mode (m/z 100-200).

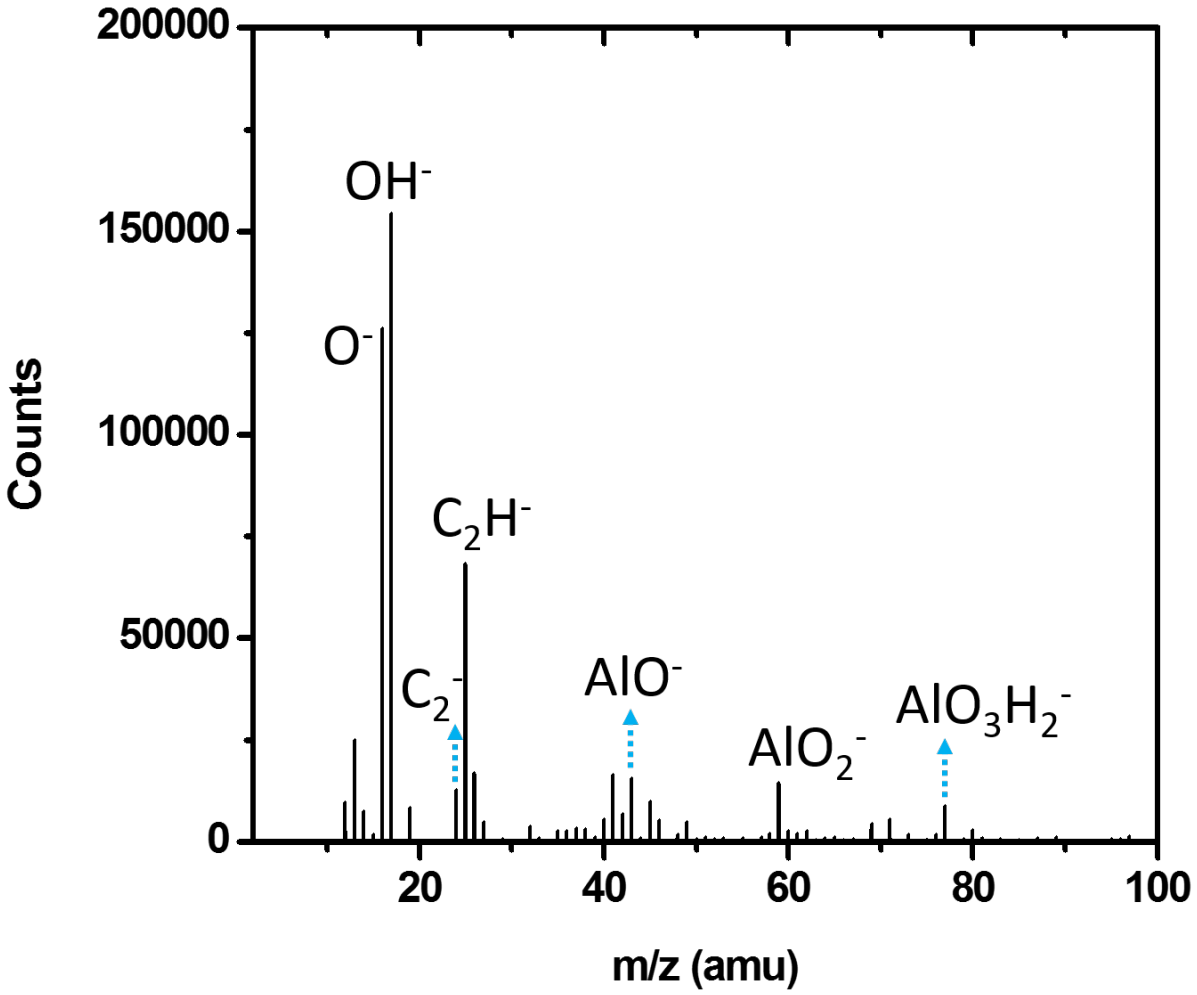

Figure 7.3. ToF-SIMS spectrum of $Si/SiO_2/Al_2O_3$ stack in negative mode (m/z 0-100).

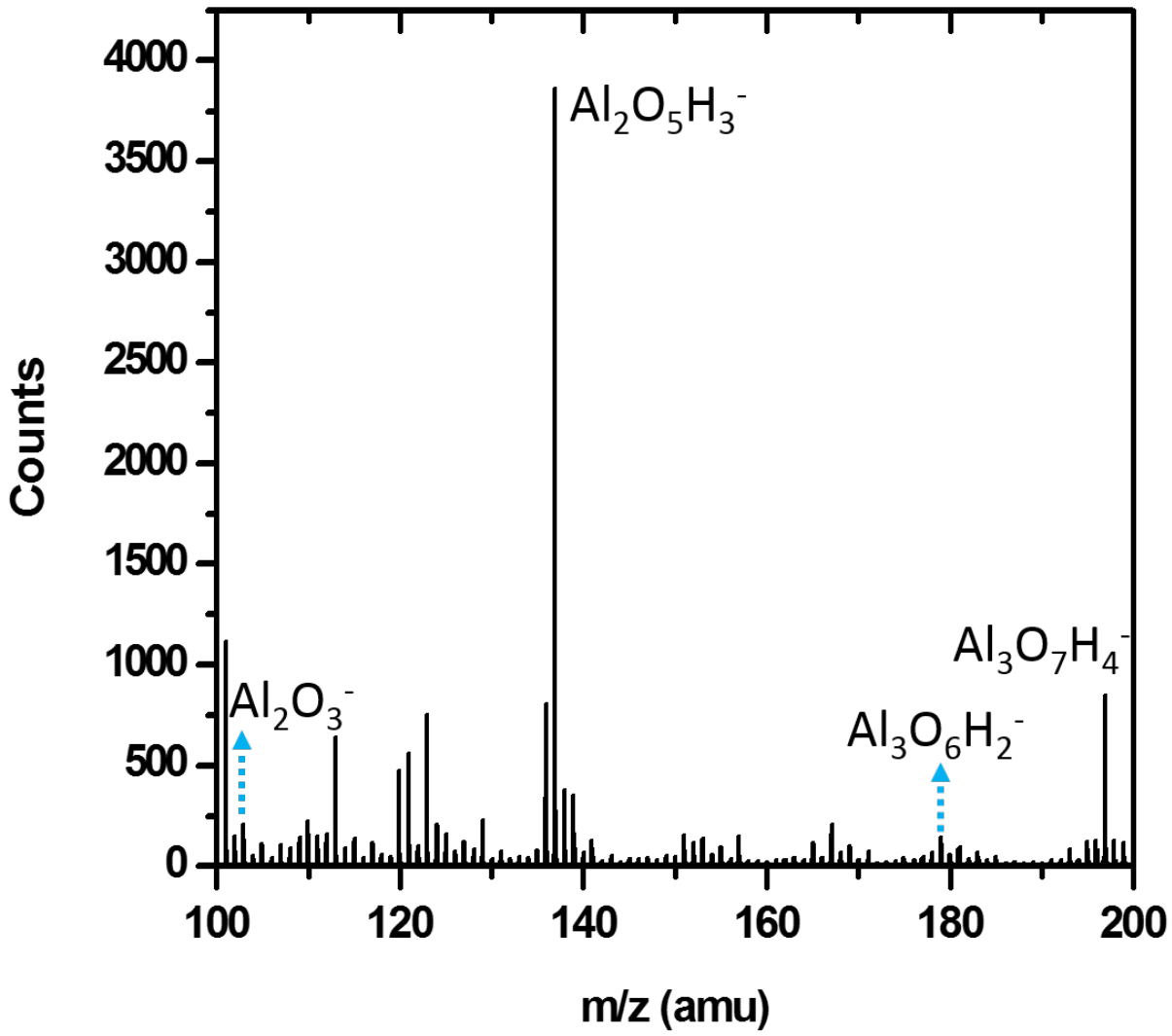

Figure 7.4. ToF-SIMS spectrum of $Si/SiO_2/Al_2O_3$ stack in negative mode (m/z 100-200).

7.5. References

1. Y. Tidiishi, S. Naka and H. Okada, Jpn J Appl Phys **47** (1), 438-440 (2008).
2. Y. Kurokawa, Y. Kobayashi and S. Nakata, Heterogen Chem Rev **1** (4), 309-327 (1994).
3. J. L. B. Maciel, E. A. Floriano, L. V. A. Scalvi and L. P. Ravaro, J Mater Sci **46** (20), 6627-6632 (2011).
4. A. A. Vasiliev, R. G. Pavelko, S. Y. Gogish-Klushin, D. Y. Kharitonov, O. S. Gogish-Klushin, A. V. Sokolov, A. V. Pisliakov and N. N. Samotaev, Sensor Actuat B-Chem **132** (1), 216-223 (2008).
5. P. M. Parthangal, R. E. Cavicchi and M. R. Zachariah, Nanotechnology **18** (18) (2007).
6. I. T. Han, B. K. Kim, H. J. Kim, M. Yang, Y. W. Jin, S. J. Jung, N. Lee, S. K. Kim and J. M. Kim, Chem. Phys. Lett. **400** (1-3), 139-144 (2004).
7. D. S. Jensen, S. S. Kanyal, V. Gupta, M. A. Vail, A. E. Dadson, M. Engelhard, R. Vanfleet, R. C. Davis and M. R. Linford, Journal of Chromatography A **1257**, 195-203 (2012).
8. D. S. Jensen, S. S. Kanyal, N. Madaan, A. J. Miles, R. C. Davis, R. Vanfleet, M. A. Vail, A. E. Dadson and M. R. Linford, J Vac Sci Technol B **31** (3), 031203 (2013).
9. D. S. Jensen, S. S. Kanyal, N. Madaan, J. M. Hancock, A. E. Dadson, M. A. Vail, R. Vanfleet, V. Shutthanandan, Z. H. Zhu, M. H. Engelhard and M. R. Linford, Surf. Interface Anal. **45** (8), 1273-1282 (2013).
10. S. S. Kanyal, D. S. Jensen, A. J. Miles, A. E. Dadson, M. A. Vail, R. E. Olsen, S. Fabien, J. Nichols, R. Vanfleet, R. Davis and M. R. Linford, J. Vac. Sci Technol. B **31** (3), 031203 (2013).

11. J. Song, D. S. Jensen, D. N. Hutchison, B. Turner, T. Wood, A. Dadson, M. A. Vail, M. R. Linford, R. R. Vanfleet and R. C. Davis, Adv Funct Mater **21** (6), 1132-1139 (2011).

12. D. S. Jensen, S. S. Kanyal, N. Madaan, M. A. Vail, A. E. Dadson, M. Engelhard and M. R. Linford, Surface Science Spectra **20**, 36-42 (2013).

13. S. S. Kanyal, D. S. Jensen, Z. Zihua and M. R. Linford, Surface Science Spectra (2014).

14. N. Madaan, S. S. Kanyal, D. S. Jensen, M. A. Vail, M. Engelhard and M. R. Linford, Surface Science Spectra **20**, 43-48 (2013).

15. N. Madaan, S. S. Kanyal, D. S. Jensen, M. A. Vail, M. Engelhard and M. R. Linford, surface Science Spectra **20**, 49-54 (2013).

16. S. S. Kanyal, D. S. Jensen, Z. Zihua and M. R. Linford, Surface Science Spectra (2014).

17. N. Madaan, S. S. Kanyal, D. S. Jensen, M. A. Vail, M. Engelhard and M. R. Linford, Surface Science Spectra **20**, 55-61 (2013).

18. S. S. Kanyal, D. S. Jensen, Z. Zihua and M. R. Linford, Surface Science Spectra (2014).

19. D. S. Jensen, S. S. Kanyal, N. Madaan, M. A. Vail, M. Engelhard and M. R. Linford, Surface Science Spectra **20**, 62-67 (2013).

20. S. S. Kanyal, D. S. Jensen, Z. Zihua and M. R. Linford, Surface Science Spectra (2014).

8. Chapter: ToF-SIMS of Thermally Evaporated Iron on an Alumina Barrier Layer

8.1. Abstract

We report the positive and negative ion ToF-SIMS spectra using Bi_3^{2+} primary ions at 50 keV of an Fe film (6 nm) that had been thermally evaporated on a thin film of alumina (ca. 35 nm) on a silicon wafer. This surface had been exposed to the air; it had previously been shown by XPS to be entirely oxidized. The positive ion SIMS spectrum shows Fe^+, FeH^+, and $Fe_xO_yH_z^+$. The negative ion spectrum shows $FeOH^-$, $Fe_xO_yH_z^+$ and OH^- species.

8.2. Introduction

A number of iron-containing thin films are known for their magnetic properties and have potential for data storage applications.[1, 2] After annealing to form nanoparticles, iron thin films are also used is as a catalyst for growth of carbon nanotube forests.[3] In the present study, a thin film of Fe (6 nm) was deposited via thermal evaporation on top of ca. 35 nm of alumina on a silicon substrate. ToF-SIMS spectra of this material were recorded in both positive and negative ion mode using Bi_3^{2+} primary ions at 50 keV. The positive ion spectra show a strong Fe^+ signal along with weaker signals due to FeH^+ and $Fe_xO_yH_z^+$ (see Figure 8.1-8.3). A small signal corresponding to Al^+ was also present. The negative ion spectra show OH^-, $Fe_xO_yH_z^-$, and $FeOH^-$ (see Figure 8.4-8.5). These different iron-containing ions are present for different isotopes of Fe. The Fe layer described herein is an essential part of the materials deposited in the preparation of microfabricated thin layer chromatography (TLC) plates.[4-8] Indeed, submissions to Surface Science Spectra have been made on the XPS and SIMS characterization of the key materials in this microfabrication,

including the silicon substrate,[9, 10] an alumina barrier layer on the Si/SiO_2 substrate,[11, 12] the Fe film on the alumina layer (the current submission and on one XPS),[13] the Fe film after annealing in H_2 to create Fe nanoparticle,[14, 15] and the carbon nanotube forest grown on the Fe nanoparticles.[16, 17]

8.3. Instrument setting

Same as section 6.3

8.4. Acknowledgement

We thank Diamond Analytics, a US Synthetic company (Orem, UT), for funding this current study. Also, a part of this research was performed at EMSL (Environmental Molecular Sciences Laboratory) located at Pacific Northwest National Laboratory.

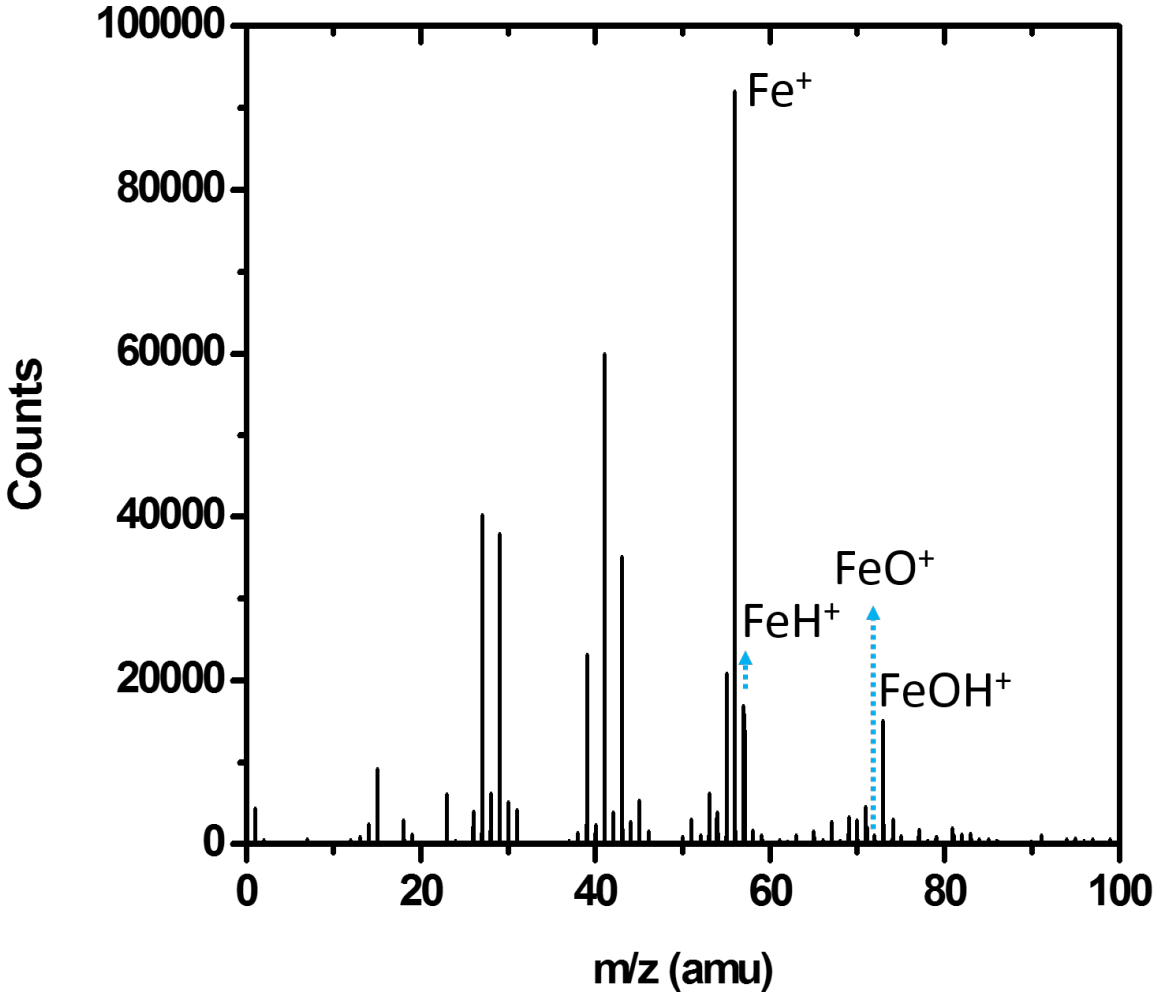

Figure 8.1. ToF-SIMS spectrum of $Si/SiO_2/Al_2O_3/Fe$ stack in positive mode (m/z 0-100).

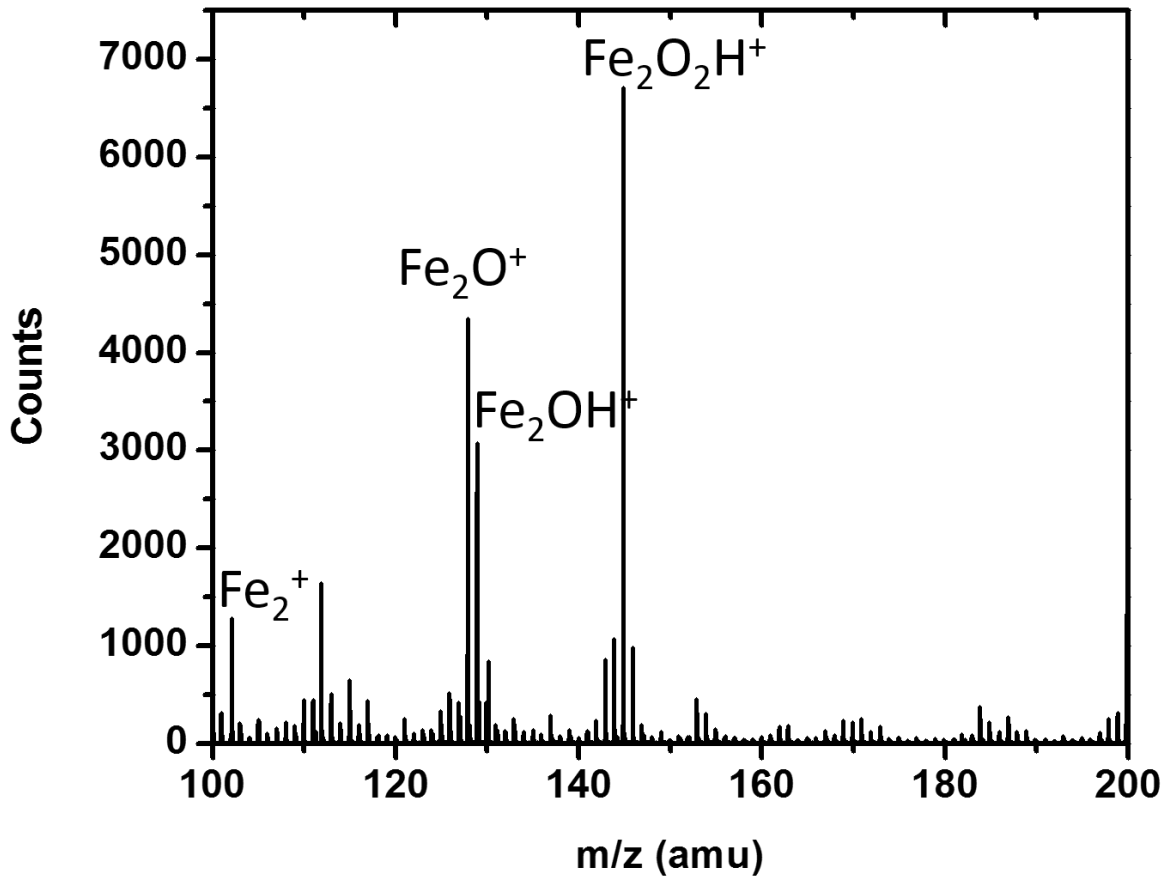

Figure 8.2. ToF-SIMS spectrum of $Si/SiO_2/Al_2O_3/Fe$ stack in positive mode (m/z 100-200).

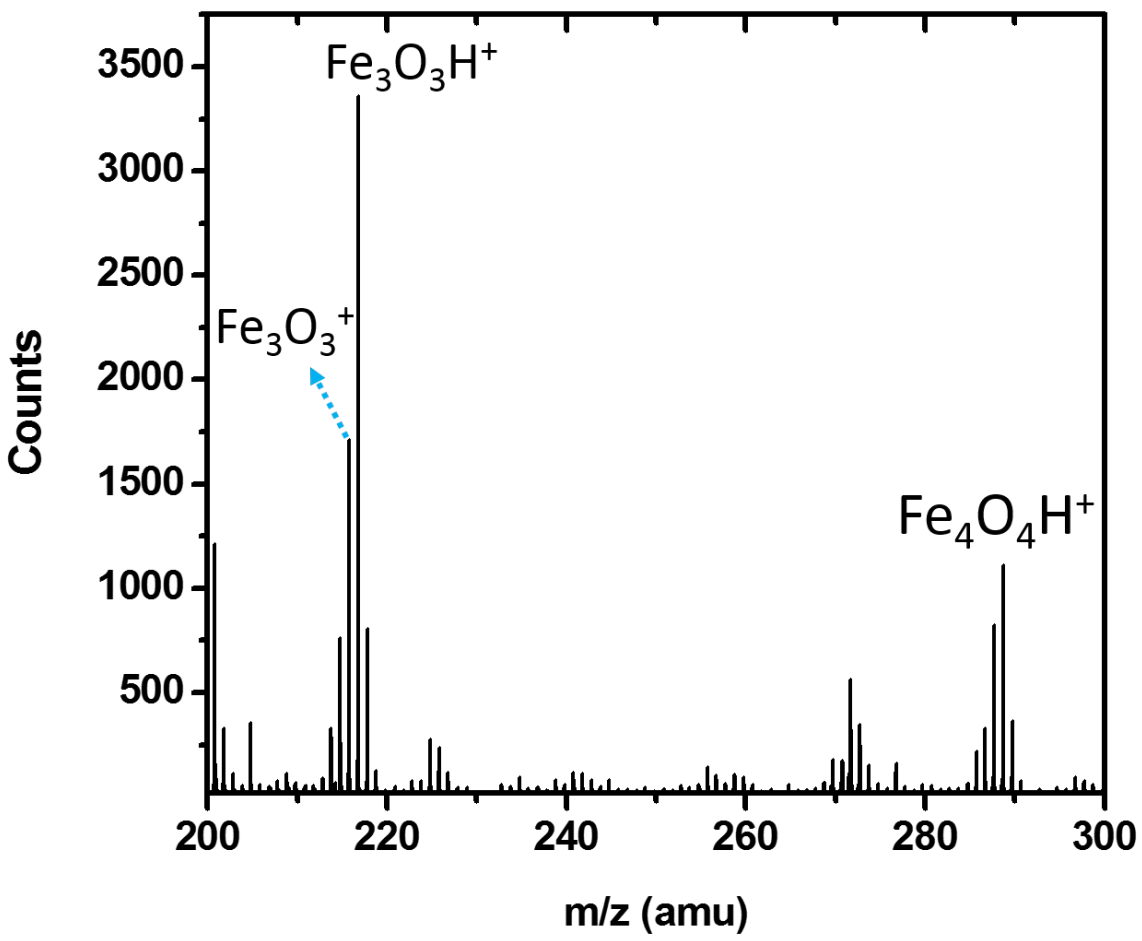

Figure 8.3. ToF-SIMS spectrum of $Si/SiO_2/Al_2O_3/Fe$ stack in positive mode (m/z 200-300).

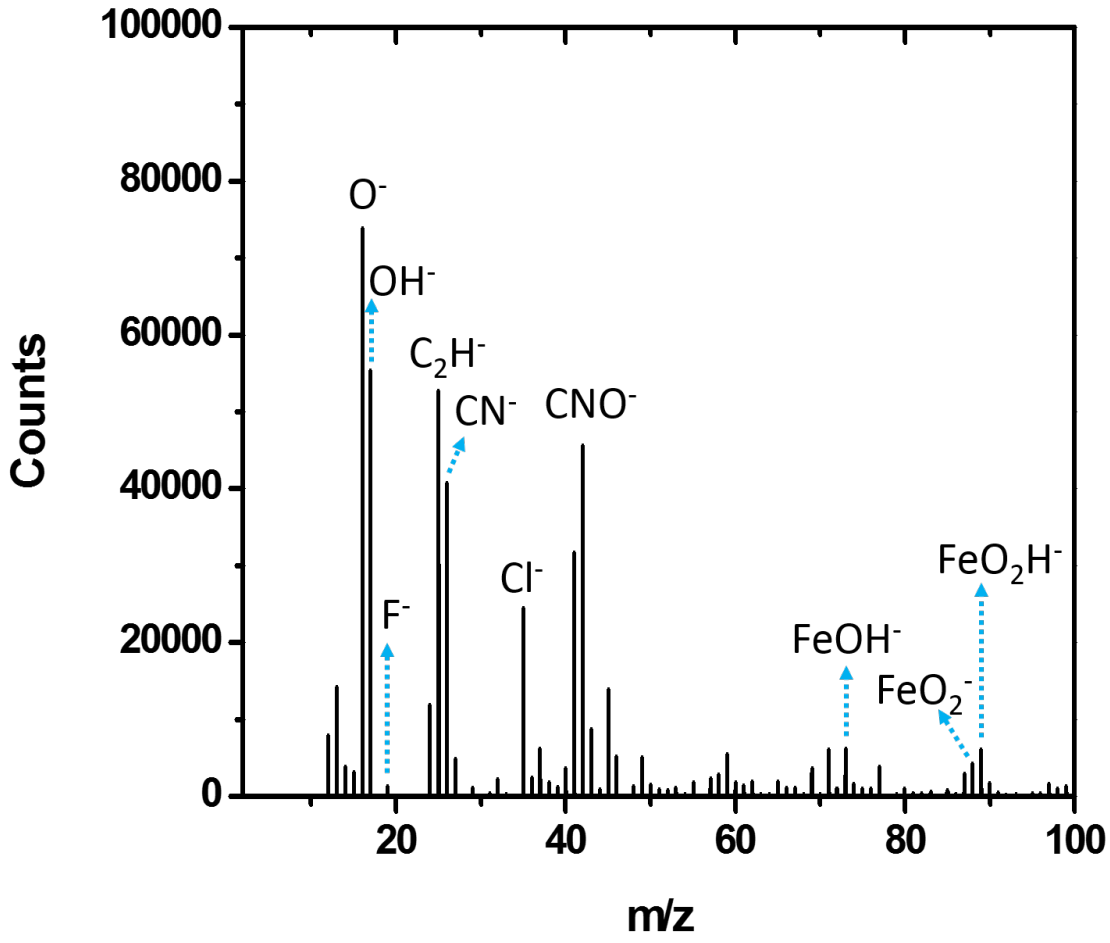

Figure 8.4. ToF-SIMS spectrum of $Si/SiO_2/Al_2O_3/Fe$ stack in negative mode (m/z 0-100).

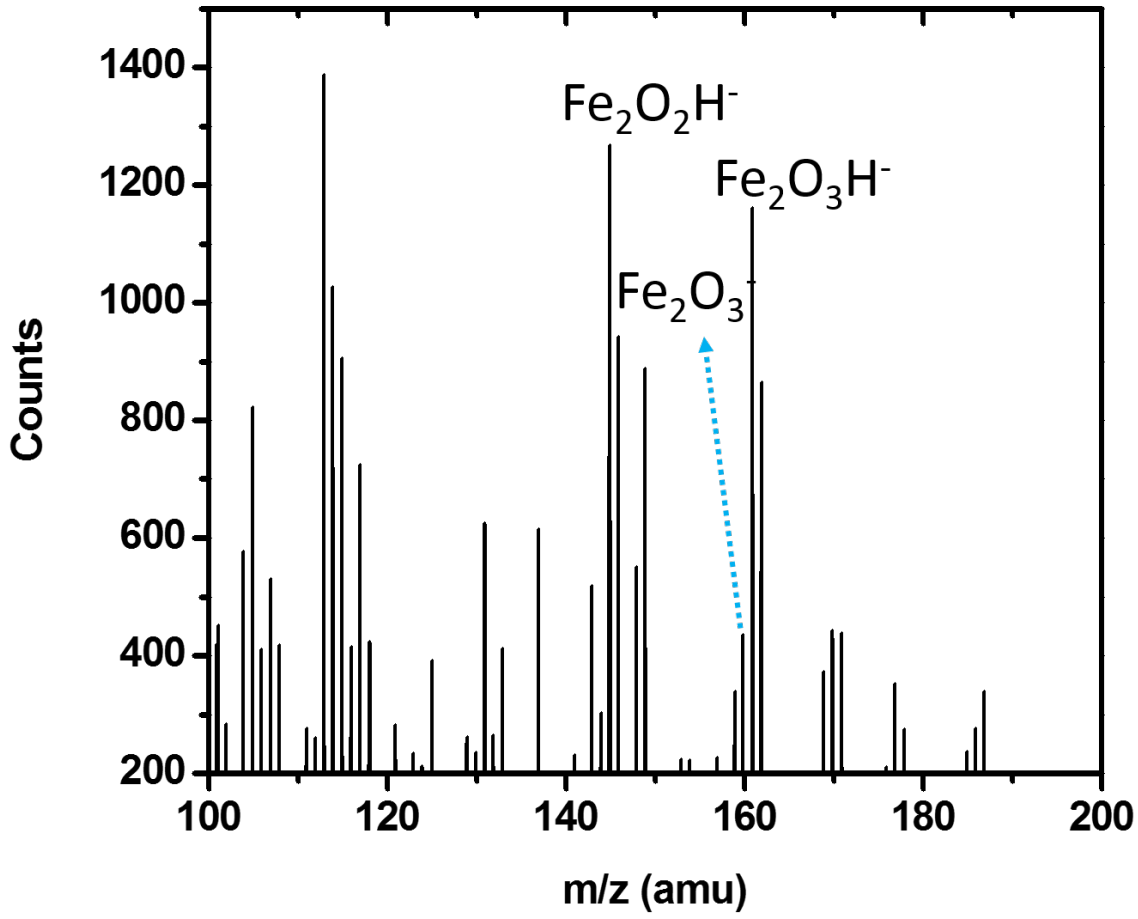

Figure 8.5. ToF-SIMS spectrum of $Si/SiO_2/Al_2O_3/Fe$ stack in negative mode (m/z 100-200).

8.5. References

1. L. Ma, Z. W. Liu, D. C. Zeng, H. Y. Yu, X. P. Zhong and X. Z. Zhang, Sci China Phys Mech **55** (9), 1594-1598 (2012).
2. G. H. Dai, Q. F. Zhan, Y. W. Liu, H. L. Yang, X. S. Zhang, B. Chen and R. W. Li, Applied Physics Letters **100** (12) (2012).
3. C. Verissimo, M. R. Aguiar and S. A. Moshkalev, J. Nanosci. Nanotechnol. **9** (7), 4459-4466 (2009).
4. D. S. Jensen, S. S. Kanyal, V. Gupta, M. A. Vail, A. E. Dadson, M. Engelhard, R. Vanfleet, R. C. Davis and M. R. Linford, Journal of Chromatography A **1257**, 195-203 (2012).
5. D. S. Jensen, S. S. Kanyal, N. Madaan, A. J. Miles, R. C. Davis, R. Vanfleet, M. A. Vail, A. E. Dadson and M. R. Linford, J Vac Sci Technol B **31** (3), 031203 (2013).
6. D. S. Jensen, S. S. Kanyal, N. Madaan, J. M. Hancock, A. E. Dadson, M. A. Vail, R. Vanfleet, V. Shutthanandan, Z. H. Zhu, M. H. Engelhard and M. R. Linford, Surf. Interface Anal. **45** (8), 1273-1282 (2013).
7. S. S. Kanyal, D. S. Jensen, A. J. Miles, A. E. Dadson, M. A. Vail, R. E. Olsen, S. Fabien, J. Nichols, R. Vanfleet, R. Davis and M. R. Linford, J. Vac. Sci Technol. B **31** (3), 031203 (2013).
8. J. Song, D. S. Jensen, D. N. Hutchison, B. Turner, T. Wood, A. Dadson, M. A. Vail, M. R. Linford, R. R. Vanfleet and R. C. Davis, Adv Funct Mater **21** (6), 1132-1139 (2011).
9. D. S. Jensen, S. S. Kanyal, N. Madaan, M. A. Vail, A. E. Dadson, M. Engelhard and M. R. Linford, Surface Science Spectra **20**, 36-42 (2013).
10. S. S. Kanyal, D. S. Jensen, Z. Zihua and M. R. Linford, Surface Science Spectra (2014).

11. N. Madaan, S. S. Kanyal, D. S. Jensen, M. A. Vail, M. Engelhard and M. R. Linford, Surface Science Spectra **20**, 43-48 (2013).

12. S. S. Kanyal, D. S. Jensen, Z. Zihua and M. R. Linford, Surface Science Spectra (2014).

13. N. Madaan, S. S. Kanyal, D. S. Jensen, M. A. Vail, M. Engelhard and M. R. Linford, surface Science Spectra **20**, 49-54 (2013).

14. N. Madaan, S. S. Kanyal, D. S. Jensen, M. A. Vail, M. Engelhard and M. R. Linford, Surface Science Spectra **20**, 55-61 (2013).

15. S. S. Kanyal, D. S. Jensen, Z. Zihua and M. R. Linford, Surface Science Spectra (2014).

16. D. S. Jensen, S. S. Kanyal, N. Madaan, M. A. Vail, M. Engelhard and M. R. Linford, Surface Science Spectra **20**, 62-67 (2013).

17. S. S. Kanyal, D. S. Jensen, Z. Zihua and M. R. Linford, Surface Science Spectra (2014).

9. Chapter: ToF-SIMS of a Thermally Annealed Iron Thin Film on an Alumina Barrier Layer

9.1. Abstract

We report the positive and negative ion ToF-SIMS spectra obtained with Bi_3^{2+} primary ions at 50 keV of an Fe film annealed in hydrogen at 750 °C to form Fe nanoparticles. This surface had been exposed to the air; it had previously been shown by XPS to be entirely oxidized. The strongest signal in the positive ion spectrum corresponded to Fe^+, with $Fe_xO_yH_z^+$ species also present. A substantial Al^+ signal was observed due to exposure of the underlying alumina substrate. The negative ion spectrum showed, O^-, OH^-, and AlO^-.

9.2. Introduction

A number of iron-containing thin films are known for their magnetic properties and have potential in data storage applications.[1, 2] After annealing to form nanoparticles, iron thin films are also used as a catalyst for growth of carbon nanotube forests.[3] Thus, characterization of these films is important. Here we report ToF-SIMS of annealed Fe films in both positive and negative ion mode using Bi_3^{2+} primary ions at 50 keV. A thin (6 nm) Fe film was deposited via thermal evaporation on top of an alumina layer (ca. 35 nm) on a silicon wafer. The alumina film acts a barrier to prevent formation of non-catalytic iron silicide. Positive ion spectra show that the strongest signal is due to Fe^+. Signals attributable to FeH^+ and $Fe_xO_yH_z^+$ are also present (see Figure 9.1-9.3). The substantial Al^+ signal is attributable to exposure of the alumina film during annealing (nanoparticle formation). The negative ion spectra show strong O^- and OH^- signals followed by a

weaker AlO^- signal (see Figure 9.4). Fluorine (F^-) and Chlorine (Cl^-) contamination is also seen in this mode. The different iron-containing ions are present for different isotopes of Fe. The Si silicon substrate described herein is an essential part of the materials created in the preparation of microfabricated thin layer chromatography (TLC) plates.[4-8] Indeed, submissions to Surface Science Spectra have been made on the XPS and SIMS characterization of the key materials in this microfabrication, including the silicon substrate,[9, 10] an alumina barrier layer on the Si/SiO_2 substrate,[11, 12] the Fe film on the alumina layer,[13, 14] current submission and on one XPS the Fe film after annealing in H_2 to create Fe nanoparticles,[15] and the carbon nanotube forest grown on the Fe nanoparticles.[16, 17]

9.3. Instrument setting

Same as section 6.3

9.4. Acknowledgement

We thank Diamond Analytics, a US Synthetic company (Orem, UT), for funding this current study. Also, a part of this research was performed at EMSL (Environmental Molecular Sciences Laboratory) located at Pacific Northwest National Laboratory.

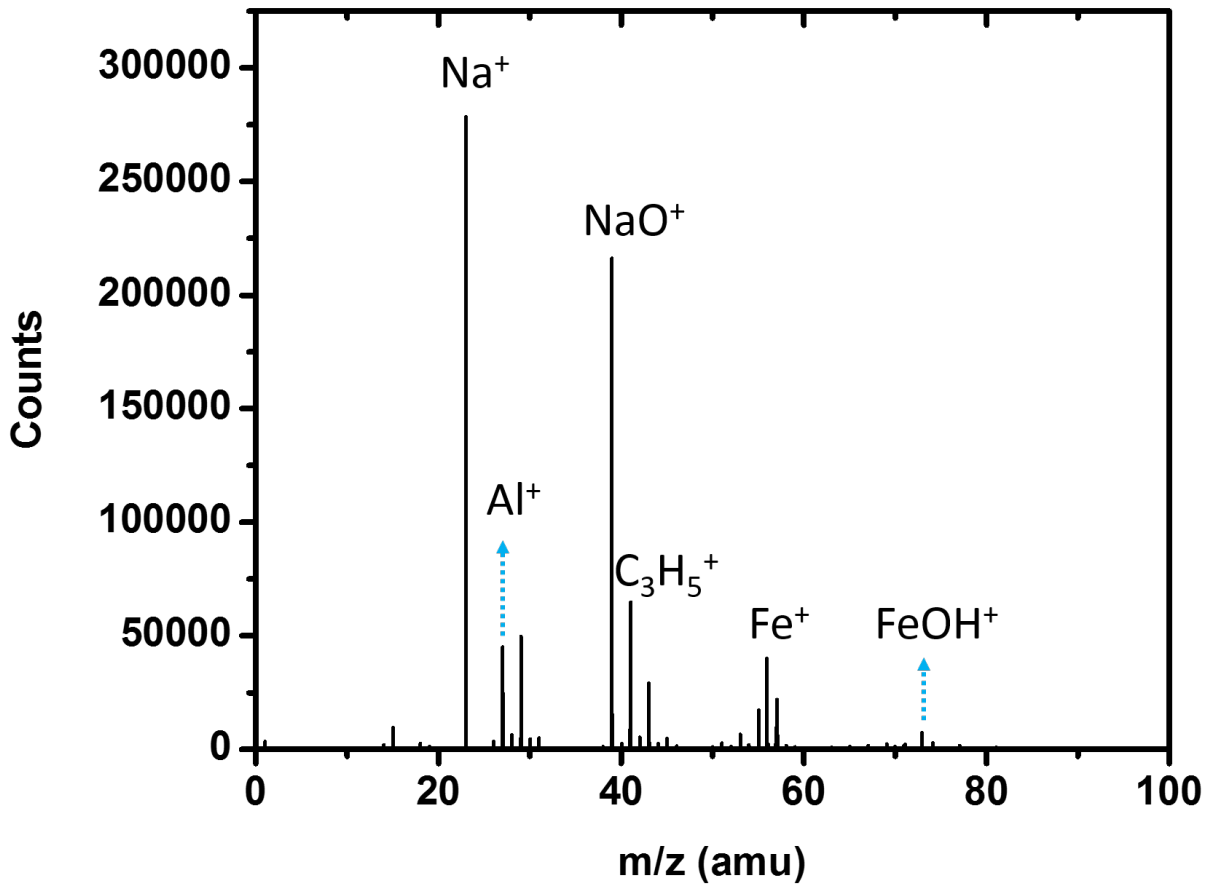

Figure 9.1. ToF-SIMS spectrum of $Si/SiO_2/Al_2O_3/Fe$(annealed) stack in positive mode (m/z 0-100)

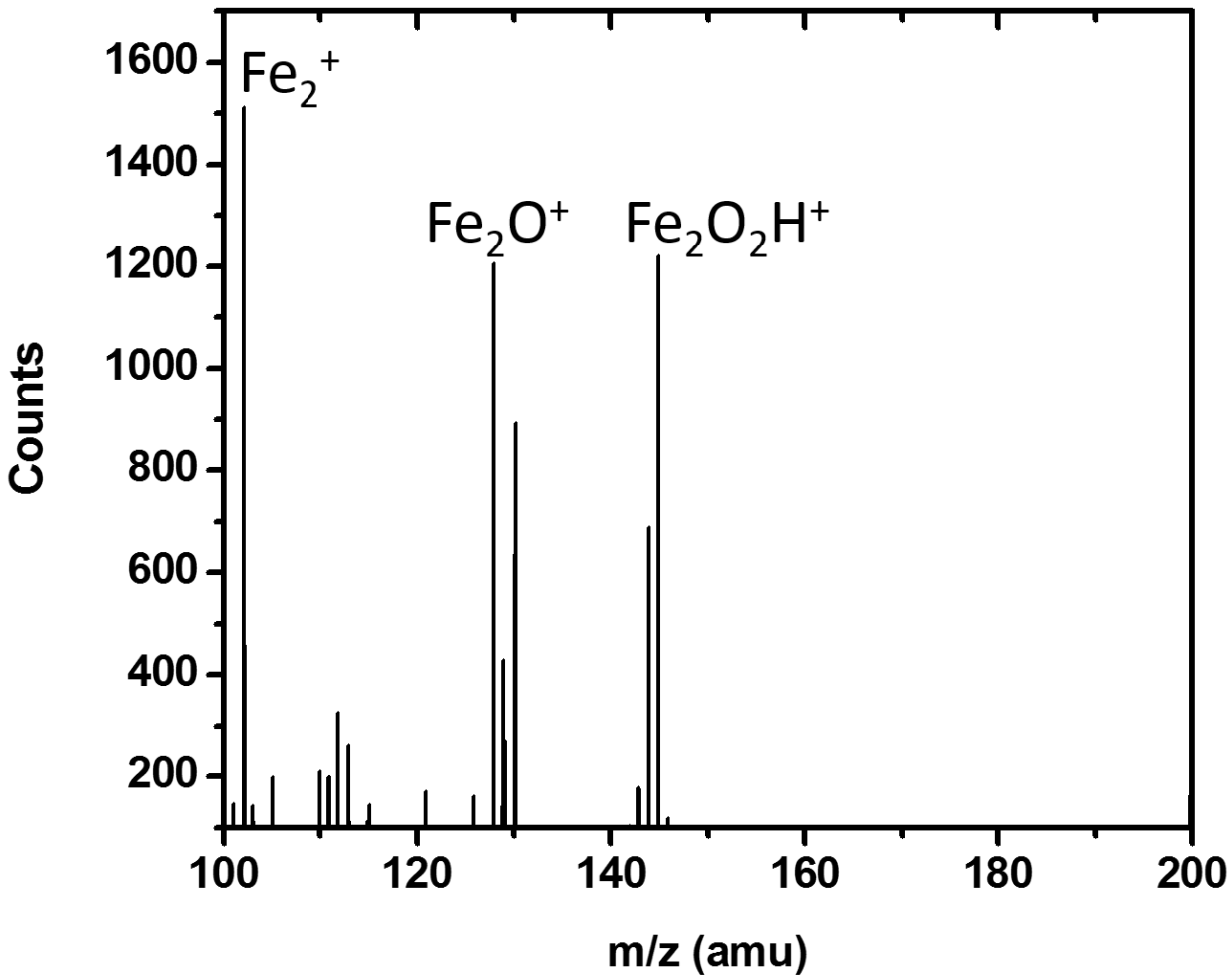

Figure 9.2. ToF-SIMS spectrum of $Si/SiO_2/Al_2O_3/Fe$(annealed) stack in positive mode (m/z 100-200).

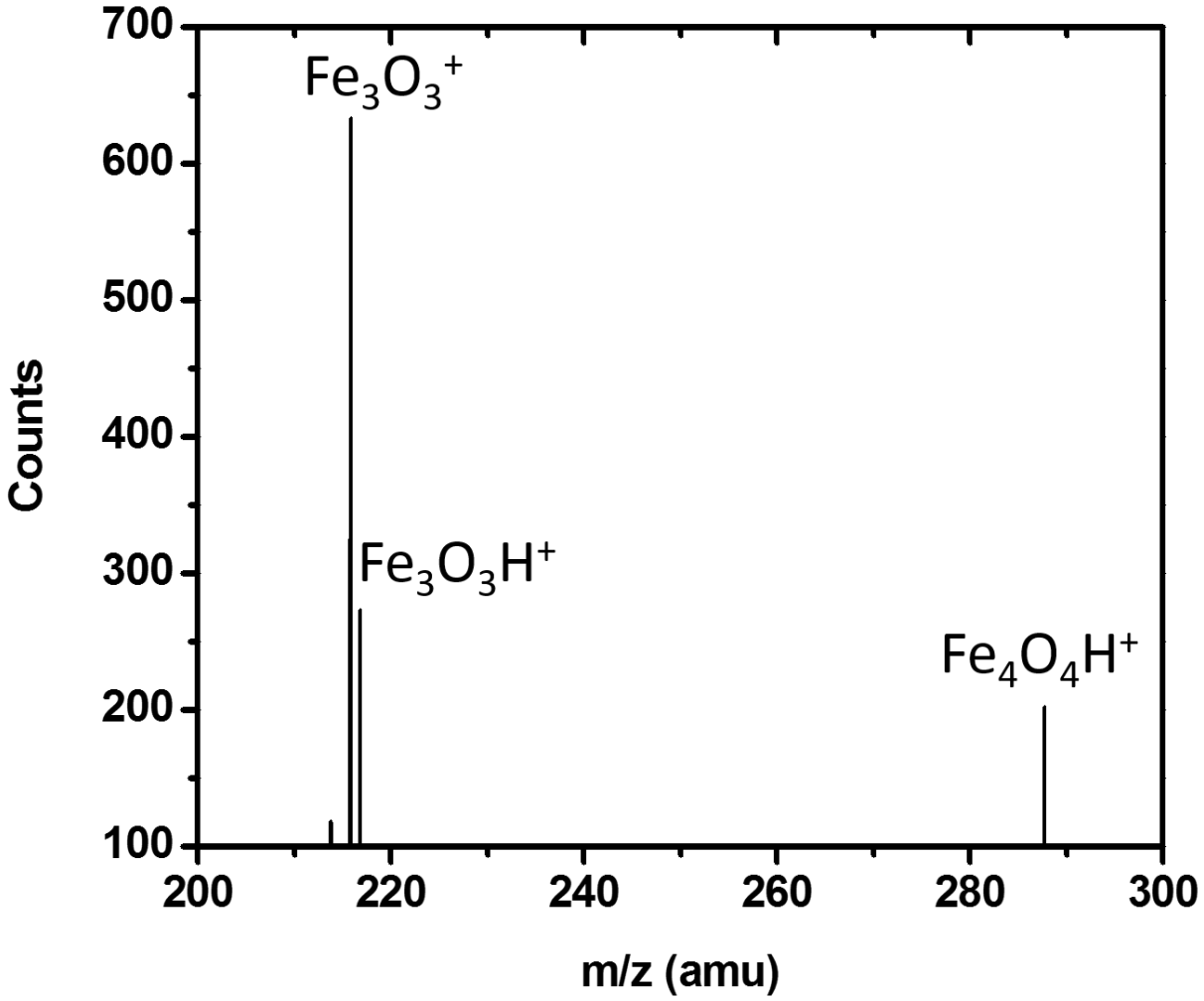

Figure 9.3. ToF-SIMS spectrum of $Si/SiO_2/Al_2O_3/Fe$(annealed) stack in positive mode (m/z 200-300)

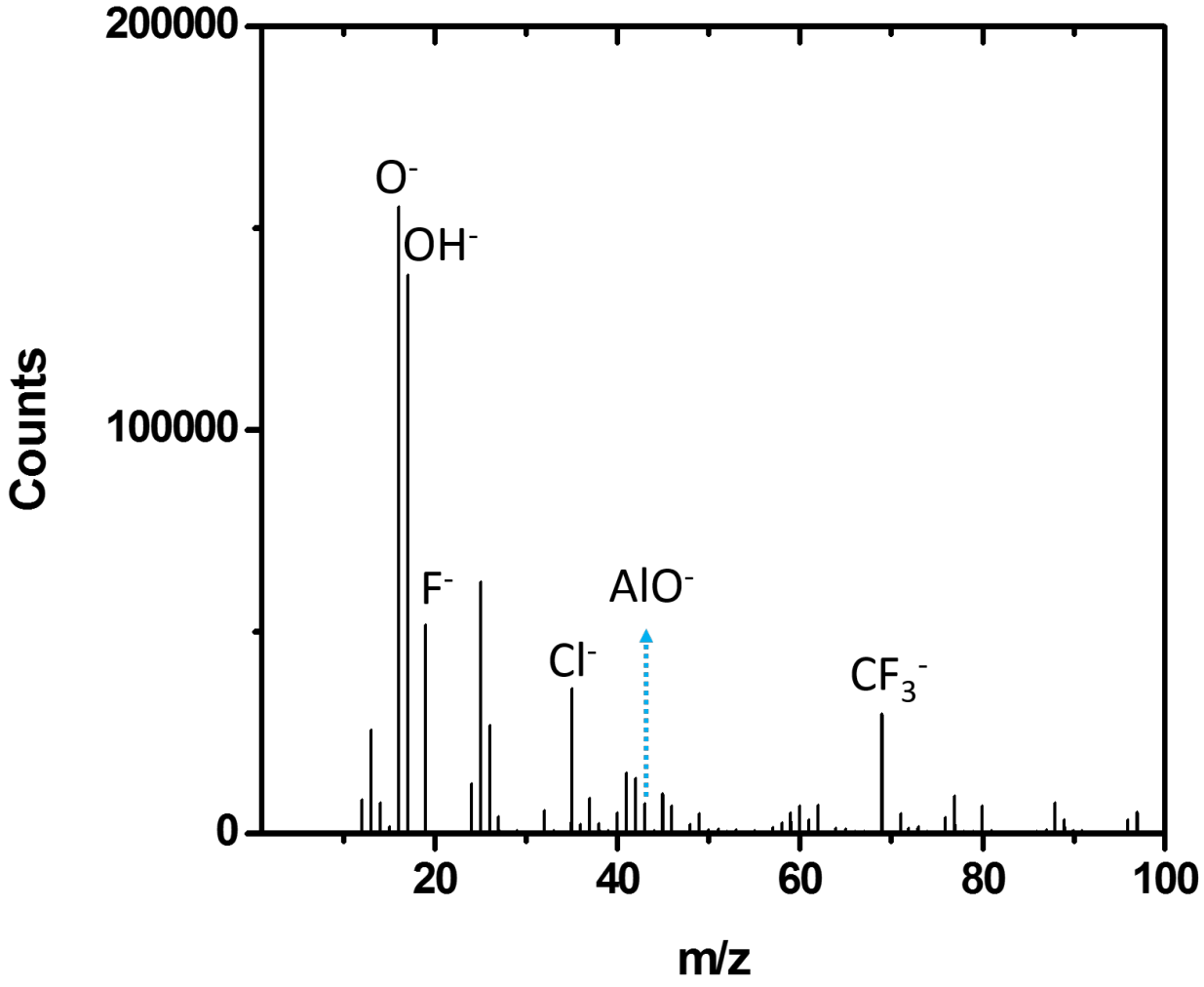

Figure 9.4. ToF-SIMS spectrum of $Si/SiO_2/Al_2O_3/Fe$(annealed) stack in negative mode (m/z 0-100)

9.5. References

1. L. Ma, Z. W. Liu, D. C. Zeng, H. Y. Yu, X. P. Zhong and X. Z. Zhang, Sci China Phys Mech **55** (9), 1594-1598 (2012).
2. G. H. Dai, Q. F. Zhan, Y. W. Liu, H. L. Yang, X. S. Zhang, B. Chen and R. W. Li, Applied Physics Letters **100** (12) (2012).
3. C. Verissimo, M. R. Aguiar and S. A. Moshkalev, J. Nanosci. Nanotechnol. **9** (7), 4459-4466 (2009).
4. D. S. Jensen, S. S. Kanyal, V. Gupta, M. A. Vail, A. E. Dadson, M. Engelhard, R. Vanfleet, R. C. Davis and M. R. Linford, Journal of Chromatography A **1257**, 195-203 (2012).
5. D. S. Jensen, S. S. Kanyal, N. Madaan, A. J. Miles, R. C. Davis, R. Vanfleet, M. A. Vail, A. E. Dadson and M. R. Linford, J Vac Sci Technol B **31** (3), 031203 (2013).
6. D. S. Jensen, S. S. Kanyal, N. Madaan, J. M. Hancock, A. E. Dadson, M. A. Vail, R. Vanfleet, V. Shutthanandan, Z. H. Zhu, M. H. Engelhard and M. R. Linford, Surf. Interface Anal. **45** (8), 1273-1282 (2013).
7. S. S. Kanyal, D. S. Jensen, A. J. Miles, A. E. Dadson, M. A. Vail, R. E. Olsen, S. Fabien, J. Nichols, R. Vanfleet, R. Davis and M. R. Linford, J. Vac. Sci Technol. B **31** (3), 031203 (2013).
8. J. Song, D. S. Jensen, D. N. Hutchison, B. Turner, T. Wood, A. Dadson, M. A. Vail, M. R. Linford, R. R. Vanfleet and R. C. Davis, Adv Funct Mater **21** (6), 1132-1139 (2011).
9. D. S. Jensen, S. S. Kanyal, N. Madaan, M. A. Vail, A. E. Dadson, M. Engelhard and M. R. Linford, Surface Science Spectra **20**, 36-42 (2013).
10. S. S. Kanyal, D. S. Jensen, Z. Zihua and M. R. Linford, Surface Science Spectra (2014).

11. N. Madaan, S. S. Kanyal, D. S. Jensen, M. A. Vail, M. Engelhard and M. R. Linford, Surface Science Spectra **20**, 43-48 (2013).

12. S. S. Kanyal, D. S. Jensen, Z. Zihua and M. R. Linford, Surface Science Spectra (2014).

13. N. Madaan, S. S. Kanyal, D. S. Jensen, M. A. Vail, M. Engelhard and M. R. Linford, surface Science Spectra **20**, 49-54 (2013).

14. S. S. Kanyal, D. S. Jensen, Z. Zihua and M. R. Linford, Surface Science Spectra (2014).

15. N. Madaan, S. S. Kanyal, D. S. Jensen, M. A. Vail, M. Engelhard and M. R. Linford, Surface Science Spectra **20**, 55-61 (2013).

16. D. S. Jensen, S. S. Kanyal, N. Madaan, M. A. Vail, M. Engelhard and M. R. Linford, Surface Science Spectra **20**, 62-67 (2013).

17. S. S. Kanyal, D. S. Jensen, Z. Zihua and M. R. Linford, Surface Science Spectra (2014).

10. Chapter: ToF-SIMS of a Multiwalled Carbon Nanotube Forest Grown via Chemical Vapor Deposition from Iron Catalyst Nanoparticles

10.1. Abstract

We report the time-of-flight secondary ion mass spectrometry (ToF-SIMS) of carbon nanotubes grown catalytically from iron nanoparticles. Both positive and negative ion spectra were obtained using a cluster ion source (Bi_3^{2+} primary ions at 50 keV). The positive mode contains an intense C^+ signal. The C_n^- peaks in the negative ion spectrum show an odd-even effect in their intensities.

10.2. Introduction

Carbon nanotubes (CNTs) are an amazing form of carbon and have remarkable mechanical and electrical properties.[1-3] Thus, their characterization is important. Here we show the ToF-SIMS characterization of multiwalled CNTs prepared from iron catalyst nanoparticles. For the preparation of this material, 35 nm of alumina, which acts as a barrier layer to prevent catalyst poisoning, was first deposited on a silicon wafer.[4] A thin film (6 nm) of iron was then deposited using a thermal evaporation process.[5-8] The substrates were then placed in a quartz tube in the presence of argon and then the temperature was slowly raised to 750 °C in the presence on H_2, followed by flow of ethylene gas for two minutes. When annealed in H_2, the Fe films reduce into Fe nanoparticle from which the carbon nanotubes grow.[7] The substrates are finally cooled to below 200 °C and retrieved. ToF-SIMS spectra were then collected in both positive and negative ion mode using a Bi_3^{2+} primary ion source. The positive ion spectrum shows a dominant signal of C^+

and various hydrocarbon fragments (see Figure 10.1). The negative ion spectrum showed an even-odd effect in the intensity of C_n^- peaks for n = 1 to 6 (see Figure 10.2-10.3). The CNT forests described herein are an essential part of the materials created in the preparation of microfabricated thin layer chromatography (TLC) plates.[9-13] Indeed, submissions to Surface Science Spectra have been made on the XPS and SIMS characterization of the key materials in this microfabrication, including the silicon substrate,[14, 15] an alumina barrier layer on the Si/SiO_2 substrate,[16, 17] the Fe film on the alumina layer[18, 19] the Fe film after annealing in H_2 to create Fe nanoparticles,[20, 21] and the carbon nanotube forest grown on the Fe nanoparticles.[22]

10.3. Instrument setting

Same as section 5.3

10.4. Acknowledgement

We thank Diamond Analytics, a US Synthetic company (Orem, UT), for funding this current study. Also, a part of this research was performed at EMSL (Environmental Molecular Sciences Laboratory) located at Pacific Northwest National Laboratory.

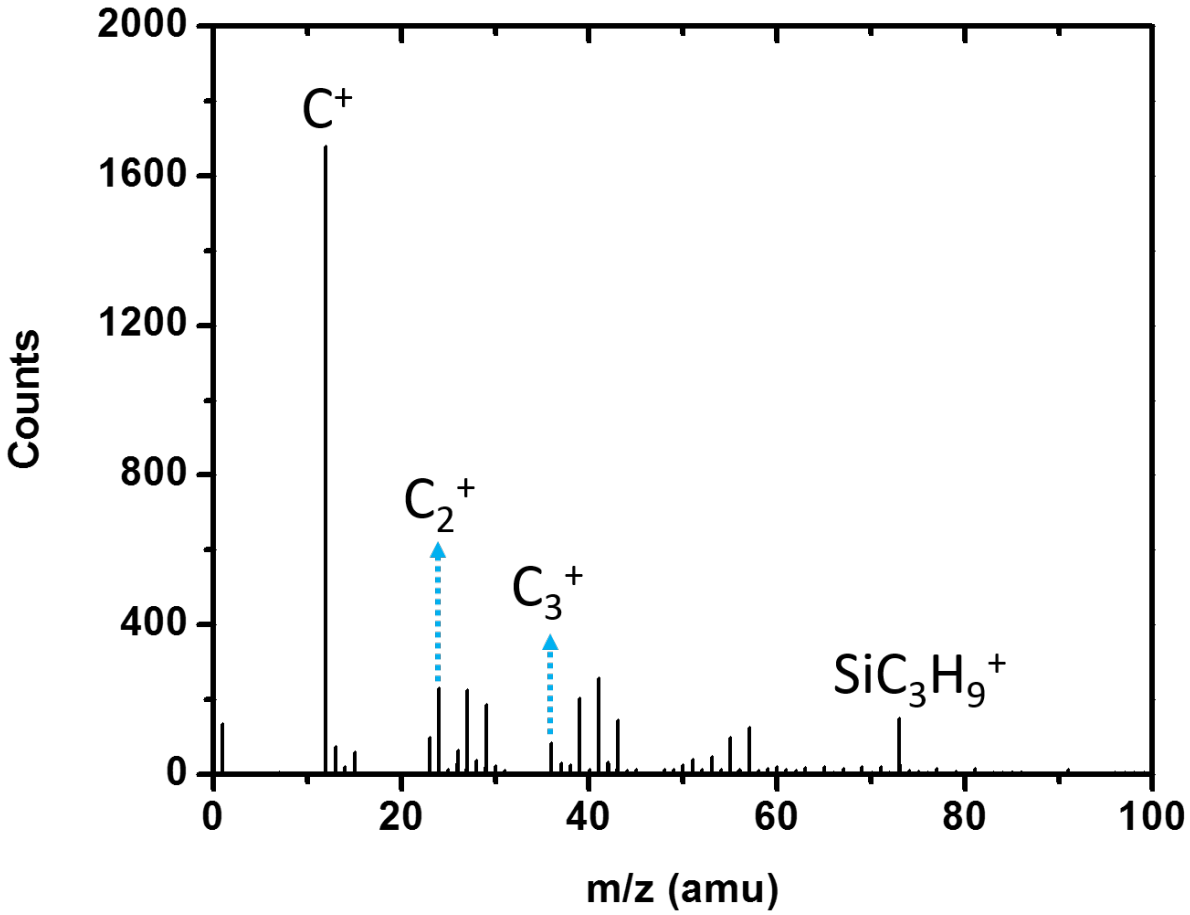

Figure 10.1. ToF-SIMS spectrum of $Si/SiO_2/Al_2O_3/Fe$(annealed)/CNT stack in positive mode (m/z 0-100).

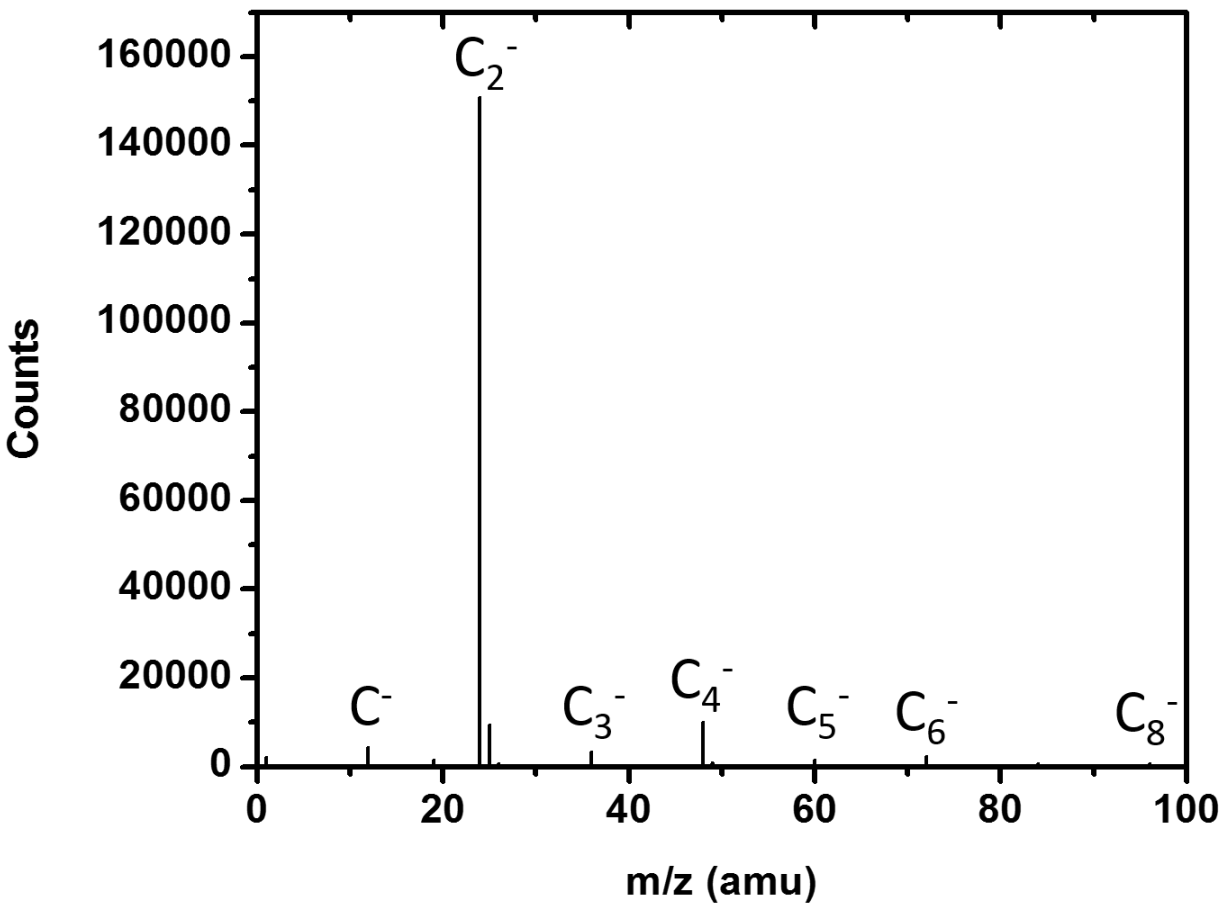

Figure 10.2. ToF-SIMS spectrum of $Si/SiO_2/Al_2O_3/Fe$(annealed)/CNT stack in negative mode (m/z 0-100).

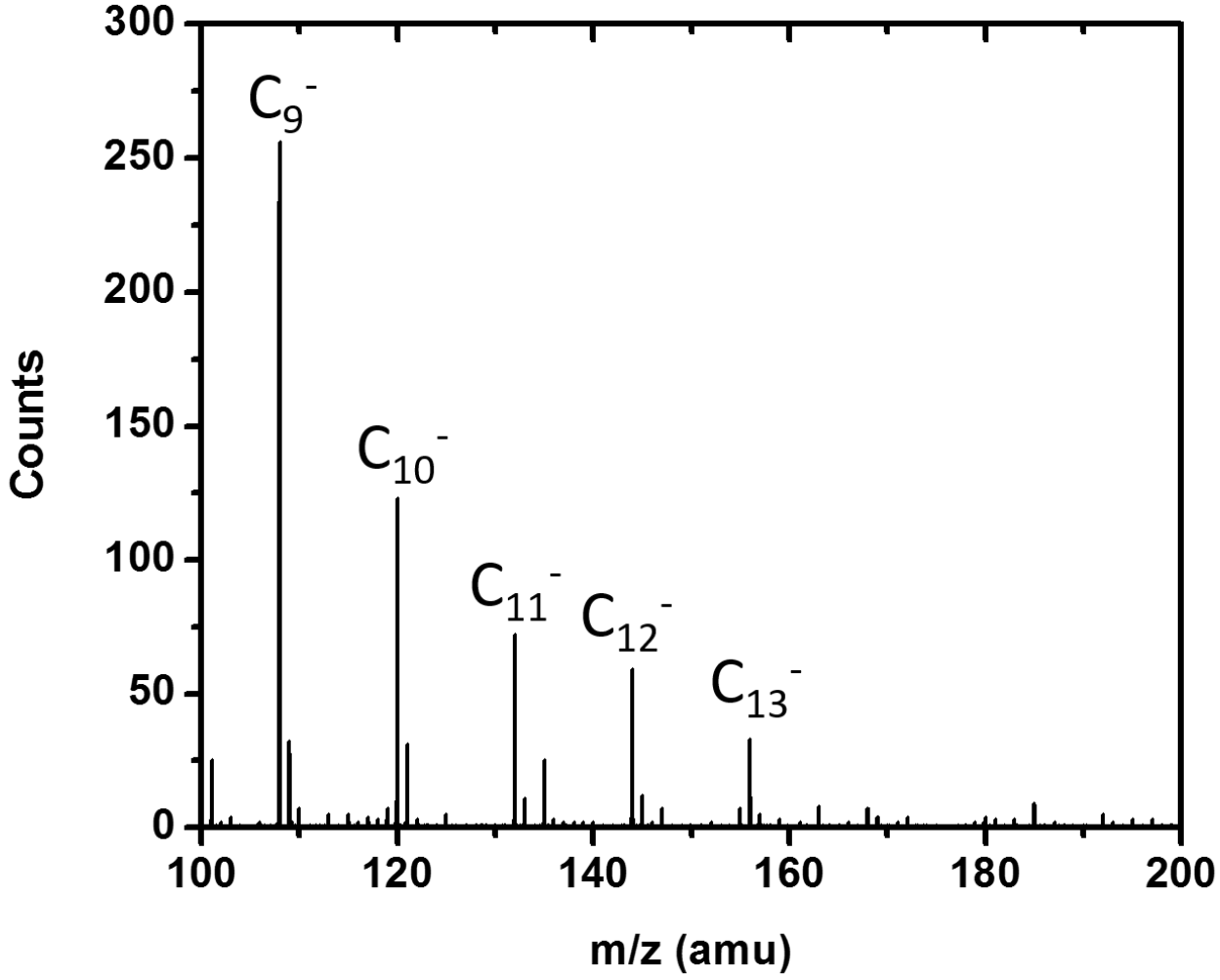

Figure 10.3. ToF-SIMS spectrum of Si/SiO_2/Al_2O_3/Fe(annealed)/CNT stack in negative mode (m/z 100-200).

10.5. References

1. H. Lee, J. K. Yoo, J. H. Park, J. H. Kim, K. Kang and Y. S. Jung, Adv Energy Mater **2** (8), 976-982 (2012).
2. C. W. Tan, K. H. Tan, Y. T. Ong, A. R. Mohamed, S. H. S. Zein and S. H. Tan, Environ Chem Lett **10** (3), 265-273 (2012).
3. D. Ahn, X. C. Xiao, Y. W. Li, A. K. Sachdev, H. W. Park, A. P. Yu and Z. W. Chen, J Power Sources **212**, 66-72 (2012).
4. S. I. Yoon, S. T. Heo, S. S. Kim, Y. K. Lee, H. T. Chun and D. G. Lee, Molecular Crystals and Liquid Crystals **499**, 472-481 (2009).
5. I. T. Han, H. J. Kim, Y. J. Park, Y. W. Jin, J. E. Jung, J. M. Kim, B. K. Kim, N. Lee and S. K. Kim, Jpn. J. Appl. Phys. **43** (6A), 3631-3635 (2004).
6. N. Bajwa, X. S. Li, P. M. Ajayan and R. Vajtai, J. Nanosci. Nanotechnol. **8** (11), 6054-6064 (2008).
7. C. Verissimo, M. R. Aguiar and S. A. Moshkalev, J. Nanosci. Nanotechnol. **9** (7), 4459-4466 (2009).
8. J. I. Sohn, C. J. Choi, S. Lee and T. Y. Seong, Japanese Journal of Applied Physics Part 1-Regular Papers Short Notes & Review Papers **41** (7A), 4731-4736 (2002).
9. D. S. Jensen, S. S. Kanyal, V. Gupta, M. A. Vail, A. E. Dadson, M. Engelhard, R. Vanfleet, R. C. Davis and M. R. Linford, Journal of Chromatography A **1257**, 195-203 (2012).
10. D. S. Jensen, S. S. Kanyal, N. Madaan, A. J. Miles, R. C. Davis, R. Vanfleet, M. A. Vail, A. E. Dadson and M. R. Linford, J Vac Sci Technol B **31** (3), 031203 (2013).

11. D. S. Jensen, S. S. Kanyal, N. Madaan, J. M. Hancock, A. E. Dadson, M. A. Vail, R. Vanfleet, V. Shutthanandan, Z. H. Zhu, M. H. Engelhard and M. R. Linford, Surf. Interface Anal. **45** (8), 1273-1282 (2013).

12. S. S. Kanyal, D. S. Jensen, A. J. Miles, A. E. Dadson, M. A. Vail, R. E. Olsen, S. Fabien, J. Nichols, R. Vanfleet, R. Davis and M. R. Linford, J. Vac. Sci Technol. B **31** (3), 031203 (2013).

13. J. Song, D. S. Jensen, D. N. Hutchison, B. Turner, T. Wood, A. Dadson, M. A. Vail, M. R. Linford, R. R. Vanfleet and R. C. Davis, Adv Funct Mater **21** (6), 1132-1139 (2011).

14. D. S. Jensen, S. S. Kanyal, N. Madaan, M. A. Vail, A. E. Dadson, M. Engelhard and M. R. Linford, Surface Science Spectra **20**, 36-42 (2013).

15. S. S. Kanyal, D. S. Jensen, Z. Zihua and M. R. Linford, Surface Science Spectra (2014).

16. N. Madaan, S. S. Kanyal, D. S. Jensen, M. A. Vail, M. Engelhard and M. R. Linford, Surface Science Spectra **20**, 43-48 (2013).

17. S. S. Kanyal, D. S. Jensen, Z. Zihua and M. R. Linford, Surface Science Spectra (2014).

18. N. Madaan, S. S. Kanyal, D. S. Jensen, M. A. Vail, M. Engelhard and M. R. Linford, surface Science Spectra **20**, 49-54 (2013).

19. S. S. Kanyal, D. S. Jensen, Z. Zihua and M. R. Linford, Surface Science Spectra (2014).

20. N. Madaan, S. S. Kanyal, D. S. Jensen, M. A. Vail, M. Engelhard and M. R. Linford, Surface Science Spectra **20**, 55-61 (2013).

21. S. S. Kanyal, D. S. Jensen, Z. Zihua and M. R. Linford, Surface Science Spectra (2014).

22. D. S. Jensen, S. S. Kanyal, N. Madaan, M. A. Vail, M. Engelhard and M. R. Linford, Surface Science Spectra **20**, 62-67 (2013).

11. Future Consideration

TLC plates manufactured via microfabrication show increased chromatographic performance. These advancements have made them industrially viable and superior to their commercial counterparts. However, further improvements may be possible as outlined below.

11.1. Optimization of channels

The channels are the arteries of microfabricated TLC plates. The speed of solvent flow across a plate can determine how fast/slow an analysis will be. In general, wider channels increase the speed of an analysis. If plates with different channel widths were available, the speed of separations could be tuned. Further work on channel optimization is needed. Data could be collected for plates with various channel widths ranging from 1-10 μm for a series of common solvents.

11.2. Optimization of hedges

The hedges of microfabricated TLC plates are the adsorbent material necessary for chromatography, and thus play an important role in separation quality. Hedges with varying widths and heights could be created to provide additional information about the optimal range in which these TLC plates can be fabricated without compromising separation quality and efficiency. Currently, we are using a hedge width of 4.5 μm and a height of 50 μm. In addition, optimization of hedge length has not been undertaken for these TLC plates.

11.3. Optimization of ZnO film and SiO_2 film thickness

Currently we put down 8 nm of ZnO to prepare fluorescent TLC plates. Additional experiments could be useful to elucidate the fluorescence phenomenon on these plates, which might include varying the ZnO film thickness and its depth from surface. The thickness of the protective ALD SiO_2 layer over the ZnO film could also be investigated.

11.4. Bonded phase TLC plates

Another possibility is to make reversed phase and other bonded phases such as amino (NH_2) and cyano (CN) phases for increasing the range of applicability of these TLC plates. We have already been successful in making amino bonded TLC plates by deposition of APTES (see Chapter 3).

11.5. Application and band analysis

It will be important to show a wide range of applications for these TLC plates. Initial results have also shown the compatibility of our M-TLC plates with mass spectrometry. Further thorough studies are needed to be able to more quantitatively analyze separated bands.